

TEMPERATURE TRAJECTORY OPTIMIZATION FOR A THERMOSTATED BATCH CRYSTALLIZATION APPARATUS

A DISSERTATION

*Submitted in partial fulfilment of the
requirements for the award of the degree*

of

MASTER OF TECHNOLOGY

in

CHEMICAL ENGINEERING

(With Specialization in Computer Aided Process Plant Design)

By

RAVENDRA SINGH



**DEPARTMENT OF CHEMICAL ENGINEERING
INDIAN INSTITUTE OF TECHNOLOGY ROORKEE
ROORKEE-247 667 (INDIA)**

JUNE, 2005

CANDIDATE'S DECLARATION

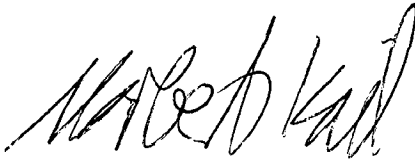
I hereby declare that the work which is being presented in the dissertation entitled "TEMPERATURE TRAJECTORY OPTIMIZATION FOR A THERMOSTATED BATCH CRYSTALLIZATION APPARATUS", in partial fulfillment of the requirement for the award of the degree of Master of Technology in Chemical Engineering with specialization in "Computer Aided Process Plant Design", submitted in the Department of Chemical Engineering, Indian Institute of Technology, Roorkee, India is an authentic record of my own work carried out during the period from September 2004 to May 2005, under the supervision of Dipl. -Ing. Norbert Kail, Research Scientist, Lehrstuhl für Prozesstechnik, RWTH Aachen University, Germany and kind guidance of Prof. Dr.-Ing. W. Marquardt, Head, Lehrstuhl für Prozesstechnik, RWTH Aachen University, Germany and Dr. Surendra Kumar, Professor, Department of Chemical Engineering, Indian Institute of Technology, Roorkee, India.

The matter embodied in this thesis has not been submitted for the award of any other degree.

Place : IIT Roorkee
Date : 29/06/2005


(RAVENDRA SINGH)


This is certified that the above statement made by the candidate is correct to the best of our knowledge.



Dipl. -Ing. Norbert Kail
Lehrstuhl für Prozesstechnik
RWTH Aachen University,
Aachen, Germany.



Prof. Dr.-Ing. W. Marquardt
Lehrstuhl für Prozesstechnik
RWTH Aachen University,
Aachen-52064,
Germany.



Prof. Dr. Surendra Kumar
Deptt. of Chemical Engineering,
Indian Institute of Technology,
Roorkee-247667,
India.

Acknowledgements

My work was supported, encouraged and inspired by a number of people. It is my great pleasure to reach the point in which I can look back in time and express my gratitude to them. First of all, I would like to thank my supervisor Dr. Surendra Kumar, Professor, Chemical Engineering Department, Indian Institute of Technology Roorkee for introducing me to the challenging and very rewarding research topic and for his guidance through the research odyssey that resulted in this project. His high standards in clear thinking and effective communication are inspiring and will always help me stand in good stead. His dedication to scientific research and hard-working attitude will always remain a role model for my work.

I can not express in few words gratitude towards my German mentor Prof. Dr.-Ing W. Marquardt, Head, Lehrstuhl für Prozesstechnik, RWTH Aachen, Germany who provided valuable guidance and direction by keeping time aside for me from his highly busy schedule and provide all the necessary facilities for carrying out this work. I thank him for his able guidance and untiring attention throughout the dissertation from inception to successful completion.

I am also grateful to Dipl.-Ing. Norbert Kail, Research Scientist, Lehrstuhl für Prozesstechnik, RWTH Aachen for supervising the master thesis and for many useful hints.

The acknowledgment transcends the reality of formality when I would like to express my deep gratitude to German Academic Exchange Service (Deutscher Akademischer Austausch Dienst) for providing me opportunity to carry out this work at German University.

Furthermore, I would like to express gratitude to Dr. (Mrs.) Shashi for careful reading of the manuscript, many valuable suggestions and comments.

I am very thankful to Dr. Bikash Mohanty, Prof. and Head, and Dr. I. M. Mishra, Prof. and Chairman, DRC, Chemical Engineering Department, Indian Institute of Technology Roorkee for providing me all the necessary facilities for carrying out this work.

During my stay in Aachen I benefited from contact with several professors as they encouraged me from time to time during my research work and provide an exposure to the recent developments in science and technology at RWTH Aachen. My special thanks to Prof. Dr.-Ing Burkhard, Director, RWTH Aachen, Germany to provide me all the facilities necessary to carry out the research work. I am also grateful to Dr. Prem Vert, Director, Indian Institute of Technology Roorkee who encouraged me for doing research work during his visit to RWTH Aachen University.

I wish to pay my heartiest thanks to Senior Engineers, Administrators, Technical Staff and Scientific Staff of LPT RWTH Aachen and Shri S. S. Mangla, Shri Ziaur Rahman, Shri Mange Ram and Ms. Tripta Garg (The staff members of Reaction Engineering lab, Chemical Engineering Department, IIT Roorkee) for their helps in many ways.

And last, but not least, I would like to thank my family for their loving support through these years.

Contents

Candidate's Declaration	i
Abstract	iii
Acknowledgements	v
List of Notations	xi
List of Figures	xvii
List of Tables	xix
1 Introduction	1
2 Literature review	5
2.1 Crystallization basics	5
2.2 Control	13
3 Experimental setup	17
3.1 Problem formulation	17
3.2 System	18
3.2.1 Batch reactor	18
3.2.2 Thermostat	20
3.2.3 Cascade control system	21
4 Tools	23
4.1 gPROMS	23
4.1.1 Modeling	24
4.1.2 Parameter estimation	24
4.1.3 Controller Tuning	28
4.1.4 Optimization	30
4.2 Labview	31
4.2.1 Control	31
4.2.2 Data acquisition	31

4.3	System identification	31
4.3.1	Experimental design	32
4.3.2	Data collection	32
4.3.3	Data Preprocessing	32
4.3.4	Model structure selection	34
4.3.5	Model estimation	35
4.3.6	D2C Conversion	35
4.3.7	Model validation	35
5	Model	37
5.1	Batch reactor	37
5.1.1	Reactor	37
5.1.2	Inner tank wall	41
5.1.3	Tempering jacket	43
5.1.4	Outer tank wall	45
5.2	Thermostat	48
5.3	Controller	49
5.3.1	Internal controller	49
5.3.2	External controller	51
5.4	Crystallization	53
5.4.1	Population balance equation	53
5.4.2	Growth rate	54
5.4.3	Nucleation rate	54
5.4.4	Production reduction rate	54
5.4.5	Mass balance	55
5.4.6	The heat of the crystallization	55
5.4.7	Supersaturation	55
5.5	Linear model of the system	56
5.5.1	Discrete time IDPOLY model	56
5.5.2	Continuous time IDPOLY model	56
5.6	Optimization problem	57
5.6.1	Linear model	57
5.6.2	<i>PID</i> controller in linear model	58
6	Results and discussion	61
6.1	Parameter estimation	61
6.1.1	System dependent parameters	61
6.1.2	Adjusting parameters	68
6.1.3	Control parameters	85
6.2	Estimated parameters	85
6.3	System identification	91
6.3.1	First estimation	91
6.3.2	Second Estimation	107
6.4	Linear model of the system	117
6.5	Temperature trajectory optimization	117
6.5.1	Optimization alone	117
6.5.2	Optimization with addition <i>PID</i>	122
6.5.3	Controller alone	130

7	Case study	133
7.1	Model	133
7.2	Result	137
8	Conclusions and recommendations	145
8.1	Conclusions	145
8.2	Recommendation for future work	146
A	Process section	147
A.1	Model	147
A.2	Linear model	152
B	System identification	155
B.1	1 Liter reactor	155
B.2	6 Liter reactor	155
C	PID controller	159
C.1	Internal controller	159
C.2	External controller	159
D	Entities in gPROMS	161
E	Case study	165
	References	167

List of Notations

Symbols

Symbol	Usage	Units
A	area	m^2
C	concentration	$\frac{kg}{m^3}$
C_p	heat capacity	$\frac{J}{kg \cdot K}$
d	diameter	m
D	diffusion coefficient	$\frac{m^2}{s}$
E	energy	J
est	estimation factor	—
h	height	m
K_c	proportional constant	—
m	mass	kg
\dot{m}	mass flow rate	$\frac{kg}{s}$
M	molecular weight	—
n	agitator speed	$\frac{revolution}{s}$
P	agitator power	$\frac{J}{s}$
p	pressure	bar

Symbol	Usage	Units
$Poly$	polynomial	—
Q	heat flow rate	$\frac{J}{s}$
S	supersaturation	—
T	temperature	K
t	time	s
T_n, T_I	integral time	s
T_v, T_D	differential time	s
V	volume	m^3
X_p	proportional gain	—

Subscripts

Index	Usage
<i>a</i>	air
<i>ag</i>	agitator
<i>amb</i>	ambience
<i>b</i>	bottom
<i>cib</i>	connect inner wall bottom
<i>cri</i>	connect reactor inner wall
<i>crc</i>	connect reactor condenser
<i>cra</i>	connect reactor ambience
<i>chs</i>	connect heat exchanger steel
<i>chob</i>	connect bottom outer wall bot- tom
<i>cis</i>	connect reactor shell
<i>coef</i>	coefficient
<i>cr</i>	crystallization
<i>csa</i>	connect steel ambience
<i>csos</i>	connect shell outer wall shell
<i>f</i>	fluid
<i>he</i>	heat exchanger
<i>i</i>	inner wall

Index	Usage
<i>ic</i>	internal controller
<i>ob</i>	outer wall bottom
<i>os</i>	outer wall shell
<i>pid</i>	external <i>pid</i> controller
<i>r</i>	reactor
<i>s</i>	shell
<i>st</i>	steel
<i>vap</i>	vapour

Greek symbols

Index	Usage
α	heat transfer coefficient
γ	variance model parameter
σ	variance
δ	thickness
ϵ	variance model parameter
ω	standard deviation
λ	heat conductivity
ν	kinematic viscosity
η	dynamic viscosity

Standard dimensionless numbers

Index	Usage
Gr	Grashof number
Nu	Nusselt number
Pr	Prandtle number
Re	Reynolds number
Sc	Schmidt number
Sh	Sherwood number

List of Figures

3.1	Problem formulation	18
3.2	Batch reactor with tempering jacket	19
3.3	Thermostat	20
3.4	Cascade control system	22
6.1	Effect of the agitator power	63
6.2	Effect of the agitator power (error)	64
6.3	Effect of the flow rate through the pump	66
6.4	Effect of the flow rate throw the pump (error)	67
6.5	Effect of the est_g	69
6.6	Effect of the est_g (enlarge)	70
6.7	Effect of the est_g (error)	71
6.8	Effect of the est_{cra}	73
6.9	Effect of the est_{cra} (error)	74
6.10	Effect of the est_α	76
6.11	Effect of the est_α (error)	77
6.12	Effect of the est_λ	79
6.13	Effect of the est_λ (error)	80
6.14	Effect of the est_{cp} (error)	82
6.15	Effect of the $cool_{min}$ (error)	84
6.16	Comparison of reactor temperature trajectory	89
6.17	Comparison of thermostat temperature trajectory	90
6.18	Input and output signal	92
6.19	Input output signal used for system identification	93
6.20	Validation 1 for <i>ARX</i> and <i>ARMAX</i> model.	96

6.21	Validation 1 for <i>OE</i> and <i>BJ</i> model.	97
6.22	Validation 1 for <i>P2DZ</i> and <i>P3DZ</i> model.	98
6.23	Input output signal used for model validation	100
6.24	Validation 2 for <i>ARX</i> and <i>ARMAX</i> model.	101
6.25	Validation 2 for <i>OE</i> and <i>BJ</i> model.	102
6.26	Input output signal used for model validation 3	104
6.27	Validation 3 for <i>ARX</i> and <i>ARMAX</i> model.	105
6.28	Validation 3 for <i>OE</i> and <i>BJ</i> model.	106
6.29	Validation 1 for <i>ARX</i> and <i>ARMAX</i> model.	108
6.30	Validation 1 for <i>OE</i> and <i>BJ</i> model.	109
6.31	Validation 2 for <i>ARX</i> and <i>ARMAX</i> model.	111
6.32	Validation 2 for <i>OE</i> and <i>BJ</i> model.	112
6.33	Validation 3 for <i>ARX</i> and <i>ARMAX</i> model.	114
6.34	Validation 3 for <i>OE</i> and <i>BJ</i> model.	115
6.35	Optimize reactor temperature trajectory in the linear model	118
6.36	Error of optimization in the linear model	119
6.37	Experimental optimize reactor temperature trajectory	120
6.38	Error of the optimization	121
6.39	Online setpoint adjustment	123
6.40	PID validation	124
6.41	PID validation error	125
6.42	Linear PID validation	126
6.43	Linear PID validation error	127
6.44	Optimization and controller both	128
6.45	Optimization and controller both error	129
6.46	Controller alone	131
7.1	Molar change of α form in unseeded crystallization	138
7.2	Molar change of β form in unseeded crystallization	139
7.3	Supersaturation of β form in unseeded crystallization	140
7.4	Molar change of α form in seeded crystallization	141
7.5	Molar change of β form in seeded crystallization	142
7.6	Supersaturation of β form in seeded crystallization	143

List of Tables

6.1	Estimated parameters	88
6.2	Comparison of the system identification methods	116
D.1	Optimization entities	163

Chapter 1

Introduction

The batch mode of production has become increasingly important in the process industry during the last decade. Batch plants can be made highly flexible, and thereby well suited for manufacturing of a large variety of product types. Batch processing is normally associated with the chemical process industries. It is however, important also in the food industry, pharmaceutical industry etc.

Temperature, pressure, concentration are the basic process variables. Among these process variables temperature is the most important for product quality as well as safety. For that reason an efficient robust temperature control technique is needed.

In many fields of process industry for example the chemical industry, pharmaceutical industry fertilizer industry, products in crystallized form are produced. In many cases products of a very specific size pattern are required for example in pharmaceutical industries. It is a challenging task to produce crystals of the desired qualities as crystal qualities strongly depend on the temperature. The temperature control in batch crystallization processes is quite difficult because of the non stationary behavior of the batch process.

In many batch processes for example crystallization the product properties depends on the temperature profile in the reactor. During the batch process it is possible to predict the desired temperature trajectory on the basis of the desired properties of the final product. To achieve the desired temperature trajectory in the reactor, a combination of a trajectory optimization and a cascade *PID* control system is used for which an accurate model of the system is required. For the optimization of the temperature trajectory, the optimization routine gOPT is used. To minimize the calculation time

of optimization the whole model of the system is simplified to a linear dynamic model with the help of the system identification tool box of Matlab.

By optimization of the temperature trajectory of the reactor we can get the desired temperature trajectory of the thermostat and that temperature trajectory of thermostat is achieved by internal *PID* controller. And hence we can achieve the desired temperature trajectory of the reactor.

Objectives

Following objectives have been formulated for the M.Tech dissertation:

1. To learn the modeling, parameter estimation and optimization routine of gPROMS.
2. To develop the model for thermostated batch crystallization apparatus with online implementation and internal control system.
3. To conduct the experiments and obtain the results.
4. To estimate model parameters based upon one set of experimental data by using parameter estimation routine of gPROMS.
5. To validate the model with other set of experimental data.
6. To develop the appropriate control technique for controlling the batch reactor temperature.
 - To obtain the simple linear model of the apparatus by using System Identification Tool Box of MATLAB.
 - To carry out the temperature trajectory optimization by using optimization routine of gPROMS.
 - To validate the temperature trajectory optimization result by the experiment.
 - To implement the external *PID* controller with provision of online setpoint adjustment of the internal *PID* controller for handling the system disturbances.

- To develop the appropriate methodology for controller parameters tuning.
7. To validate the developed control technique by the experiment.
 8. To perform a cause study for the crystallization of the L-glutamic acid.

Chapter 2

Literature review

2.1 Crystallization basics

Crystallization is a solid-liquid separation process where mass is transferred from a solute dissolved in a liquid phase to a solid (crystal pure) phase. Batch crystallization is considered as one of the important unit operation used for separation and purification in chemical engineering. This is because batch crystallizers are simple, flexible and usually involve less process development. Also, the solid product can be obtained at high purity and at low costs. [HJKA03].

Supersaturation

The number of units per unit volume of fluid phase can be given as follows:

$$\frac{n \cdot N_A}{V} = c \cdot N_A \quad (2.1)$$

A saturated fluid phase having concentration c_{eq} is in thermodynamic equilibrium with the solid phase at the relevant temperature. If the solution is liquid, the saturation concentration often depends strongly on temperature but only slightly on pressure. If a fluid phase has more units than $c_{eq} \cdot N_A$, it is said to be supersaturated [Mer95]. Crystallization process can take place only in supersaturated phases, and the rate of crystallization is often determined by the degree of supersaturation. Supersaturation is expressed as difference in concentration [Mer95].

$$\Delta c = c - c_{eq} \quad (2.2)$$

Relative supersaturation can be expressed as:

$$S = \frac{(c - c_{eq})}{c_{eq}} \quad (2.3)$$

Nucleation

Crystals are formed by the repetition of unit cells in 3-D space. Formation of new nucleus is called nucleation. Crystals are created when nuclei are formed and then grow. The kinetic processes of nucleation and crystal growth require supersaturation, which can generally be obtained by a change in temperature (cooling in the cause of a positive gradient of the solubility curve or heating in the cause of a negative gradient), by removing the solvent (evaporative crystallization), or by adding a drowning-out agent or reaction partners. The system then attempts to achieve thermodynamic equilibrium through nucleation and the growth of nuclei [Mer95]. Process of nucleation can be classified as follows:

1. Primary nucleation
 - Primary homogeneous nucleation
 - Secondary homogeneous nucleation
2. Secondary nucleation

Primary nucleation

Primary nucleation is the formation of a new solid phase from a clear liquid. This type of nucleation can be further subdivided into homogeneous and heterogeneous nucleation. Both homogeneous and heterogeneous nucleation take place in the absence of solution-own crystals. This occurs when a specific supersaturation, known as the meta stable supersaturation is exceeded in the system.

Homogeneous primary nucleation

If a solution contains neither solid foreign particles nor crystals of its own type, nuclei can be formed only by homogeneous nucleation. If supersaturation is sufficiently high, more and more elementary units can join together and create increasingly larger nuclei known as clusters [Mer95].

Heterogeneous primary nucleation

In heterogeneous nucleation, nucleation starts on foreign substrates of mostly microscopic particles, e.g. dust or dirt particles. The presence of foreign interfaces allows the nuclei of the new phase to be supported by a surface, which reduces their surface energy and globally increases the nucleation rate, thus reduces the width of the meta stability zone and the induction period. Concerning modeling aspects, kinetic laws are similar to the laws used for homogeneous nucleation.

Secondary nucleation

Secondary nucleation refers to the birth of new crystals at the interface of parent crystals. Contrary to the relatively high super saturation required for primary nucleation, secondary nucleation already occurs at low to moderate values of the supersaturation. There are various types of secondary nucleation, but the most important source of secondary nuclei in crystallization is attrition. Attrition, also referred to as contact nucleation, occurs as a result of crystal-pump, crystal-vessel wall or crystal-crystal collisions.

The driving force for attrition is determined by the concentration of the various sized crystals and their relative motion with respect to the pump blades, vessel walls or other crystals. The relative kinetic energy of a collision is determined by the size and relative velocity of the particle, which in turn is a function of the slurry motion, viscosity and particle inertia (thus particle size). The rate coefficient or resistance for attrition is a function of the shape, surface roughness and mechanical properties of the colliding crystal. The rate coefficient is also indirectly influenced by the supersaturation, which determines factors such as surface roughness and healing of corners and surfaces damaged due to previous collisions.

The formation of secondary nuclei is a complex process depending on the hydrodynamics inside a crystallizer, the attrition behavior of the crystalline material and the outgrowth (survival) of the attrition fragments. In draft tube, draft tube baffle and forced circulation crystallizers the attrition is mainly caused by collisions between crystals and the pump or impeller, whereas in fluidized bed crystallizers collisions between crystals are considered the dominating source of attrition.

Secondary nucleation refers to several mechanisms of nuclei production which have

all in common mechanical aspects induced by the stirring of the medium and the interaction between the crystals already present and their environment: fluid, stirrer, reactor wall, and other crystals. Contact nucleation refers to the breakage of parent crystals due to shocks with walls, stirrer,... and release of small fragments which act as secondary nuclei. True secondary nucleation is less known, it refers to the existence of a cluster or nuclei reservoir in the boundary layer of the parent crystals. These nuclei are released into the liquid medium by shocks or shearing effect of the fluid. From a modeling point of view, the nucleation rate generally depends on the stirring rate, on the parent crystals mass or/surface area and on super saturation level (S-1) with an exponent ranging between 0.5 and 2.5. Consequently, the corresponding metastability zone is narrower than for primary nucleation. Secondary nucleation is predominant in continuous industrial crystallizers operated at low supersaturation levels. On the contrary, in precipitator, in which supersaturation, is much higher, primary nucleation is the main source of nuclei.

Crystal growth and dissolution

Crystal growth is the addition of solute molecules from a supersaturated solution to the crystal lattice. Besides being a mechanism responsible for increasing crystal size, crystal growth, or more specifically the relative growth rates of the crystal faces, also largely determines crystal morphology. Finally, the crystal face growth rates together with the growth mechanism determine the surface structure and purity of the crystal[HJR00].

The growth rate of a particular crystal face is mostly described by its linear growth rate, which refers to the growth rate of that face in the direction normal to the face. Since the growth rates of the various crystal faces are usually not equal, an overall linear growth rate is often used.

Crystal growth is a three-step process consisting of mass transfer, surface integration and heat transfer. Mass transfer and surface integration occur sequentially and in parallel with heat transfer. Mass transfer involves the diffusion of growth units, i.e. molecules, atoms or ions, to the crystal surface. Surface integration consists of surface diffusion, orientation and the actual incorporation into the lattice. Various mechanisms exist for surface integration, the most important being spiral growth, 'birth and spread'

growth and rough growth. Spiral growth is the most encountered growth mechanism under normal operating conditions[HJR00]. It is important to note that the super saturation, i.e. the difference in chemical potential of the crystallizing substance in the liquid and solid phase, need not to be the same for each crystal. While the chemical potential in the liquid phase may be the same, the chemical potential of two neighboring crystals may differ due to differences in lattice structure and/or lattice strain. As a result, similarly sized crystals exposed to identical growth conditions can exhibit different growth rates. This phenomenon is called growth rate dispersion[RJT90]. The mass transfer rate coefficient is a function of the diffusion coefficient, crystal size and local hydrodynamics. Besides on the surface integration mechanism, the rate coefficient for surface integration also depends on the size of the growth units (because of surface diffusion and steric orientation) and the lattice structure.

Crystal dissolution is not the exact opposite of crystal growth. dissolution does not require surface diffusion and orientation of atoms, ions or molecules, and is therefore in general limited by mass transfer. Crystal dissolution thus has a first order dependency on the supersaturation, its driving force. The rate coefficient for dissolution is a function of the diffusion coefficient, crystal size and local hydrodynamics. Because dissolution is usually mass transfer limited, dissolution at crystal edges and corners is faster due to steric favoring. For this reason, crystals are easily rounded off once dissolution starts.

Agglomeration

The agglomerate is defined as the mass formed by the cementation of individual particles, probably by chemical forces. A mass formed by a group of particles held together by only inter particle forces is called an aggregate.

Agglomerates are usually undesirable because they contain mother liquor between the primary crystals that form the agglomerate. This liquor is hard to remove during drying, and promotes caking of the product during storage. Furthermore, agglomerates also tend to break more easily than solid crystals, during which they also release solvent. There are however also cases where agglomeration is stimulated, namely when the primary particles are too small for acceptable downstream solids handling.

Agglomeration first of all requires the collision of two or more crystals. The collision

mechanism depends on the sizes of the crystals involved. Per kinetic (due to Brownian motion; small particles), orthokinetic (due to fluid shear) or inertia (due to differences in relaxation time; differently sized particles). Next, these crystals must form an aggregate as a result of interparticle forces, such as VanderWaals (attractive), electrostatic (repulsive) and steric (repulsive) forces. Finally, cementation of these crystals as a result of growth, before the aggregate is disrupted, is required to create agglomerate.

The driving force for agglomeration is the supersaturation. Without super saturation, aggregates can be formed but agglomerates cannot. The rate coefficient or kernel for agglomeration is a function of the number of particles (collision chance), the sizes of the particles involved (agglomeration mechanism), and in the case of orthokinetic agglomeration the fluid shear or energy dissipation (collision chance, time between collision and disruption).

The collision frequency increases with increasing shear rate, but if the shear rate becomes too high, aggregates are disrupted before sufficient cementation has taken place. As a result, the rate constant for orthokinetic agglomeration first increases and subsequently decreases with shear rate.

Breakage

Similar to attrition, breakage can occur as a result of crystal-pump, crystal-vessel wall or crystal-crystal collisions. The difference between breakage and attrition is not a distinct one. The fracture of a particle into one slightly smaller particle and many much smaller fragments is defined as attrition. Breakage involves the fracture of a particle into two or more pieces. To accomplish the total fracture of a particle it required considerably more energy than that needed for attrition. If the impact energy of a single collision is not sufficient, repeated collisions, which result in accumulation of crystal stress, are required for breakage.

The driving force and rate coefficient for breakage are mainly a function of the same process conditions and particle properties as discussed for attrition. In addition, the rate coefficient or resistance for breakage is also influenced by the collision history of the particles involved.

Segregation

Segregation is not a crystallization mechanism in the sense that it forms a particle, increases its size or reduces its size. However, as it can have a significant effect on the final product quality it is discussed here. Particle segregation is a result of slip with respect to the liquid motion. An important effect that can only be described if segregation is taken into account is the non-uniform distribution of solids in a crystallizer. For instance, if the circulation intensity is lowered in a crystallizer, the relative amount of solids in the lower part of the crystallizer will increase. Particle segregation is a function of particle size, liquid velocity, solids concentration, and the difference in material density between the liquid and solid phase.

To achieve a desired *CSD* it is important to control supersaturation through cooling temperature and agitation rate, among other factors. Crystals are formed when nuclei appear and then grow. In the cooling crystallization process, the kinetics of nucleation and crystal growth require supersaturation, which is obtained by a change in temperature. In continuous processes it is important to keep supersaturation at an optimum value that will yield a growth rate as high as possible and a low nucleation rate for a sufficiently coarse crystal product to be formed. This condition is difficult to be achieved in batch crystallization because supersaturation changes from the beginning to the end of the processing. Therefore, it is desirable to set a cooling profile that keeps supersaturation almost constant to prevent high nucleation rates and limits the number of new nuclei formed. On the other hand, agitation exerts an additional influence on *CSD*. Low values induce agglomeration, aggregation, and flocculation of particles, whereas high values produce attrition and breakage. Again, it is desirable to establish an agitation profile that increases mass transfer but reduces crystal destruction. A right combination of temperature and agitation profiles may induce optimal operation of batch crystallizers [PEBL04].

Dynamic behavior

Process conditions may vary with time. Consequently, the product quality resulting from a crystallization process will not always be constant in time. Dynamics in product quality are usually most noticeable in the crystal size distribution. Batch processes are inherently dynamic, but continuous processes can also exhibit dynamic behavior.

Dynamics in continuous processes do not only occur as a result of process disturbances or set point changes, but can also occur when the process inputs are kept constant and no disturbances occur. In the latter case, unstable process behavior is usually a result of the interaction between crystallization mechanisms such as nucleation and growth. For instance, a period of low nucleation rates will result in a decrease in the volume specific crystal surface area available for growth, which will lead to an increase in the level of super saturation and hence in the crystal growth rate. As the same crystal mass is being deposited on a smaller number of crystals, the average crystal size will increase. The increase in super saturation and crystal size can respectively lead to an increase in primary and secondary nucleation rates. Consequently, the super saturation level and average crystal size will decrease, thus leading to a new period of low nucleation rates[Mer95].

As decisions taken during design determine to a great extent the controllability of a process, the effect of process dynamics on product quality and process performance should not be postponed to the control system design stage. Dynamic modeling of crystallization processes is therefore essential from the process design stage onwards.

Polymorphism

Polymorphism is the phenomenon that a compound has more than one crystalline arrangement. Different polymorphic structures exhibit different physical and chemical properties such as crystal morphology, solubility, and color, which effect the performance of the products. L-Glutamic acid is known to have two polymorph, the α and β form. If α form crystals are put in a saturated aqueous solution, a solvent mediated transformation from the α form to the β form will take place [OtHJ04].

The solvent mediated transformation process is a combination of the dissolution of the α form and the nucleation and subsequent growth of the β form. The model parameters for the dissolution of the α form and the nucleation and growth of the β form were determined with the aid of the experimental data. The growth rate of the β form is the rate limiting step in the transformation[OtHJ04].

2.2. Control

A control system is an essential part to ensure that the desired operating conditions can be maintained as close as possible during the course of a batch run [API05]. Achieving the optimal operation of the batch reactor is quite difficult due to the complexity of the batch process which can be characterized as [API05]

- Batch processes are generally highly nonlinear in behavior for instance crystallization rate depends on the temperature and the concentration both.
- In the batch process most of the variables and parameters are time variant for instance in batch crystallization process temperature and concentration both changes w.r.t. time. Some system parameters (e.g. heat transfer coefficient) may also change significantly w.r.t. time.
- Some properties (e.g. molecular weight) are difficult to measure during the batch run and can be measured only at the end of the process while these need to be controlled during the batch run or if they can be measured (e.g. concentration) there is significant time delay.
- Due to the difficulties in the measurement of the other properties in most of the cases temperature is used to control the other process properties. This type of indirect control is not so efficient.

Usually controllers try to track the prespecified setpoint profiles for the process variables for which measurements are available (e.g. temperature) in order to obtain desired product properties. The prespecified setpoint profile can be obtained by offline optimization. Because of modeling errors and external disturbances, even if the optimal profiles are tracking perfectly, the final properties may significantly differ from the desired values. To account for the modeling errors and disturbances, new optimal profiles may be recomputed once new product property measurements are obtained. Gattu and Zafiriou have formulated a state estimation model based algorithm for on line modification of setpoint profiles utilizing infrequent and delayed measurement information of the properties to be controlled, with the goal of obtaining the desired values of the properties in the minimum batch time. The algorithm modifies the setpoint profile for the remainder of the batch after every measurement by making one step in the right

direction instead of attempting to find a completely new optimal profile. This results in robustness with respect to model error and allows improvement even with infrequent product property measurements [GZ99].

The uncertainty in the parameters may also lead to the inefficient controller performance for instance uncertainty in the heat transfer coefficient and the kinetic parameters may lead to an unstable response. In the system under consideration some parameters like the heat transfer coefficient between the reactor liquid and the bath fluid and between the bath fluid and the environment are uncertain and need to be adjusted. Sampath and Palanki proposed a robust nonlinear control strategy for temperature tracking problems in the jacketed batch reactors in the presence of the parametric uncertainty. A multiloop controller design methodology is used in which the inner loop is used as a nominal model, based on nominal parameter values, to approximately linearize the system in an input/output (I/O) sense. The outer loop is designed for both robust stability as well as nominal performance using recent results from robust control theory. In the methodology proposed by sampath and Palanki only bounds of the uncertain parameters are required to reduce the performance degradation. The uncertain parameters are pulled out from the state space equations into a block diagonal perturbation to obtain an equivalent system where the state space matrices do not depend on uncertain parameters. The closed loop system is then reduced to the standard feed back form [SPCC02].

How accurately the desired operating conditions are achieved in batch processes also depends on the type of controller used. The most common controllers used for batch processes are generic model control (GMC), dual mode control (PI , PID), and model predictive control (MPC). Aziz et.al have conducted an experiment for studying the performance of the dual mode control and the generic model control [NHI00]. First they obtained the optimum temperature profile by solving the off line optimization problem. The optimum temperature profile thus obtained is then used as the setpoint to be tracked by different types of controller.

GMC is a model based control strategy developed by Lee and Sullivan [PS88]. The main advantage of the GMC is that the nonlinear process models do not need to be linearized because it directly inserts nonlinear process models in to the controller itself. In addition, the GMC algorithm is relatively easy to implement. The desired response

can be obtained by incorporating only two tuning parameters [NHI00].

In the study [NHI00] it is found that a *PI* controller shows a large offset while *PID* and *GMC* controllers were able to track the reactor temperature with little offset. Based on the amount of the desired product achieved, the controller performance using the *PID* is found to be slightly better than that obtained by using the *GMC*. It is due to the larger rise time for the *GMC* controller compared with the *PID* controller. The performance of the *GMC* controller is found to be more stable compared with other controllers. The response of *PI* and *PID* controllers are more sluggish than *GMC* in tracking the dynamic setpoints.

The model predictive control (MPC) uses an internal model of the system to be controlled. This model is utilized to calculate predictions of the future behavior of the system. These predictions are then employed to, at each instant in time, to optimize the future behavior of the system over the input variables. The solution to this optimization problem is the optimal input signal to the system at that particular time. The model predictive control is the most suitable control system for the batch process but online optimization is required to implement the *MPC*. The neural network estimator is required to implement the generic model control. The *PID* is the most suitable controller for the system under consideration in the absence of an online optimization tool and neural network.

Chapter 3

Experimental setup

3.1 Problem formulation

In many chemical industries (e.g. crystallization, polymers, pharmaceutical etc.) batch mode of the production is preferred because batch process offers many advantages such as it is quite flexible, it can adopt to small volume production of various products, product can be modified according to market trends and new technology developed, it is quite safe for handling dangerous as well as expensive materials. A control system is essential in the batch process to obtain the desired properties of the product. The control system ensures that the desired operating conditions can be maintained as close as possible during the course of a batch run. However it is quite difficult to maintain the optimal operating conditions in the batch run and still it is a challenging and interesting problem.

In the system under consideration a thermostat is used to maintain the optimal temperature profile in the jacketed reactor. The reactor fluid exchanges the heat from the bath fluid and the bath fluid is heated or cooled in the thermostat. A prespecified temperature trajectory of the thermostat can be tracked by the internal PID controller. The temperature trajectory of the thermostat which gives the optimal temperature trajectory in the reactor is needed to be estimated. The optimal temperature trajectory of the bath fluid can be obtained by the optimization routine of gPROMS for which an accurate mathematical model of the system is needed. Due to the complexity of the system the optimization time is very high and hence the optimization run is infeasible. In order to make the optimization run feasible a linear model of the system is needed.

Since the linear model is not behaving exactly as the system under consideration hence an external controller is also needed to adjust the prespecified temperature trajectory of the bath fluid. The overall problem can be formulated in figure 3.1.

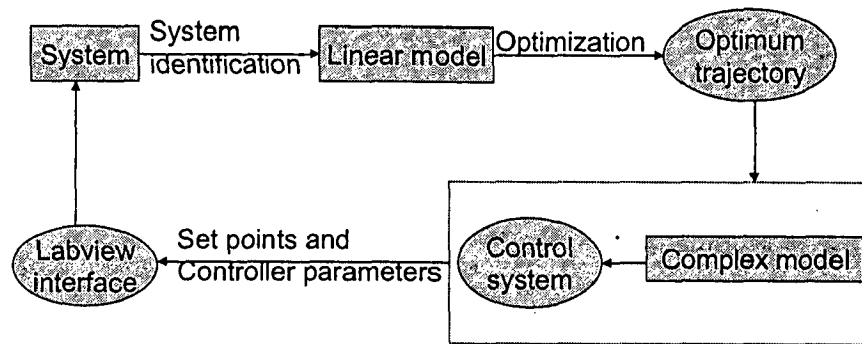


Figure 3.1: *Problem formulation*

3.2 System

The system under consideration is a stirred tank batch crystallizer. The whole system under consideration can be classified in to three major parts:

- Batch reactor
- Thermostat
- Cascade control system

3.2.1 Batch reactor

It is a flat flange vessel of the type ADAV (cylindrical, jacketed, with bottom outlet valve) with tempering jacket. It is manufactured by HWS [hm]. The reactor is shown

in figure 3.2, which was taken from the manufactures brochure[hm]. The reactor is closed by a glass lit and both reactor and lit are made of borosilicate glass (DINI SO 3585), required physical properties are given in Appendix A.1. Values for the various dimensions of the vessel are listed in Apendix A.1. The pressure in the reactor is constant (1 bar). A blade agitator of turbine type is mounted in the reactor. The revolution of the agitator can be adjusted at the control panel of the agitator engine or in the LABVIEW interface. A temperature sensor in the reactor measures the reactor temperature permanently and transmits the temperature data to the LABVIEW control panel. The inner reactor tank is surrounded by the tempering jacket, in which the bath fluid is circulated around the reactor tank. The bath fluid enters the tempering jacket at the bottom in tangential direction and leaves the jacket shell at the top of the tempering jacket

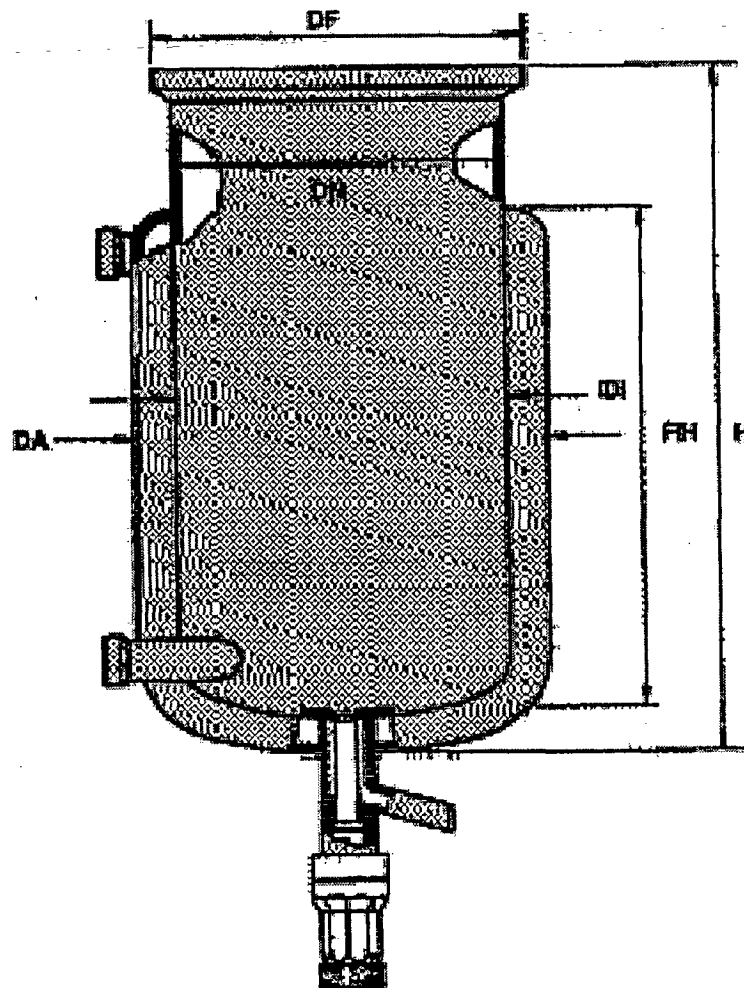


Figure 3.2: stirred batch reactor with tempering jacket

3.2.2 Thermostat

The Thermostat is used for controlling the temperature of the reactor. It is connected to the reactor with two insulated tubes at the inlet and outlet of the tempering jacket [hg]. The thermostat Julabo Presto LH 46 as depicted in Figure 3.3 tempers the bath fluid by means of an internal temperature controller[hg]. The bath fluid is heated/cooled in a heat exchanger tank inside the thermostat and circulated through the tempering jacket via a circulating pump. The bath fluid in the heat exchanger is well mixed due to a bypass in the heat exchanger around the tempering jacket. The bath fluid is heated by an electrical heater with a maximum capacity of 1.8 KW. The cooling is realized with a compression cooling cycle. The maximum cooling duty depends on the temperature difference between the cooling liquid in the cooling coils and the bath fluid in the heat exchanger tank.

The heat exchanger tank, which is surrounded by a steel cage, and the cooling aggregate in turn are cooled with a combination of forced air flow by a fan and cooling water (from the tap). The heat exchanger tank of the thermostat is connected to a reservoir for maintaining the required level of bath fluid in the heat exchanger tank as well as the tempering jacket of the reactor. The entire system is located in a laboratory of the institute and therefore exposed to the ambient air at room temperature.

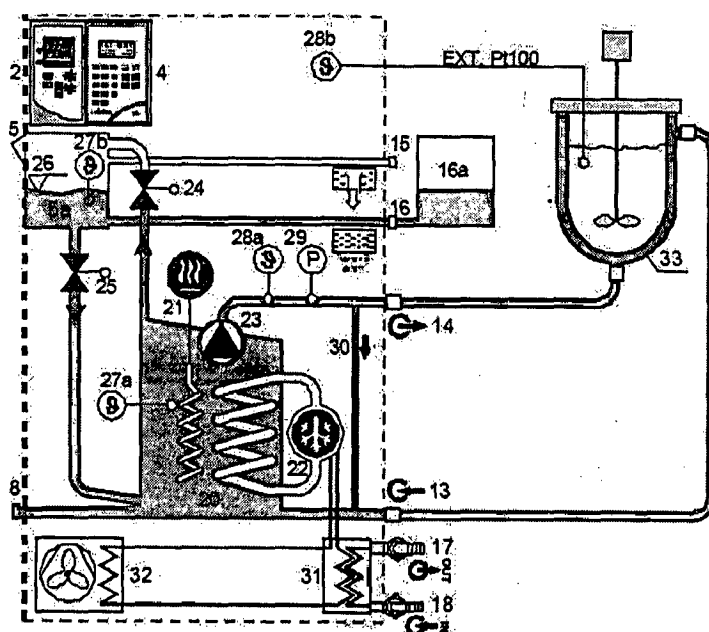


Figure 3.3: *Thermostat and reactor*

Code : Name	Code : Name
2 : Local control panel	21 : Heater
4 : Removable operating device RD	22 : Cooler
5 : Filling funnel	23 : Circulating pump
5a: Internal reservoir	26 : Level sensor
8 :Exit	27a : Temperature safety sensor
13, 14 : Connection with reactor	27b : Label safety sensor
15 : Over flow	28a : Internal control sensor
16 : Connection with 16a	28b : External control sensor
16a : External reservoir	29 : Pump pressure
20 : Heat exchanger	30 : Internal bypass
23 : Circulating pump	31 : Water cooler
25 : Filling valve	32 : Air cooler
17 : Outflow for cooling water	33 : Reactor with tempering jacket
18 : Inflow for cooling water	

3.2.3 Cascade control system

The reactor temperature is controlled by a cascade control system. An internal PID controller is used to control the thermostat temperature and an external PID controller is used to control the reactor temperature. The thermostat temperature setpoint is obtained by off line optimization of the reactor temperature trajectory.

The cascade control system is shown in figure 3.4. The adjusted setpoint temperature $T_{he-set-adj}$ is tracked by the thermostat temperature T_{he} with the help of the internal *PID* controller. The setpoint temperature profile of the thermostat, T_{he-set} , obtain by the off line optimization of the linear model is adjusted online with the help of the external *PID* controller.

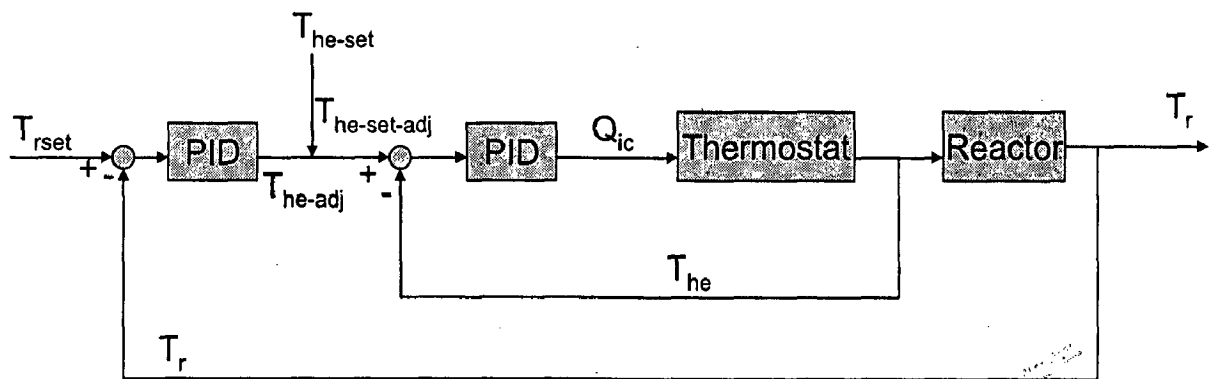


Figure 3.4: *Cascade control system*

Chapter 4

Tools

4.1 gPROMS

gPROMS is a general process modeling system widely used for simulation, optimization and parameter estimation of various processes. gPROMS is a leading software in the dynamic modeling and simulation field.

1. gPROMS allows the user to write equations almost as they would appear on paper.
2. All solvers have been designed specifically for large scale systems and there are no limits regarding problem size other than those imposed by the available machine memory. Our system also consist a large number of equations so gPROMS is an appropriate modeling tool for it.
3. The physical and chemical behavior of most processes are inherently discontinuous. gPROMS is able to handle processes with discontinuities.
4. In gPROMS it is very easy to construct models of complex flow sheets and procedures by decomposing them in to sub-models. So gPROMS has a modeling hierarchy and there is no limit on the number of levels in this modeling hierarchy.
5. gPROMS was the first modeling system to have formal, mathematical algorithm for automatically optimizing large-scale dynamic processes.
6. It has facilities for estimating model parameters through optimization from both steady-state and dynamic experimental data.

4.1.1 Modeling

A model contains a mathematical description of the physical behavior of a given system. All the equations of the model are specified in the model section of gPROMS. gPROMS has a facility of decomposing a big model into smaller models. All the models have its own worksheet which have many subsections such as parameter, distribution domain, variable, stream, equation etc. The variables and the parameters used in the model are declared under the subsection parameter and variable respectively. All the variables that are declared in the model section can be categories in different types for example all temperatures can be placed in to one group and all energies can be placed in another group and so on. The name of each group of variables must be specified in the variable types section. The name of the variable types, it's lower bound, default value, upper bound and unit are specified in the separate table. There should be one connecting model where all the models are connected to each other.

The values of all parameters are specified in the process section. The variables used in the model can be placed in to two groups, the time dependent variables and the time independent variables. The time dependent variables are calculated by gPROMS and these variables must be equal to the number of the equations used in the mathematical model. The remaining variables are time independent and the values of these variables are specified in the process section. The initial conditions required for solving the differential equations are also specified in the process section. The number of the initial conditions must be equal to the number of the differential equations.

4.1.2 Parameter estimation

Introduction

During dynamic modeling and simulation there are many parameters involved. Parameters are time invariant quantities and in many cases some of these parameters are unknown. The value of these parameters which give the best agreement between the mathematical model and the experimental unit is determined by the parameter estimation routine of gPROMS.

Parameter estimation in gPROMS is a reverse process. Experimental data is required as an input and values of the parameters are estimated by the parameter esti-

mation routine of gPROMS in order to minimize the error between the experimental result and the mathematical model. Required information is specified in parameter estimation and experiment entity.

Parameter estimation entity

In this section parameters to be estimated and their initial guess lower bound and upper bound are specified. The accuracy of estimated parameters depends on the initial guess, the lower bound and the upper bound specified. The parameter estimation routine of gPROMS searches the values of parameters within the specified range. If the actual values of the parameters lie below the specified lower bound of the parameters then the parameter estimation routine of gPROMS will give the lower bound as the estimated parameter similarly if actual values of the parameters lie above the specified upper bound then the specified upper bound will be obtained as the value of the estimated parameter, which may be inaccurate values. Parameters to be estimated must be declared in the assign section of the gPROMS model and their guess values must be specified in the process section.

The full gPROMS path of the variables measured by the experiment are also specified in this section. The accuracy of the estimated parameters can be increased by using more than one variables measured by the experiment for parameter estimation but estimation time may also increase accordingly. For example in the system under consideration the parameters can be estimated by using the experimental data of either reactor temperature or thermostat temperature (or any other measured variables) but in order to get more accurate values of the estimated parameters, the experimental data of both that is the reactor temperature and the thermostat temperature should be used simultaneously. The mathematical model predicts the values obtained by the experiment. The variance model used for the prediction of experimental values is specified for each measured variable. The name of the variance model and its mathematical description are given in the following table:

Name	Mathematical description
Constant variance	$\sigma^2 = \omega^2$
Constant relative variance predicted values	$\sigma^2 = \omega^2 * Z^2 + \epsilon$
Constant relative variance measured values	$\sigma^2 = \omega^2 * \tilde{Z}^2 + \epsilon$
Heteroscedastic predicted values	$\sigma^2 = \ \omega^2 * Z^2 + \epsilon\ ^\gamma$
Heteroscedastic measured values	$\sigma^2 = \ \omega^2 * \tilde{Z}^2 + \epsilon\ ^\gamma$

Where

σ is the variance.

ω is the standard deviation.

γ is a parameter.

ϵ is a very small but non zero number calculated by gPROMS.

Selection of variance model

The selection of a variance model for a particular measured variable depends on its characteristics. A short description of each variance model can be given as follows:

- In a constant variance model, the measurement error has a constant standard deviation ω .
- In a constant relative variance model, the measurement error depends on the magnitude of the predicted or measured values.
- In case of a heteroscedastic variance model, the measurement error also depends on the measured or predicted values, but is proportional to for example $\tilde{z}^{0.5y}$ or $z^{0.5y}$, respectively.

There are many possibilities for selecting a variance model. Some of them are listed below.

- A measured variable may be characterized by different variance models in two (or more) different experiments.
- A measured variable may be characterized by the same variance model in two or more different experiments but the values of the parameters (ω, γ) may be different in the two cases.

- A measured variable may have the same statistical variance model with the same parameters over all experiments.

Selection of ω and γ

An initial guess, a lower bound and an upper bound of ω and γ is required for parameter estimation. The accuracy of the estimated parameters very much depends on the initial guess, lower bound and the upper bound specified. The hierarchical approach is used to determine the appropriate value of the initial guess lower bound and the upper bound of the ω and γ For a particular mathematical model. The concept behind the hierarchical approach used is that for an accurate value of the initial guess, lower bound and the upper bound of the ω and γ , there should be the best agreement between gPROMS model output and parameter estimation output. The step wise description of the hierarchical approach used can be described as follows:

1. Assign any arbitrary value of the parameters to be estimated in the process section of gPROMS model and run the gPROMS model.
2. The experimental data of some variables are required for parameters estimation. These variables are called measured variables. The data for the measured variables are collected from the execution output of the gPROMS model instead of the experiment as described in step 1.
3. Fix any initial guess, lower bound and the upper bound of ω and γ .
4. The data for measured variables collected in step 2 are used for parameter estimation.
5. Specify the same initial guess of the parameters to be estimated as used in the mathematical model.
6. Estimate the parameters by parameter estimation routines of gPROMS.
7. Compared the estimated values of the parameters with the specified values. If both values are almost the same then the specified initial guess, the lower bound and the upper bound of ω and γ are correct values for the selected mathematical model otherwise specify the other values for ω and γ and estimate the parameters

again. Repeat the steps until getting the desired values of the initial guess, lower bound and the upper bound of ω and γ .

For the mathematical model under consideration the most suitable initial guess, lower bound and upper bound of ω and γ obtained by hierarchical method are given in the following table:

	Initial guess	Lower bound	Upper bound
ω	1	0.01	10
γ	0.5	0.001	1

The experiment entities

Full gPROMS path of measured variables followed by measured data from the experiment is specified in this section. The total number of the intervals followed by the duration of each interval of measured data is also specified. If there is any piecewise constant in the model then the value of this piecewise constant in each intervals should be also specified.

4.1.3 Controller Tuning

The *PID* controller consist of three parameters, K_c , T_I and T_d . To find out the appropriate values of these parameters is called parameter setting. A systematic procedure is required for parameter setting. There are three methods generally used for tuning of *PID* controller.

- Heuristic method
- Continuous cycling method(Ziegler Nichols method)
- Integral method

Hierarchical method

An approximated value of the controller parameters can be determined by this method. The procedure to achieve an optimal controller setting is described in following steps:

1. Eliminate the derivative and integral action by setting T_D to zero and T_I to as large value as possible.
2. Increase the controller gain K_c starting from very low value until continuous cycling occurs that is sustained oscillation with constant amplitude and set K_c to the half of this value.
3. Decrease T_I in small increments until continuous cycling occurs again and set T_I three times of this value.
4. Increase T_D until continuous cycling occurs and set T_D equal to one third of this value.

This method is quite time consuming and it gives just approximated value of controller parameters.

Ziegler Nichols method

In the classical paper by Ziegler and Nichols (1942) a tuning rule is given [JN42]. In order to determine the controller parameters by this method first find out the ultimate controller gain K_{cu} . It is obtained in second step of Heuristic method as described in previous section. At this value of controller gain determine the period of oscillation which is the ultimate period P_u . The Ziegler Nichols settings are calculated from these values to provide a 1/4 decay ratio. $K_c = 0.6K_{cu}$, $T_I = \frac{1}{2}P_u$, $T_D = \frac{1}{8}P_u$

The Ziegler Nichols setting results in a very good disturbance response for integrating processes but gives poor performance for process with a dominant delay [Sko04].

Integral method

This method is based on analytical criteria. In order to determine the controller parameters an objective function is minimized. Based on the objective function there are several possible criteria that we can use, some are summarized below:

Name of criterion	Objective function
Integral of the absolute value of the error	$IAE = \int_0^t (Error) dt$
Integral of the squared error	$ISE = \int_0^t (Error)^2 dt$
Integral of the time weighted absolute error	$ITAE = \int_0^t (Error) t dt$

This method gives an accurate value of the controller parameters for which the error is minimal. Among these methods *ITAE* is preferred because it results in conservative settings. In *ITAE* criteria errors are multiplied by the corresponding time hence smaller errors also take in to account in minimization of objective function while in *IAE* and *ISE* criteria smaller errors have no considerable effect in optimization of objective function.

Controller tuning using gOPT

A dynamic optimization tool is required for controller tuning with *ITAE* criteria. We use gOPT for minimizing the objective function of *ITAE*.

4.1.4 Optimization

Dynamic optimization is a very effective tools of gPROMS. In optimization we can minimize or maximize our objective function with various equality and inequality constraints. Dynamic optimization in gPROMS seeks to determine the following optimum variables:

- The time horizon
- The values in each interval of the time variant parameters
- The values of the time invariant parameters
- The time variation of the control variables, over the entire time horizon

The specification which are required for the optimization are given in the table *D.2*. The result of optimization very much depends on the specification. Following points can help for better optimization results.

- Initial guess, lower bound and upper bound of time horizon and for each interval should be as accurate as possible for reducing execution time of optimization but if not sure about accuracy then take longer range.
- Piecewise constant and piecewise linear variables should be accurate but if not sure then do not specify initial values, gPROMS will automatically calculate these specifications.

- End point equality, end point inequality, interior point inequality should be specified according to the need of process. gPROMS will perform optimization only within the constraints limit.

4.2 Labview

The system under consideration is connected with the labview interface. Labview is used to supply the required input data to the system, collecting the output data from the system and controlling the operating condition of the system.

4.2.1 Control

The setpoint temperature profiles of the thermostat temperature and reactor temperature are specified in the VI interface. The internal PID controller tracks the setpoint temperature profile of the thermostat while external *PID* controller tracks the setpoint temperature trajectory of the reactor temperature. The appropriate values of the controller parameters and the batch run time are specified in the VI of the labview. The prespecified temperature and the actual temperature of the reactor, the prespecified, adjusted and the actual temperature of the thermostat are displayed in every specified interval. The graph of the reactor temperature trajectory as well as thermostat temperature trajectory during batch run are also displayed.

4.2.2 Data acquisition

Data of all the measured variables are stored in the specified file.

4.3 System identification

System Identification is a kind of inverse problem selection. When obtaining a model by using the theory of system identification, the input sequence and the system response to that particular sequence are used. It is now the task of the system identification to find a model structure and a set of corresponding model parameters which best describe the behavior of the system given with respect to the available data. The steps of system identification can be structured as follows:

- Experimental design
- Data collection
- Data preprocessing
- Model structure selection
- Model estimation
- D2C conversion (special to our needs)
- Model validation

4.3.1 Experimental design

Experiment design is about designing a proper experiment, which reveals as much information about the system to be modeled as possible.

4.3.2 Data collection

Once the experiments are designed the actual input and output sequences, the data, have to be collected. In the system under consideration the setpoint temperature of the thermostat is the input sequence and the reactor temperature is the output sequence. Input sequence is generated by modeling in gPROMS. A Labview interface is used to supply the input and to collect the output sequence from the experimental unit.

4.3.3 Data Preprocessing

The measured data often have offsets, outliers, periods of missing values, drift, low frequency disturbances, high frequency disturbances, and other anomalies. The anomalies may lead to an improperly identified system. In order to remove these sources of errors, data preprocessing is often required. after the data has been collected it should be transformed in frequency and time domain to determine if it needs to be preprocessed.

The Following common processes are performed in data preprocessing:

Outliers detection

When recording experimental data occasional large measurement errors may occur. Such errors can be caused by disturbances, conversion failures etc. The corresponding abnormal data points are called outliers. The outliers can be easily determined from a residual. As they appear as spikes in the sequence of prediction errors.

Detrending

Detrending of a signal involves the removal of a trend from the signal as like removing the mean values or linear trends, low frequency drifts and very low frequency disturbances etc.

Selecting data range

The whole recorded data may not be suitable for identification due to undesired features as missing or bad data, outburst of disturbances etc. In this cause only a fraction of the data should be used as working data, however remaining data can be used as validation data. Initially up to some span of time there is more fluctuation in the output of the system. The system could also become unstable at the end of process. Unstable response of the system is not reflecting the true behavior of the system. For identification only that fraction of the data should be taken which reflects stable behavior of the system.

Prefiltering

Is used for removing high frequency noise in the data of input and output signals. The same filter should be used for all signals. In some cases it is required that the identified model should be based on some specific frequency ranges. By prefiltering it is possible to make sure that the model concentrates on the important frequency ranges.

In some cases following processes also required for data preprocessing:

- Re-sampling, to increase estimation speed and accuracy.
- Scaling to balance variability in signal levels.

- Decimation, to remove redundancy in signals.

4.3.4 Model structure selection

When selecting a model structure, the container for the final model is chosen. That is, the number of parameters and how they appear in the model. The system identification toolbox provides three methods for model estimation.

Parametric estimation

In the system identification tool box of Matlab ARX, ARMAX, Output error (OE), Boxjenkins (BJ), state space and user defined models are available. Any model can be selected and the model order can be edited in order to get the best fit.

Process model estimation

The focuss is on lower order, continuous time models that are characterized by a time constant static gain, a possible dead time, and a possible process zero and poles. The structure of the estimated model is customized on the basis of knowledge of the system .

The Transfer function of the process is obtained directly by this method. It is useful for further implementing the controller in the model or implementing the model in Labview. This method of model estimation is also useful when possible disturbances of the system is not known. A model estimated by this method can be implemented in gPROMS. But this method has certain limitations as like model having zeros more than one and poles more than three can not be estimated by this method and flexibility in the selection of model is also limited.

Nonparametric estimation

It uses spectral and correlation analysis methods and estimate frequency functions directly. Spectral analysis is performed using data window techniques to estimates the transfer function and the noise spectrum. Correlation analysis is performed using automatic prewhitening of the input signal.

4.3.5 Model estimation

The estimation of the model deals with transforming the input and output sequences into the chosen container, by assigning the unknown parameters to appropriate value. It is a heuristic process of determining the dynamic model of the given system. The Model having the best agreement with the experimental unit is to be found out by this process.

4.3.6 D2C Conversion

Parametric estimation method estimates the model in discrete time domain. In order to implement the identified model in gPROMS it is converted in continuous time domain. The Discrete model is converted in to continuous domain with the help of matlab command window. The discrete model is transported in to the matlab workspace where by using the following command it is converted in to continuous domain:

```
mc = d2c(ans)
```

4.3.7 Model validation

The last part of the system identification problem, model validation, deals with finding out how well the above mentioned transformation went. That is, it aims at answering the difficult question of whether a good model was found or not. Validation data should be different to estimation data for comparison the dynamic behavior of the estimated model and the experimental setup. The identified model is analyzed and compared with the validation set as follows:

- The Dynamic behavior of both models can analyzed directly in the model output.
- The outputs of the estimated model and the validation data is compared in the residual analysis.
- Bode plot of estimated model is shown in frequency response from which damping levels and resonance frequency can be determined.
- The behavior of the model for step or impulse input can be analyzed by transient response. The disturbance spectra of the output signal of identified model can be

analyzed in the noise spectra.

The deviation of the identified linear model from the original system can be analyzed more accurately by following analytical criteria:

Fit

The fitness is given by the following equation:

$$Fit = \left[1 - \frac{|Y - \hat{Y}|}{|Y - MEAN(Y)|} \right] \cdot 100 \quad (4.1)$$

Where Y is the measured output and \hat{Y} is the simulated/predicted model output. A higher value of fit means a better model.

Loss function

It represents the determinant of the estimated covariance matrix of the noise source $e(t)$. Generally for better fit the loss function should be minimum. But when comparing the loss function values between different structures that use very different disturbance models, an output error model may have a better input–output fit, even though it displays a higher value of the loss function.

Final prediction error

The accuracy of fitness of linear model is also determined in terms of final prediction error (FPE) which is calculated by following equation.

$$FPE = V \cdot (1 + d/N)/(1 - d/N) \quad (4.2)$$

Where V is the loss function, d is the number of estimated parameters and N is the number of estimation data.

Chapter 5

Model

5.1 Batch reactor

5.1.1 Reactor

Assumptions

The mathematical model of the reactor is based on the following assumptions:

- The liquid in the reactor is assumed to be ideally mixed therefore the temperature and the concentration variation inside the reactor are considered to be uniform. In practice there may be temperature and concentration variation along radial and axial direction inside the reactor especially for a large reactor.
- There are no chemical reactions occurring in the reactor.
- The tank is cylindrical in shape, made of borosilicate glass.
- There is no inflow and outflow during process from the reactor hence total mass of the liquid is constant and hence mass balances are not included in the mathematical model.
- The air above the liquid surface is neglected for modeling therefore heat of evaporation is assumed to be equal to the heat of condensation of the liquid at the surface of the lid.
- The total heat of the condensation is lost to the environment which is same as the heat of the evaporation of the liquid in the reactor.

- The heat transfer between the liquid and the air phase is neglected.
- The rate of the energy dissipation through the agitator is assumed to be constant throughout the process although it depends on the temperature and concentration profiles of the reactor.

Energy balance

The liquid in the reactor is considered as the system for the energy balance.

$$\frac{dE}{dt} = -Q_{cri} - Q_{crc} + Q_{cra} + P \quad (5.1)$$

Where E is the energy holdup in the reactor, Q_{cri} is the rate of the heat exchange between the reactor liquid and the inner tank wall, Q_{crc} is the rate of the heat loss to the environment due to the condensation of the vapor at the lid of the reactor, Q_{cra} is the rate of the heat exchange between the surface of the reactor uncovered with jacketed shell and the environment and P is the rate of the heat dissipation through the agitator.

Energy holdup

The holdup of the energy in the reactor is calculated as:

$$E = mass_r \cdot c_p \cdot (T_r - 273.15K) \quad (5.2)$$

Where T_r is the temperature of the liquid inside the reactor and $mass_r$ is the mass and c_p is the heat capacity of the liquid phase which is the function of the reactor temperature.

$$c_p = \text{poly}(T_r) \quad (5.3)$$

Heat exchange between the reactor liquid and inner reactor wall

The rate of the heat exchange between the reactor liquid and the inner reactor wall is given as.

$$Q_{cri} = A_{cri} \cdot \alpha \cdot (T_r - T_{i0}) \quad (5.4)$$

α is the heat transfer coefficient which is related to the nusselt number and the heat conductivity by the following equation.

$$\alpha = \frac{Nu \cdot \lambda}{dn} \quad (5.5)$$

The Nusselt number is calculated from the following correlation [VW]

$$Nu = 1.31 \cdot Re^{\frac{2}{3}} \cdot Pr^{\frac{1}{3}} \cdot \left(\frac{\eta_r}{\eta_{i0}}\right)^{0.14} \cdot \left(\frac{d_{ag}}{dn}\right)^{0.39} \cdot \left(\frac{h_{ag}}{dn}\right)^{0.34} \quad (5.6)$$

with the Reynolds number being

$$Re = \frac{d_{ag}^2 \cdot n \cdot \rho}{\eta_{fl}} \quad (5.7)$$

Where d_{ag} is the diameter of the blade, h_{ag} is the height of the blade, n is the revolutions per second of the agitator, η_r is the dynamic viscosity of the reactor liquid (water) at reactor temperature and η_{i0} is the dynamic viscosity of the reactor liquid at the temperature of the inner side of the inner tank wall.

The area of the the heat transfer which is the wet area on the inner side of the reactor tank is estimated by the following equation:

$$A_{cri} = \pi \cdot dn \cdot h_f + \frac{1}{4} \pi \cdot dn^2 \quad (5.8)$$

The height of the liquid in the reactor is estimated as:

$$h_f = \frac{V_r}{\frac{1}{4} \pi \cdot dn^2} \quad (5.9)$$

The volume of the liquid in the reactor is estimated as:

$$V_r = \frac{mass_r}{\rho} + V_{ag} \quad (5.10)$$

The volume of the stirrer-system V_{ag} is also included in the volume for determining the heat transfer area

Heat of condensation

The rate of evaporation of the liquid from the surface is given as [Ren]:

$$\frac{dm}{dt} = A_{crc} \cdot est_g \cdot g_{coeff} \cdot \frac{\xi_s}{1 - \xi_s} \quad (5.11)$$

with A_{crc} being the surface area, g_{coeff} the mass transfer coefficient and ξ_s the mass concentration above the surface (the mass concentration at the glass lit is assumed to be zero). est_g is an adjusting (estimation) factor that adjusts the mass transfer

coefficient g_{coeff} for better fitting of the modeled temperature profiles. The value of est_g is determined by the parameter estimation. ξ_s can be derived using the ideal gas law.

$$\xi_s = \frac{1}{1 + \left(\frac{p_r}{p_{vap}} - 1 \right) \cdot \frac{R_r}{R_a}} \quad (5.12)$$

p_r is the pressure in the reactor, p_{vap} is the vapor pressure of the reactor liquid (water) at the reactor temperature and R_r and R_a are the gas constants of vaporized reactor liquid and air, respectively.

The mass transfer coefficient g_{coeff} can be obtained from the analogy of heat and mass transfer [Ren]:

$$g_{coeff} = \frac{Sh \cdot \rho_s \cdot D}{0.9 \cdot dn} \quad (5.13)$$

$0.9 \cdot dn$ is the characteristic length of the circular surface, ρ_s denotes the density at the surface, D the diffusion coefficient of vapor in air and the Sherwood number Sh is the mass transfer analog to the Nusselt number in heat transfer.

The density at the surface ρ_s can be computed from the density of the vapor ρ_{vap} , the density of air ρ_a (both at the temperature of the reactor) and the mass concentration ξ_s

$$\rho_s = \frac{\frac{1}{\xi_s}}{\frac{1}{\rho_{vap}} + \frac{1-\xi_s}{\rho_a \cdot \xi_s}} \quad (5.14)$$

The expression for the binary diffusion coefficient D in gaseous mixtures at low pressures can be found on page Da33 in the VDI Wärmeatlas [VW]:

$$D = 10^{-4} \cdot 10^{-3} \cdot T_r^{1.75} \cdot \sqrt{\frac{M_r + M_a}{M_r \cdot M_a}} \cdot \frac{1.013}{p_r \cdot \left(diffvol_r^{1/3} + diffvol_a^{1/3} \right)^2} \quad (5.15)$$

In this expression, M_r and M_a are the molecular weights for the liquid in the reactor and air respectively; P_r is the pressure (1bar) in the reactor and $diffvol_r$ and $diffvol_a$ denote the diffusion volumes of the liquid in reactor and air, respectively. The diffusion volumes can be found on page Da33 in the VDI Wärmeatlas [VW].

The Sherwood number Sh as the analogue to the Nusselt number can be derived from a correlation of the form

$$Sh = C \cdot Gr^m \cdot Sc^n \quad (5.16)$$

The Grashof number Gr is used in this Sherwood correlation since evaporation is analogue to natural convection (heat transfer). The Grashof number for mass transfer

can be calculated from

$$Gr = \frac{g \cdot (0.9 \cdot dn)^3 \cdot (\rho_a - \rho_s)}{\nu_a^2 \cdot \rho_a} \quad (5.17)$$

with ν_a being the kinematic viscosity of air at the reactor temperature.

The Schmidt number Sc amounts to

$$Sc = \frac{\nu_a}{D} \quad (5.18)$$

The appropriate Nusselt correlation that is analogue to the required Sherwood correlation was found to be the correlation for natural convection at horizontal circular plates with laminar flow and surface temperature higher than ambient temperature. The Nusselt number was substituted with the Sherwood number:

$$Sh = 0.54 \cdot (Gr \cdot Sc)^{\frac{1}{4}} \quad (5.19)$$

Finally, the heat flow due to evaporation across the surface of the reactor liquid can be obtained:

$$Q_{crc} = \frac{dm}{dt} \cdot h_{v,r} \quad (5.20)$$

with $h_{v,r}$ being the heat of evaporation of the liquid in the reactor at its respective temperature. $h_{v,r}$ is evaluated at the respective reactor temperature in a polynomial

The heat exchange between the reactor and the environment

$$Q_{cra} = est_{cra} \cdot (T_{amb} - T_r) \quad (5.21)$$

The estimation factor est_{cra} stands for the product of the area of heat transfer and the heat transfer coefficient.

5.1.2 Inner tank wall

Assumptions

- No heat flow in tangential direction. This assumption is reasonable if the tank is perfectly symmetrical and there is no radial temperature gradient in the liquid inside the reactor as well as in the liquid in the cooling jacket which is true for the

ideally mixed liquid in the reactor and for the small thickness of the temperature jacket.

- The heat flow along the wall (axial in the cylindrical ring and radial in the base) can be neglected in compared to the heat flow across the wall. This assumption is reasonable only when there is no temperature gradient in the axial as well as in the radial direction in the liquid inside the reactor and in the liquid inside the cooling jacket. The axial velocity of the liquid in the tempering jacket is kept high which insures the negligible axial temperature gradient inside the tempering jacket.

Energy balance

The above assumptions ensure that the heat flow only along the thickness of the inner wall. The heat balance in the cylindrical ring of the thickness y_i is given as:

$$\rho_{glass} \cdot est_{c_{p_{glass}}} \cdot c_{p_{glass}} \cdot \frac{dT_i(y)}{dt} + \frac{dq_{y(y)}}{dy_i} = 0 \quad (5.22)$$

$est_{c_{p_{glass}}}$ is an adjusting (estimation) factor that adjusts the heat capacity of the wall $c_{p_{glass}}$ for better fitting of the modeled temperature profiles.

The heat conduction in the axial direction $qy(y_i)$ is given by

$$qy(y_i) = -est_{\lambda} \cdot \lambda_{glass} \cdot \frac{T_i(y_i)}{dy_i} \quad (5.23)$$

est_{λ} is an adjusting (estimation) factor that adjusts the heat conductivity of the wall λ_{glass} for better fitting of the modeled temperature profiles. The value of est_{λ} is determined by parameter estimation. The following boundary condition is apply at the inner side of the inner wall.

$$qy(0) = \frac{Q_{cri}}{A_{cri}} \quad (5.24)$$

with A_{cri} being the area of the interface to the reactor liquid.

The following boundary condition is apply at the outer side of the inner wall.

$$qy(S_i) = \frac{Q_{cis} + Q_{cib}}{A_{cis/cib}} \quad (5.25)$$

with $A_{cis/cib}$ being the combined outer area of the inner tank wall and Q_{cis} and Q_{cib} are the rate of the heat transfer in to the liquid inside the tempering jacket from the shell part and the bottom part of the outer side of the inner wall respectively.

5.1.3 Tempering jacket

The bath fluid enters at the edge of the bottom part of the tempering jacket and spreads around the center of the bottom hence the liquid in the bottom part of the tempering jacket is assumed to be ideally mixed while the liquid in the shell part of the tempering jacket can not be considered ideally mixed in axial direction. Hence the bottom and the shell part of the tempering jacket is modeled separately.

Bottom

The mass holdup in the bottom of the tempering jacket is assumed to be constant. The rate of the change of the energy in the bottom part of the tempering jacket is governed by the following equation:

$$\frac{dE}{dt} = \dot{E}_{in} - \dot{E}_{out} - Q_{cbob} + Q_{cib} \quad (5.26)$$

\dot{E}_{in} and \dot{E}_{out} denote the energy flow in and out the bottom part of the jacket:

$$\dot{E}_{in} = \dot{m} \cdot c_{pin} \cdot (T_{in} - 273.15K) \quad (5.27)$$

$$\dot{E}_{out} = \dot{m} \cdot c_p \cdot (T_b - 273.15K) \quad (5.28)$$

Q_{cib} is the rate of the heat exchange between the bath fluid in the bottom and the inner tank wall:

$$Q_{cib} = A_{cib} \cdot est_{\alpha} \cdot \alpha \cdot (T_i(Si) - T_b) \quad (5.29)$$

$$\alpha = \frac{Nu \cdot \lambda}{d_{char}} \quad (5.30)$$

$$Nu = \frac{0.03 \cdot Re^{0.875} \cdot Pr \cdot \eta_b^{0.14}}{(Re^{0.125} + 1.74 \cdot (Pr - 1)) \cdot \eta_{iSi}^{0.14}} \quad (5.31)$$

Q_{cbob} is the rate of the heat exchange between the bath fluid in the bottom part of the tempering jacket and the outer tank wall:

$$Q_{cbob} = A_{cbob} \cdot q_{cbob} \quad (5.32)$$

$$q_{cbob} = est_{\alpha} \cdot \alpha \cdot (T_b - T_{ob}(0)) \quad (5.33)$$

The energy in the bottom phase is calculated from

$$E = \rho \cdot V_b \cdot c_p \cdot (T_b - 273.15\text{K}) \quad (5.34)$$

with V_b being the volume of the bottom part of the jacket.

Shell

Assumptions

- The temperature gradient of the bath fluid in the shell part of the tempering jacket is negligible in the tangential as well as radial direction.
- The temperature gradient is considered in the axial direction because the heat is exchanged between the bath fluid in the tempering jacket and the liquid in the reactor as well as with the outer tank wall. There is no axial mixing of the bath fluid in the shell part of the tempering jacket.
- The holdup of the bath fluid in the shell part of the tempering jacket is constant.
- The conductive heat flow in the axial direction is neglected in comparison to the convective heat flow due to the high velocity of the bath fluid.

Energy balance

The rate of the change of the energy in the shell part of the tempering jacket is governed by the following equation:

$$\begin{aligned} & \rho(z_s) \cdot c_p(z_s) \cdot \frac{dT_s(z_s)}{dt} + v(z_s) \cdot \rho(z_s) \cdot c_p(z_s) \cdot \frac{dT_s(z_s)}{dz_s} \\ &= \frac{d_i \cdot q_{cis}(z_s) - 2 \cdot \left(\frac{1}{2}d_i + \delta_{jacket}\right) \cdot q_{csos}(z_s)}{\left(\frac{1}{2}d_i + \delta_{jacket}\right)^2 - \left(\frac{1}{2}d_i\right)^2} \end{aligned} \quad (5.35)$$

$$q_{csos}(z_s) = est_\alpha \cdot \alpha(z_s) \cdot (T_s(z_s) - T_{os}(0)) \quad (5.36)$$

The rate of the heat exchange between the bath fluid in the shell and the outer tank wall is averaged as:

$$q_{csos_{av}} = \frac{\pi i \cdot (d_i + 2\delta_{jacket})}{A_{csos}} \cdot \int_0^{L_s} q_{csos}(z_s) \quad (5.37)$$

with A_{csos} being the area of the interface.

The axial velocity of the bath fluid in the shell part of the tempering jacket is computed as:

$$v(z_s) = \frac{\dot{m}_{in}}{\rho(z_s) \cdot A_s} \quad (5.38)$$

with A_s being the cross sectional area of the shell.

5.1.4 Outer tank wall

The heat exchange between the outer side of the outer tank wall and the ambient air is governed by natural convection, which differs for the horizontal and vertical interface. Therefore the rate of the heat exchange between the ambient air and the bottom part of the tempering jacket is differ to that of the ambient air and the shell part of the outer tank wall. Hence the bottom part and the shell part of the outer tank wall is modeled separately. The inner tank wall and the outer tank wall are symmetric and concentric and the jacket width is relatively small. Therefore the same heat transfer correlations and adjusting factors are taken for the outer tank wall as in the inner tank wall.

Assumptions

- The heat is transferred only in axial direction, the radial and the tangential heat transfer are neglected due to the ideally mixed bath fluid in the bottom part of the tempering jacket.
- The conductive heat between the bottom and the shell part of the tempering jacket is neglected due to the small thickness of the outer tank wall.

Energy balance

$$\rho_{glass} \cdot est_{cp} \cdot c_{p_{glass}} \cdot \frac{dT_{ob}(y_o)}{dt} + \frac{dqy(y_o)}{dy} = 0 \quad (5.39)$$

The heat conduction in axial direction $qy(y_o)$ is governed by

$$qy(y_o) = -est_{\lambda} \cdot \lambda_{glass} \cdot \frac{dT_{ob}(y_o)}{dy_o} \quad (5.40)$$

The boundary conditions are given as:

$$qy(0) = q_{cbob} \quad (5.41)$$

$$qy(S_o) = q_{coba} \quad (5.42)$$

The rate of the heat flux between the bottom part of the outer tank wall and the ambience is given as:

$$q_{coba} = \alpha \cdot (T_{amb} - T_{ob}(S_o)) \quad (5.43)$$

The heat transfer coefficient can be calculated from

$$\alpha = \frac{Nu \cdot \lambda}{0.9 \cdot da} \quad (5.44)$$

with $0.9 \cdot da$ being the characteristic length for the circular interface.

At the different conditions the nusselt number is computed as:

1. laminar flow

- wall temperature higher than ambient temperature

$$Nu = 0.58 \cdot (Gr \cdot Pr)^{\frac{1}{5}} \quad (5.45)$$

- wall temperature lower than ambient temperature

$$Nu = 0.54 \cdot (Gr \cdot Pr)^{\frac{1}{4}} \quad (5.46)$$

2. turbulent flow (only for wall temperature lower than ambient temperature)

$$Nu = 0.14 \cdot (Gr \cdot Pr)^{\frac{1}{3}} \quad (5.47)$$

The constraint for laminar flow is

$$Gr \cdot Pr < 8 \cdot 10^6 \quad (5.48)$$

The Prandtl number (as the data for kinematic viscosity of air, and heat conductivity of air) needs to be evaluated at the medium temperature T_m , which is the arithmetic average of the ambient temperature T_{amb} and the wall temperature $T_{ob}(S)$:

$$T_m = 0.5 \cdot (T_{amb} + T_{ob}(S_o)) \quad (5.49)$$

$$Gr = \frac{g \cdot (0.9da)^3 \cdot \frac{1}{T_{amb}} \cdot (T_{amb} - T_{ob}(S))}{\nu^2} \quad (5.50)$$

ν is the kinematic viscosity of air at the medium temperature, $0.9da$ is the characteristic length of the circular interface and $T_{amb} - T_{ob}(S_o)$ is the temperature difference at the transition wall - ambient air.

Outer tank wall shell

The rate of heat transfer in the tangential and the axial direction is assumed to be negligible in comparison to the radial direction. The energy balance is given as:

$$\rho_{glass} \cdot est_{cp} \cdot c_{p_{glass}} \cdot \frac{dT_{os}(y_o)}{dt} + \frac{dq_y(y_o)}{dy_o} = 0 \quad (5.51)$$

The heat conduction in axial direction $q_y(y_o)$ is formed by

$$q_y(y_o) = -est_{\lambda} \cdot \lambda_{glass} \cdot \frac{dT_{os}(y_o)}{dy_o} \quad (5.52)$$

The boundary conditions are given as:

$$q_y(0) = q_{csos_{av}} \quad (5.53)$$

$$q_y(S_o) = q_{cosa} \quad (5.54)$$

$$q_{cosa} = \alpha \cdot (T_{amb} - T_{os}(S_o)) \quad (5.55)$$

$$\alpha = \frac{Nu_{cylinder} \cdot \lambda}{L_s + S_o} \quad (5.56)$$

with $L_s + S_o$ being the characteristic length for the area of heat exchange.

The Nusselt correlation is valid for $10^{-1} < Gr \cdot Pr < 10^{12}$ and for both wall temperature higher and lower than ambient temperature

$$Nu = \left(0.825 + 0.387 \cdot (Gr \cdot Pr \cdot f(Pr))^{\frac{1}{4}} \right)^2 \quad (5.57)$$

The Grashof number is calculated from

$$Gr = \frac{g \cdot (L_s + S_o)^3 \cdot \frac{1}{T_{amb}} \cdot (T_{os}(S_o) - T_{amb})}{\nu^2} \quad (5.58)$$

Where ν is the kinematic viscosity of air at the medium temperature, h is the height of the outer side of the outer tank wall, $T_{amb} - T_{os}(S)$ the temperature difference at the transition wall - ambient air and $f(Pr)$ a correction factor:

$$f(Pr) = \frac{\left(Pr^{\frac{9}{16}} + 0.492^{\frac{9}{16}}\right)^{-\frac{16}{9}}}{\left(Pr^{\frac{9}{16}}\right)^{-\frac{16}{9}}} \quad (5.59)$$

The Prandtl number is calculated at the medium temperature, which is the arithmetic average of the ambient temperature T_{amb} and the wall temperature at the outer side $T_{os}(S_o)$:

$$T_m = 0.5 \cdot (T_{amb} + T_{os}(S_o)) \quad (5.60)$$

The Nusselt number that is calculated with the above mentioned Nusselt correlation applies for vertical discs. The correction for cylinders is carried out as follows:

$$Nu_{cylinder} = Nu + 0.97 \cdot \frac{L_s + S_o}{da} \quad (5.61)$$

5.2 Thermostat

The mass holdup is constant in the heat exchanger tank and perfect insulation of the pipe connecting the thermostat to the tempering jacket is assumed and hence heat exchange of the bath fluid with the ambience through the connecting pipe is neglected. The energy balance in the heat exchanger of the thermostat is formulated as:

$$\frac{dE}{dt} = \dot{E}_{in} - \dot{E}_{out} + Q_{ic} - Q_{chs} \quad (5.62)$$

The energy holdup is related to the thermostat temperature by the following equation:

$$E = \rho \cdot V_{he} \cdot c_p \cdot (T_{he} - 273.15K) \quad (5.63)$$

\dot{E}_{in} and \dot{E}_{out} are the energy flows in and out of the heat exchanger:

$$\dot{E}_{in} = \dot{m}_{in} \cdot c_{pin} \cdot (T_{tout} - 273.15K) \quad (5.64)$$

$$\dot{E}_{out} = \dot{m}_{out} \cdot c_p \cdot (T_{he} - 273.15K) \quad (5.65)$$

with T_{tout} being the temperature of the bath fluid leaving the tempering jacket that leads to the thermostat.

Q_{ic} is the rate of the heat exchange with heating/cooling system and Q_{chs} is the heat exchange with the steel cage of the heat exchanger tank which is computed as:

$$Q_{chs} = \alpha \cdot A_{chs} \cdot (T_{he} - T_{st}) \quad (5.66)$$

with T_{st} being the steel cage temperature. The heat balance in the steel cage is given as

$$\frac{dE_{st}}{dt} = Q_{chs} + Q_{csa} \quad (5.67)$$

where Q_{csa} is the rate of the heat exchange between the steel cage and the ambient air. The energy holdup in the steel cage is given as:

$$E_{st} = m_{st} \cdot c_{pst} \cdot (T_{st} - 273.15K) \quad (5.68)$$

The rate of the heat exchange with the environment is given as:

$$Q_{csa} = \alpha \cdot A_{csa} \cdot (T_{amb} - T_{st}) \quad (5.69)$$

with A_{csa} being the estimated area of heat exchange and $T_{amb} - T_{st}$ being the temperature difference between the air flow at ambient temperature and the steel cage.

$$\alpha = \frac{Nu_m \cdot \lambda}{l_{csa}} \quad (5.70)$$

$$Nu_m = \sqrt{Nu_{laminar}^2 + Nu_{turbulent}^2} \quad (5.71)$$

with the scope of the application ranging from

$$10^1 < Re < 10^7 \quad (5.72)$$

$$Nu_{laminar} = 0.664 \cdot \sqrt{Re} \cdot Pr^{\frac{1}{3}} \quad (5.73)$$

$$Nu_{turbulent} = \frac{0.037 \cdot Re^{0.8} \cdot Pr}{1 + 2.443 \cdot Re^{-0.1} \cdot (Pr^{\frac{2}{3}} - 1)} \quad (5.74)$$

The Reynolds number is computed from

$$Re = \frac{u \cdot l_{csa}}{\nu} \quad (5.75)$$

with ν being the kinematic viscosity of air at the ambient temperature, u being the velocity of the air and l_{csa} is the characteristic length of the area of heat exchange.

5.3 Controller

5.3.1 Internal controller

The structure of the internal controller is provided by the manufacture according to which the the controller is designed. The integrator of the internal controller is modeled by

$$\frac{dI_{error}}{dt} = error \quad (5.76)$$

and the proportional and integral part of the internal controller are summed up as

$$PIvalue = \frac{1}{xp} \cdot \left(error + \frac{1}{Tn} \cdot I_{error} \right) \quad (5.77)$$

with xp being the range of proportional gain and Tn being the integral time. The equation for the differentiator then reads

$$Dvalue + Tv \cdot \frac{dDvalue}{dt} = \frac{1}{xp} \cdot Tv \cdot din \quad (5.78)$$

with $Dvalue$ being the output of the differentiator, Tv being the differential time and din being the rate of energy change in the heat exchanger as illustrated below. Finally, the outputs of the PI controller and the differentiator are combined by

$$PIDvalue = Dvalue - PIvalue \quad (5.79)$$

The output of the internal controller $PIDvalue$ still has to be scaled and brought to the corresponding value of the heating/cooling duty, which is done in the model.

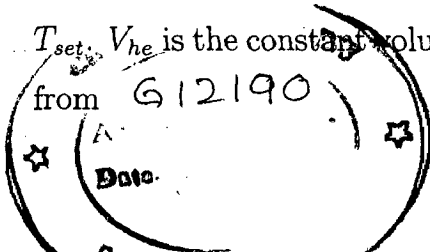
$$din = \dot{E}_{in} - \dot{E}_{out} + Q_{ic} - Q_{chs} \quad (5.80)$$

The setpoint can still be specified as setpoint temperature T_{set} , but the corresponding energy in the heat exchanger has to be calculated as the pseudo command variable *setpoint*:

$$setpoint = \rho \cdot V_{he} \cdot c_p \cdot (T_{set} - 273.15K) \quad (5.81)$$

with the density ρ and heat capacity c_p being evaluated at the setpoint temperature T_{set} . V_{he} is the constant volume of the heat exchanger tank. The error is then calculated

$$error = in - setpoint \quad (5.82)$$



which is the difference between the actual (*in*) and desired energy (*setpoint*) of the heat exchanger tank.

$$maxcool = poly(T_{he}) \quad (5.83)$$

$$maxheat = Q_{max} + cool_{min} \cdot maxcool \quad (5.84)$$

$cool_{min}$ is a figure smaller than one that models the persisting minimum flow of cooling fluid running through the cooling coils even when the thermostat is in heating mode.

Note that the maximum cooling duty $maxcool$ is a negative value. The effective maximum heating duty still depends on the bath fluid temperature to a slight extent since the minimum cooling $cool_{min} \cdot maxcool$ depends on the bath fluid temperature.

$$Q_{ic} = maxheat; \text{ (If } PIDvalue > 1)$$

$$Q_{ic} = maxcool; \text{ (If } PIDvalue < -1)$$

$$Q_{ic} = Q_{max} \cdot PIDvalue + cool_{min} \cdot maxcool; \\ \text{(If } -1 < PIDvalue < 1)$$

Alternate PID controller

An alternate internal *PID* controller is modeled (similar to the external *PID* controller) in which the temperature is specified as the setpoint instead of energy. The controller heat is calculated as:

$$Q_{ic} = \frac{1}{xp} \left\{ error + \frac{1}{Tn} \int_0^t (error) dt - \frac{Tv \cdot \frac{d(error)}{dt}}{1 + Tv \cdot \frac{d(error)}{dt}} \right\} \quad (5.85)$$

Where error is given as:

$$error = T_{set} - T_{he} \quad (5.86)$$

for detail refer appendix C.1.

5.3.2 External controller

It is difficult to implement a *PID* controller in gPROMS. For implementing a model in gPROMS, the number of initial conditions must be equal to the number of differential equations in the model. Integration of a function w.r.t time can not be directly expressed in the gPROMS model builder while it can be expressed in the form of differential equation. Due to the simultaneous operation of differentiation

and integration of the error in a single equation gPROMS requires two initial conditions. On specification of two initial conditions gPROMS gives the error of *DAE* (differential-algebraic equation) index greater than one. The *PID* controller is implemented in gPROMS by special model formulation. By optimization we can achieve the desired temperature trajectory in the reactor but exact tracking of desired temperature trajectory is not possible by using only optimization, to achieve that we need an external controller.

Controller input

$$Error = T_{rset} - T_r \quad (5.87)$$

Controller output

$$Q_{pid} = K_c \left(Error + \frac{I_{Error}}{T_I} + T_d \cdot D_{Error} \right) \quad (5.88)$$

Integral error

$$\frac{dI_{Error}}{dt} = Error \quad (5.89)$$

Differential error

$$D_{Error} = \frac{d(Error)}{dt} \quad (5.90)$$

Instead of using differential equation (5.90), D_{Error} can be expressed in terms of basic variable, reactor temperature by algebraic equation given below (for detail description see Appendix C.2)

$$D_{Error} = f(T_r, T_{rset}) \quad (5.91)$$

Online setpoint adjustment

The setpoint temperature of the thermostat is tracked by the internal controller but the prespecified thermostat setpoint temperature trajectory may not lead to the desired reactor temperature trajectory hence online modification of the thermostat setpoint temperature is needed for obtaining the desired reactor temperature trajectory. The external controller is used for online modification of the setpoint temperature of the thermostat.

In order to track the reactor setpoint temperature trajectory, the predicted energy holdup of the thermostat heat exchanger is calculated from the equation given below:

$$\frac{dE_{predicted}}{dt} = \dot{E}_{in} - \dot{E}_{out} + Q_{ic} - Q_{chs} + Q_{PID} \quad (5.92)$$

On the basis of the predicted energy holdup the thermostat temperature can be predicted with the help of the following equation:

$$E_{predicted} = \rho \cdot V_{he} \cdot c_p \cdot (T_{he_{predicted}} - 273.15K) \quad (5.93)$$

The deviation of the predicted thermostat temperature from the actual temperature is calculated as follows:

$$\nabla T_{he} = T_{he} - T_{predicted} \quad (5.94)$$

The new setpoint of the thermostat temperature is calculated as follows:

$$T_{set_{ad}} = T_{set} - \nabla T_{he} \quad (5.95)$$

5.4 Crystallization

Assumptions

The following assumptions are considered in the modeling of the crystallization process.

- The ideally mixed constant volume batch cooling crystallizer is used.
- The density of the solute and the solvent are constant.
- The attrition, breakage and agglomeration are also considered by introducing the production reduction term.

5.4.1 Population balance equation

The population density distribution of the crystals is governed by the following partial differential equation:

$$\frac{\partial n_T}{\partial t} + V \cdot \frac{\partial G_T}{\partial L} = V \cdot [B^0 + \alpha(L)] \quad (5.96)$$

Where n_T is the total number of the crystal per unit size of the crystal at any instant and is given as:

$$n_T = n \cdot V \quad (5.97)$$

Where n is the population density of the crystals and V is the magma volume.

The rate of the crystal production per unit magma volume is given as:

$$G_T(L) = G(L) \cdot n \quad (5.98)$$

5.4.2 Growth rate

The linear growth rate of the crystal is assumed to be the function of the super saturation (S) as well as agitator speed (N) and its dependency is correlated as:

$$G(L) = K_g \cdot S^g \cdot N^q \quad (5.99)$$

Where the growth kinetic coefficient K_g , growth order, g and q are the adjusting parameters that has to be estimated by the parameter estimation routine of gPROMS in order to obtain the best agreement between the mathematical model and the experimental results.

5.4.3 Nucleation rate

The rate of the generation of the new crystal particles per unit magma volume is correlated with the supersaturation, the crystal mass and the agitator speed with following equation:

$$B^0 = K_b \cdot S^b \cdot M_c^j \cdot N^p \quad (5.100)$$

Where nucleation kinetic coefficient (K_b) and the nucleation orders, b , j and p are adjusting parameters that have to be estimated by the parameter estimation routine of the gPROMS.

5.4.4 Production reduction rate

The combined effect of the crystal breakage, attrition, and the crystal agglomeration on the population density distribution is considered by using a single term known as production reduction rate which is given by the following equation:

$$\alpha(L) = K_a \cdot S^d \cdot M_c^k \cdot N^r \quad (5.101)$$

Where the adjusting parameters, the production reduction kinetic coefficient (K_a) and the production reduction orders, d , c and r have to be estimated by the parameter estimation routine of the gPROMS.

The mass of the crystals are estimated as:

$$M_c = \rho_c \cdot K_v \cdot \mu_3 \quad (5.102)$$

Where ρ_c is the crystal density and it is assumed to be constant throughout the crystallization process. The K_v is the crystal shape factor and μ_3 is the third moment defined as:

$$\mu_3 = \int_0^{L_T} n \cdot L^3 dL \quad (5.103)$$

Where L is the size of the crystal and L_T is the the size of the largest crystal.

5.4.5 Mass balance

The mass of the solute is transferred from the liquid phase to the solid crystalline phase. The rate of the change of the solute concentration in the liquid phase is governed by the following equation:

$$\frac{dc}{dt} = -3\rho_c \cdot K_v \cdot \frac{V}{M_w} \left[\int_0^{L_T} G_T(L) \cdot L^2 dL + B^0 \cdot L_0^3 \right] \quad (5.104)$$

It is assumed that some fine crystals of size L_0 were present initially as impurity in the magma.

5.4.6 The heat of the crystallization

The heat of the crystallization is the function of the reactor temperature so it is correlated as:

$$\Delta H_c = est_1 + est_2 \cdot T_r \quad (5.105)$$

Where est_1 and est_2 are the adjusting factors. These adjusting factors are determined by using the fact that the difference in the temperature trajectory of the reactor obtained by without crystallization and with crystallization is due to the heat of the crystallization. These adjusting factors are estimated by the parameter estimation routine of gPROMS for better fitting the modeled temperature trajectory with the experimental temperature trajectory.

5.4.7 Supersaturation

The driving force for the crystallization, the supersaturation is related to the solute concentration by the following equation:

$$S = \frac{(C - C_{eq})}{C_{eq}} \quad (5.106)$$

5.5 Linear model of the system

With the help of the system identification toolbox of Matlab, the reactor temperature is related to the thermostat temperature by a second order differential equation. Values of reactor temperature and thermostat setpoint temperature w.r.t.time are used for system identification. Thermostat setpoint temperature is used as an input signal while the reactor temperatures are used as an output signal.

5.5.1 Discrete time IDPOLY model

In discrete time domain the linear model is expressed by the following equation

$$A(q)y(t) = B(q)u(t) + e(t) \quad (5.107)$$

Where $u(t)$ denotes the input and $y(t)$ denotes the output signal which are the thermostat temperature and reactor temperature respectively. The order of the estimated model is represented as $[na \ nb \ nk]$. The corresponding terms in order represent the number of poles, zeros+1, and delays respectively. The coefficient $A(q)$ is a function of q and na and can be expressed by following equation.

$$A(q) = 1 + a_1q^{-1} + \dots + a_{na}q^{-na} \quad (5.108)$$

The coefficient $B(q)$ represents the delay terms and can be expressed by following equation.

$$B(q) = b_1q^{-nk} + b_2q^{-(nk+1)} \quad (5.109)$$

5.5.2 Continuous time IDPOLY model

In continuous time domain the above model can be represented as

$$A(s)y(t) = B(s)u(t) + C(s)e(t) \quad (5.110)$$

Where $A(s)$, $B(s)$, and $C(s)$ are the transfer functions characterizing the behavior of input signal, output signal and disturbances respectively and are given in appendix B.1.

If an experiment is repeated with the same input, the output will typically be some what different, due to the presence of some unpredictable noise sources. The noises are represented by the term $e(t)$ in the identified model. It contains all the influence on the measured y , known and unknown, that are not contained in the input u . Prediction of noise source $e(t)$ at time t is difficult even if past data up to the time $(t-1)$ have been measured very accurately. The transfer function $C(s)$ is just a convenient way of capturing their character.

The disturbance model $e(t)$ have an importance when the model is used for prediction and it can be modeled by analyzing the possible disturbances on the system. We want to use the model for simulation, i.e., the responses to various inputs are to be studied. Hence the disturbance model plays no immediate role and can be neglected.

Taking the Laplace transformation of the simplified linear model we get the following second order differential equation.

$$\frac{d^2y}{dt^2} + a\frac{dy}{dt} + by = c\frac{du}{dt} + du \quad (5.111)$$

Where u , and y represent the input and output signal respectively. In the system under consideration u is the thermostat setpoint temperature and y is the reactor temperature.

5.6 Optimization problem

In order to maintain similarity with the gPROMS model the formulation of the optimization problem given here is same as it is required for implementing in gPROMS:

5.6.1 Linear model

$$\frac{dT_r}{dt} = x \quad (5.112)$$

$$\frac{dx}{dt} + ax + bT_r = c\frac{T_{he}}{dt} + dT_{he} \quad (5.113)$$

$$\frac{T_{he}}{dt} = slope \quad (5.114)$$

The time can be defined in gPROMS as follows:

$$\frac{dt}{dt} = 1 \quad (5.115)$$

The desired trajectory of the reactor temperature is defined as:

$$\frac{T_{r_{set}}}{dt} = constant \quad (5.116)$$

Where constant is the slope of reactor temperature which varies as a piecewise constant with respect to time.

Objective function for the trajectory optimization

Following objective function is used for temperature trajectory optimization:

$$Obj = \int_0^t |T_r - T_{r_{set}}| dt \quad (5.117)$$

In order to determine the temperature of the bath fluid in the thermostat T_{he} , the objective function is to be minimized by the dynamic optimization tool of gPROMS subject to following conditions:

- Piecewise constant variable = slope
- Interior point inequality constraint:
 - $300 < T_r < 400$
 - $300 < T_{he} < 400$

- Time horizon for dynamic optimization is to be fixed as 20000 seconds and it is divided into 20 intervals.

5.6.2 *PID* controller in linear model

For controller parameter tuning gOPT is used. The optimization in complex model is not practicable due to the complexity of the model hence the same *PID* controller is also implemented in the linear model as in the complex model.

The controller heat is calculated as:

$$Q_{pid} = K_c \cdot (Error + \frac{I_{Error}}{T_I} + T_D \cdot D_{Error}) \quad (5.118)$$

Integral error is defined as:

$$I_{Error} = \int_0^t (Error) dt \quad (5.119)$$

error is calculated as:

$$Error = T_{r_{set}} - T_r \quad (5.120)$$

Differential error is related to the slope of the setpoint and actual reactor temperature as:

$$D_{Error} = constant - x \quad (5.121)$$

The external *PID* controller in the linear model is also used to adjust the setpoint of the internal controller for which controller energy should be related to the thermostat temperature. There is no energy balance in the linear model even then controller energy can be related to the thermostat temperature by the following equation:

$$Q_{pid} = -\rho \cdot V_{he} \cdot C_p \cdot (slope_{set} - slope) \quad (5.122)$$

Where ρ is the density of the bath fluid in the thermostat which is related to the thermostat temperature by a 3rd degree polynomial. The coefficients of the polynomial are given in the appendix A.2.

$$\rho = poly(T_{he}) \quad (5.123)$$

C_p the heat capacity of the bath fluid is also related to the thermostat temperature by 3rd degree polynomial and coefficients of polynomial is given in the appendix A.2.

$$C_p = poly(T_{he}) \quad (5.124)$$

V_{he} is the volume of the heat exchanger tank

The thermostat setpoint temperature is defined as:

$$\frac{T_{he_{set}}}{dt} = slope_{set} \quad (5.125)$$

In order to achieve the reactor setpoint temperature the prespecified thermostat setpoint temperature is adjusted as

$$\Delta T_{he} = T_{he_{set}} - T_{he} \quad (5.126)$$

The controller parameters are tune using *ITAE* criteria which is given as:

$$ITAE = \int_0^t t \cdot |error| dt \quad (5.127)$$

In order to determine the controller parameters the *ITAE* is minimized using the optimization routine of gPROMS.

Chapter 6

Results and discussion

6.1 Parameter estimation

The mathematical model involves many parameters. The accuracy of the Mathematical model depends on the fact that how accurately these parameters are adopted in the model. The parameters involved in the model can be divided into three groups, system dependent parameters, adjusting parameters and control parameters.

6.1.1 System dependent parameters

These parameters are directly related to the system under consideration. Most of these parameters are known or can be calculated with the help of the properties data supplied by the manufacture and the remaining parameters are estimated by the parameter estimation routine of gPROMS. The system under consideration comprises of two subsystems, The batch reactor and the thermostat so the system-dependent parameters can be subdivided into two groups, reactor dependent parameters and the reactor independent parameters. The system dependent parameters which depend either on the batch reactor or batch reactor and thermostat are placed in the group of reactor dependent parameters and other parameters are placed in the group reactor independent parameters. For the same thermostat the reactor independent parameters will remain the same. The reactor dependent parameters which have to be estimated are the power of the agitator and the volumetric flow rate through the pump in the thermostat.

Power dissipated through the agitator

The power dissipated through the agitator directly influences the temperature trajectory of the reactor. The effect of the power dissipated through the agitator is shown in figure 6.1. The graph shows that the greater the rate of energy generated by the agitator the higher the temperature of the reactor at any instant.

The deviation of the temperature trajectories obtained from the mathematical model from the experimental temperature trajectory are shown in figure 6.2. The power dissipated through the agitator depends on the power intake to the agitator and type and dimensions of the agitator. In the system under consideration the power dissipated through the agitator is a parameter which is estimated by the parameter estimation routine of gPROMS. The temperature trajectory obtained from the mathematical model at $0.002KW$ (estimated value) shows the best agreement with the experimental temperature trajectory.

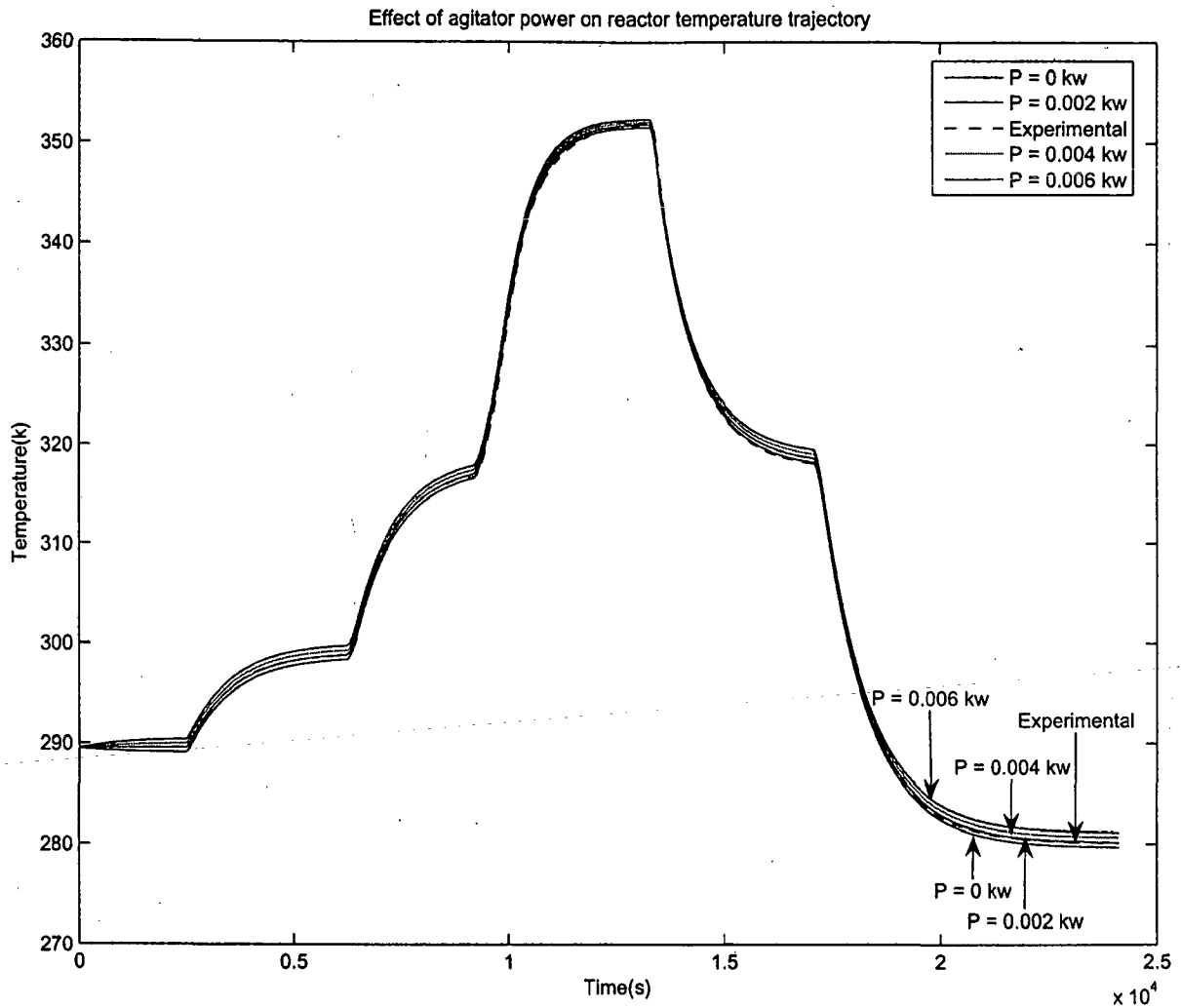


Figure 6.1: *This graph shows the effect of the agitator power on the reactor temperature trajectory.*

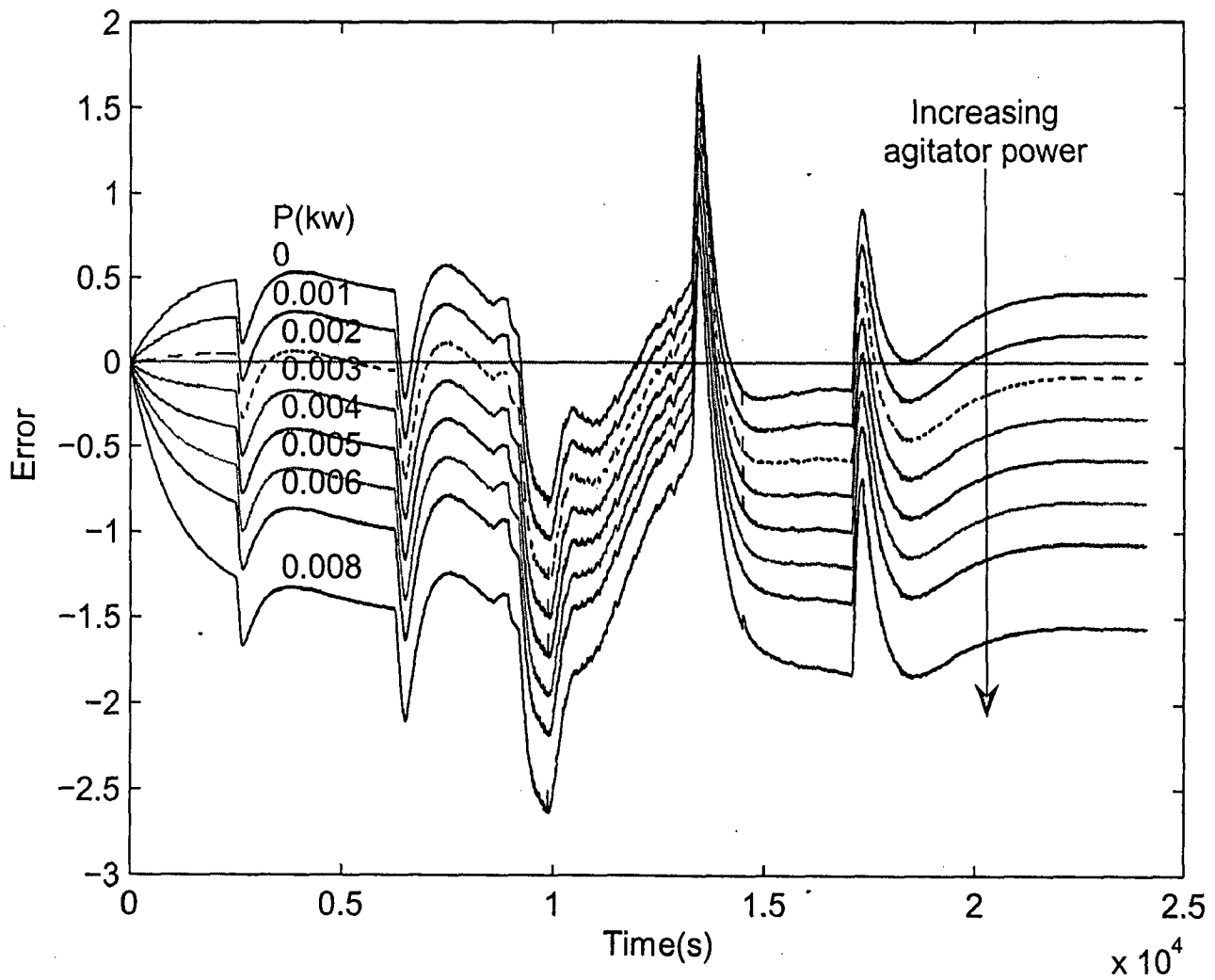


Figure 6.2: This graph shows the difference of the experimental temperature trajectory and the temperature trajectories obtained by the model at different agitator power intake.

Volumetric flow rate through the pump

The effect of the volumetric flow rate through the pump is shown in figure 6.3. The whole range of operating time can be divided in to two parts, heating time and cooling time. Which is shown in the graph with the help of a vertical line. The left portion of the graph shows the heating and the right portion shows the cooling. The graph shows that the higher the volumetric flow rate through the pump the higher will be the heating as well as the cooling effect.

The deviation of the temperature trajectories obtained from the model are shown in figure 6.4. The volumetric flow rate through the pump should be proportional to the volume of the tempering jacket. It is an unknown parameter for the system under consideration. It is estimated by the parameter estimation routine of gPROMS. The graph shows that the temperature trajectory obtained from the mathematical model at $0.24E - 3 \text{ m}^3/\text{s}$ (estimated value) of the volumetric flow rate through the pump gives best agreement with the experimental temperature trajectory. In the system under consideration, on increasing the volumetric flow rate through the pump, the value of the experimental temperature minus the temperature obtained by the mathematical model decreases in the heating zone while it increases in the the cooling zone at any instant.

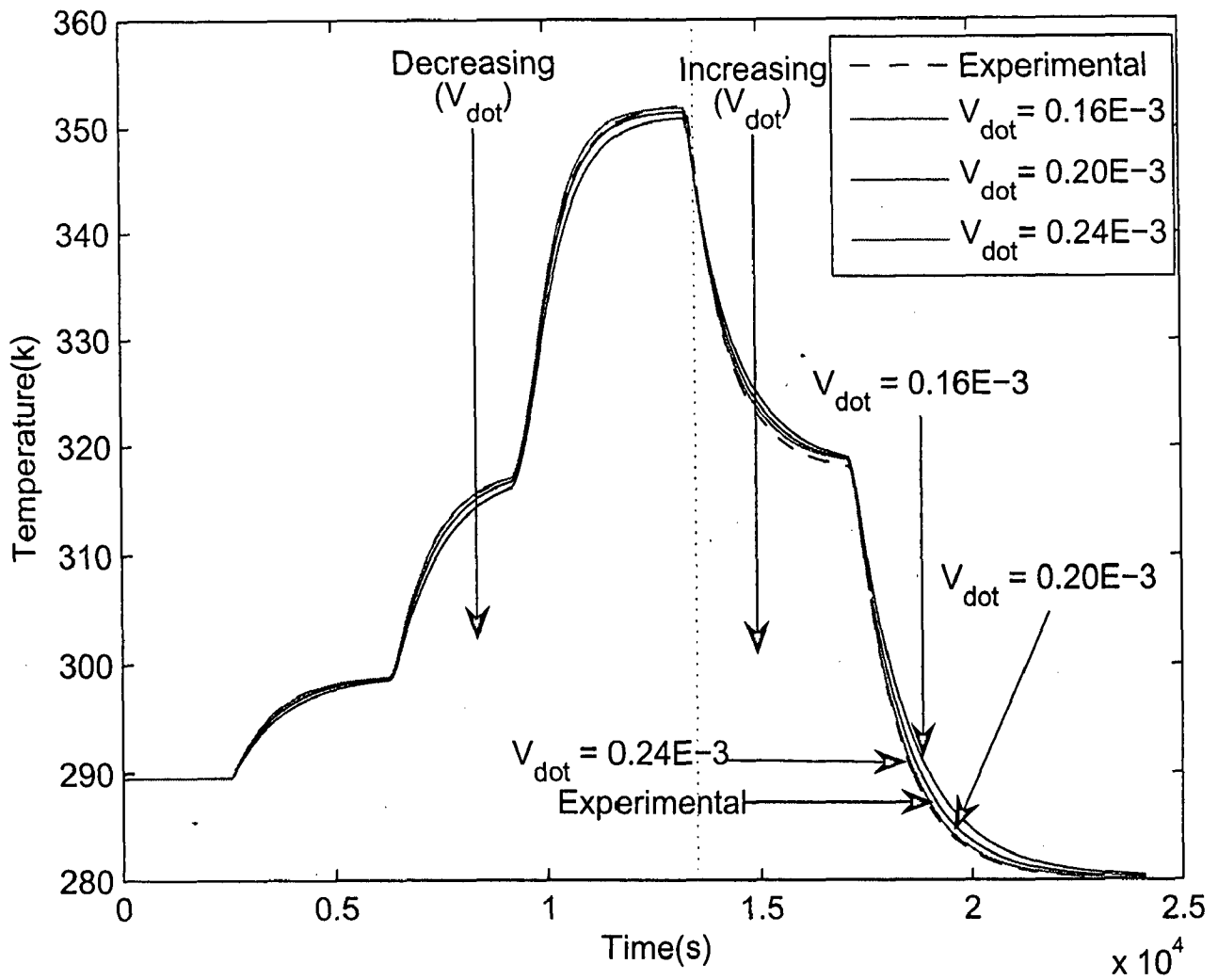


Figure 6.3: This graph shows the effect of the volumetric flow rate through the pump on the reactor temperature trajectory.

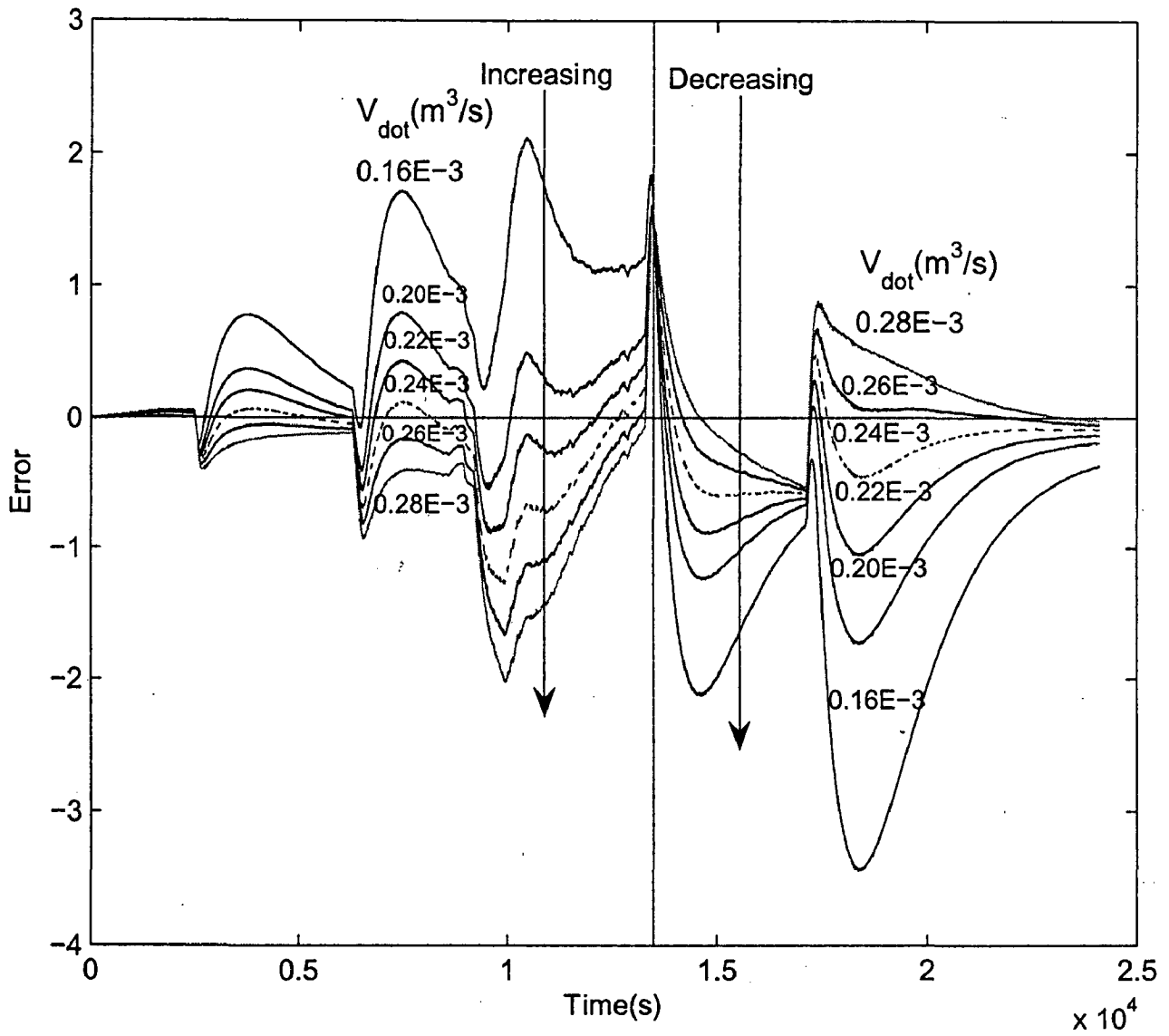


Figure 6.4: This graph shows the difference of the experimental temperature trajectory and the temperature trajectories obtained by the model at different volumetric flow rates through the pump.

6.1.2 Adjusting parameters

In order to obtain the best agreement between the mathematical model and the system under consideration some adjusting parameters are introduced in the model. For an ideal mathematical model the values of these parameters should be unity. The values of these parameters are estimated by the parameter estimation routine of gPROMS.

Mass transfer coefficient at the liquid surface

The liquid in the reactor is vaporized in to the air above the liquid surface and it condenses at the lit of the reactor. The heat of condensation is lose to the environment. The parameter est_g is used to adjust the mass transfer coefficient for mass transfer from the liquid surface by the evaporation. The more the value of the est_g the more will be the rate of evaporation and hence the rate of the condensation heat loss to the environment. This effect is also shown in figure 6.5. The graph shows that on increasing the value of the est_g the temperature of the reactor decreases. The rate of the heat loss through the lit is proportional to the temperature difference between the reactor and the environment hence the effect of the parameter est_g is greater at higher temperatures of the reactor.

The portion of the figure 6.5 enclosed within the rectangle is shown in figure 6.6 in enlarged form. The graph shows that the smallest deviation of the temperature trajectory obtained by the mathematical model from the experimental temperature trajectory is at a est_g value of 0.5 (estimated value). The value of est_g is proportional to the area of interface between the liquid surface and the air above the liquid surface. The effect of the est_g is independent of the heating and cooling range, for the same difference of reactor temperature and environmental temperature it's effect will be the same in both regions as shown in figure 6.7.

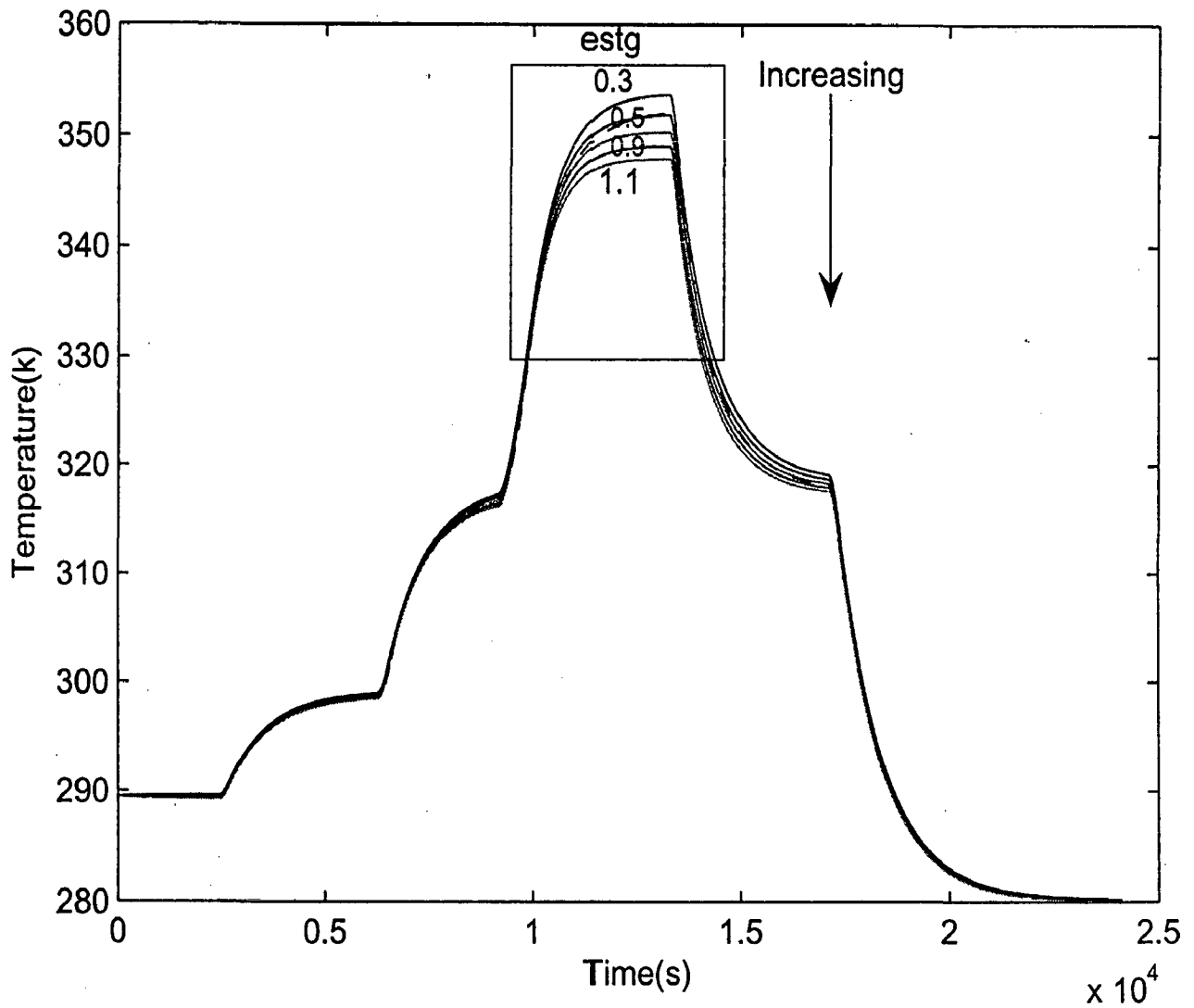


Figure 6.5: This graph show the effect of the factor of the mass transfer coefficient at the surface (est_g) on the reactor temperature trajectory.

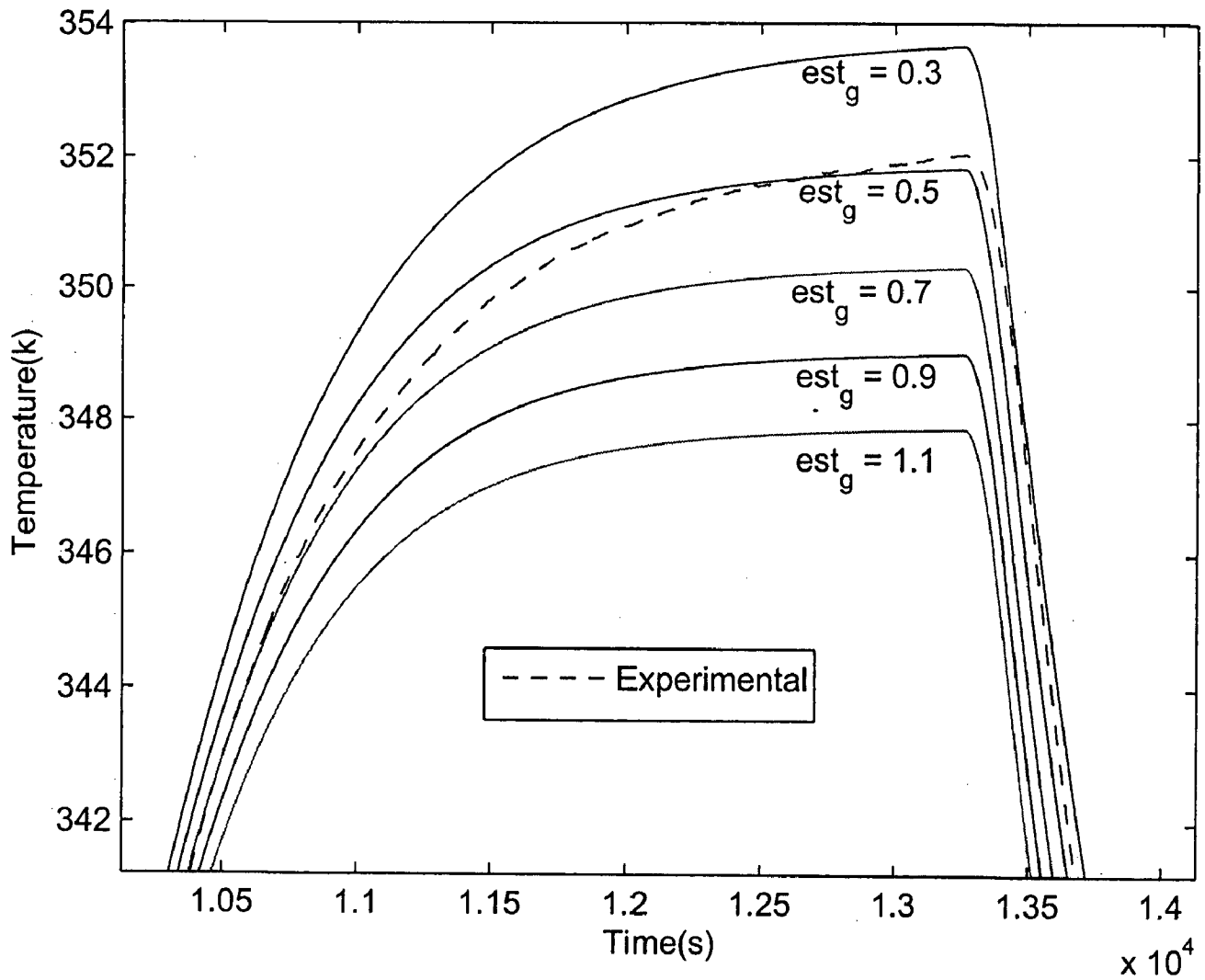


Figure 6.6: This graph shows the enlarged form of a portion of the previous graph enclosed within the rectangle.

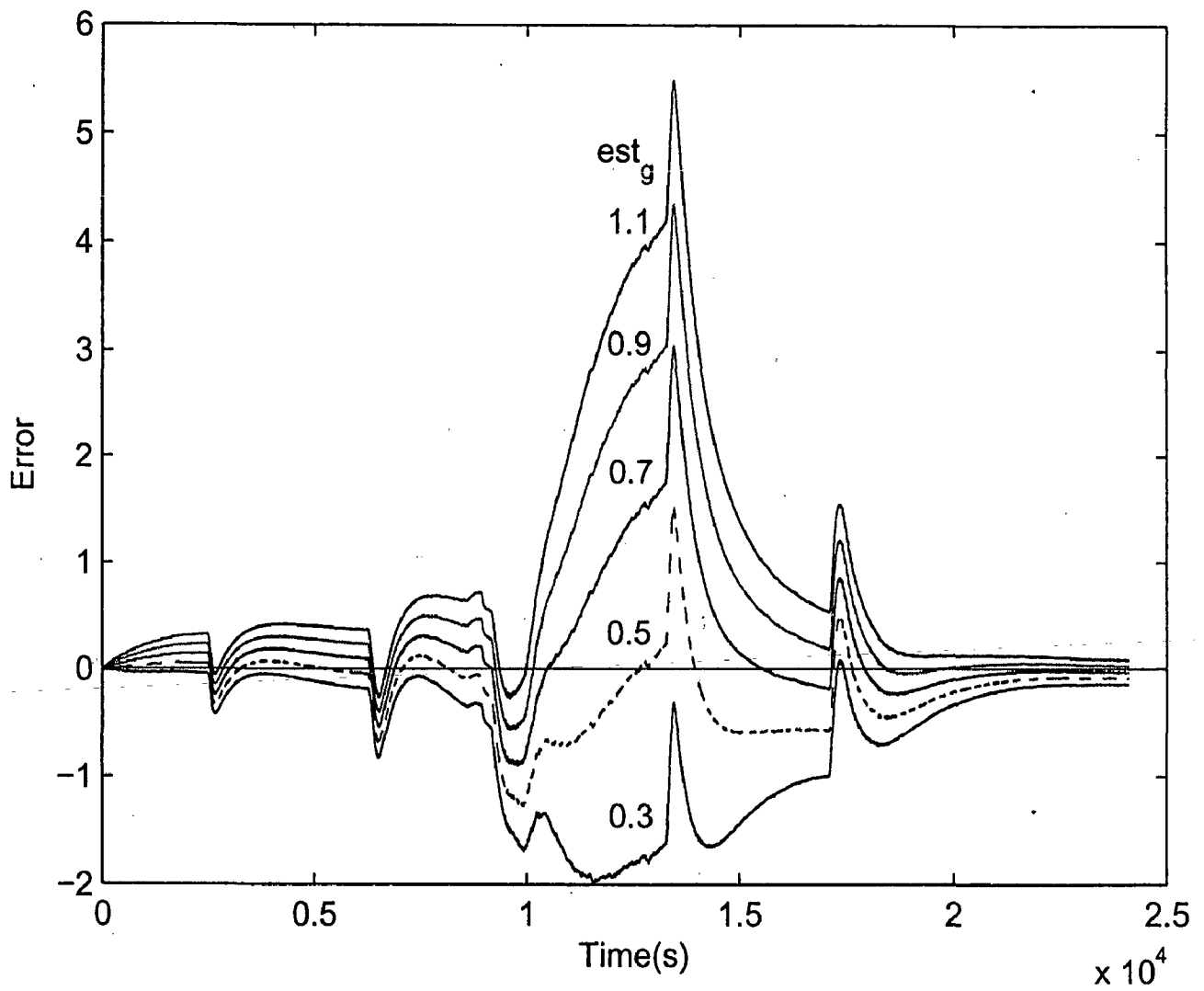


Figure 6.7: This graph shows the difference of the experimental temperature trajectory and the temperature trajectories obtained by the model at different values of the factor of the mass transfer coefficient at the surface (est_g).

Product of the heat transfer coefficient and the area of heat exchange between reactor liquid and ambient air

For the sake of simplicity, the rate of the heat lost to the environment is modeled by using one model. The effect of the factor est_{cra} on the temperature trajectory of the reactor is shown in figure 6.8. The total time span is divided in two parts by a vertical line. In the left portion of the graph the reactor temperature is above the ambient temperature hence heat is transferred from the system to the environment. In this time span the higher the value of est_{cra} the higher will be the heat loss to the environment hence less will be the reactor temperature at any instant. The right portion of the graph shows the heat gain from the environment to the system hence in this portion the higher the value of the est_{cra} the higher will be the reactor temperature. The effect of the factor est_{cra} on the reactor temperature trajectory will be higher if the difference of the reactor temperature and the ambient temperature will be more.

The deviation of the temperature trajectory obtained by the mathematical model from an experimental temperature trajectory is shown in figure 6.9. It is clear from the graph that the mathematical model having the value of the parameter est_{cra} as $1.2E - 4$ (estimated value) shows the best agreement with the experimental result.

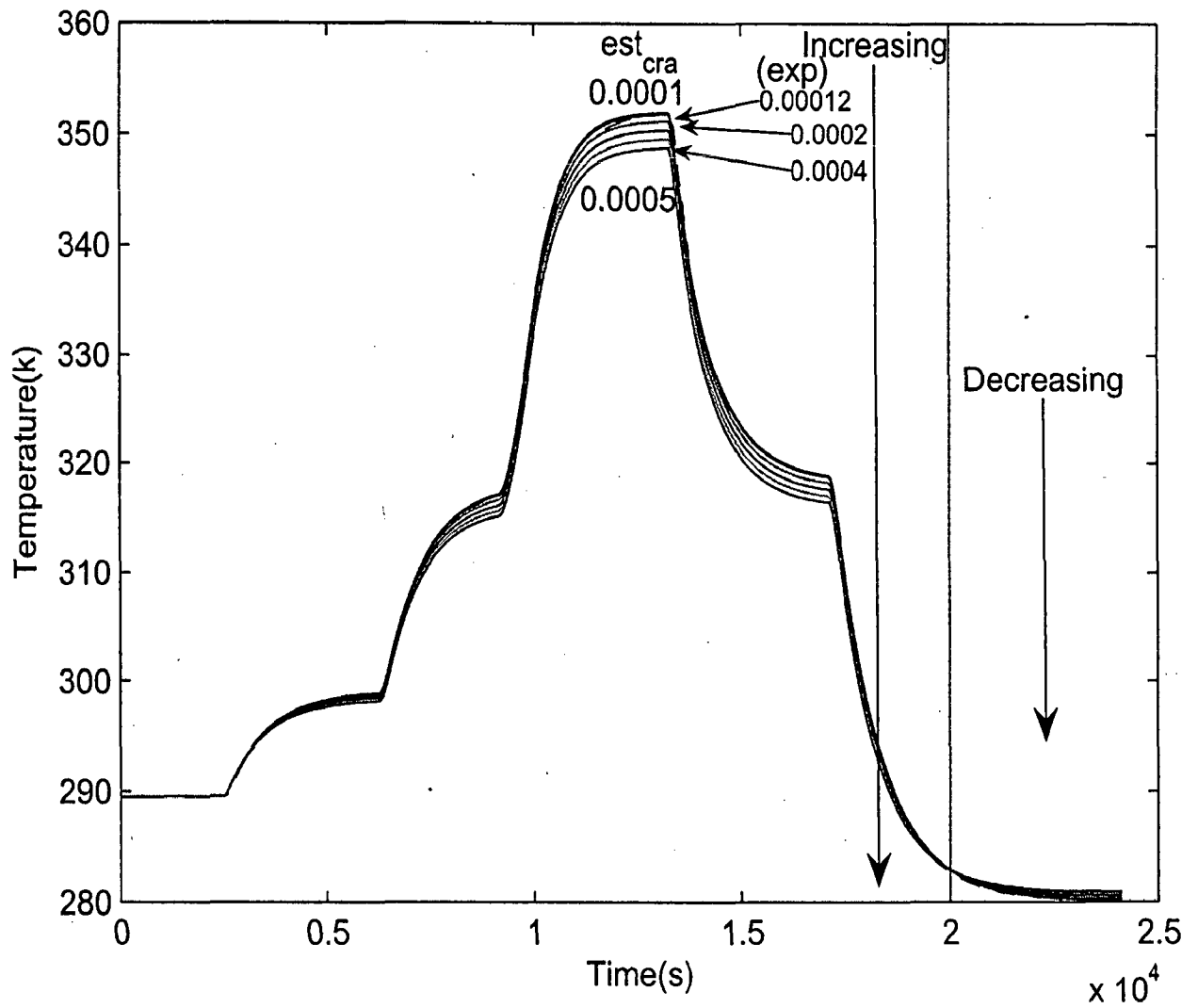


Figure 6.8: This graph shows the effect of the product of the heat transfer coefficient and the area of heat exchange between reactor liquid and ambient air (est_{cra}) on the reactor temperature trajectory.

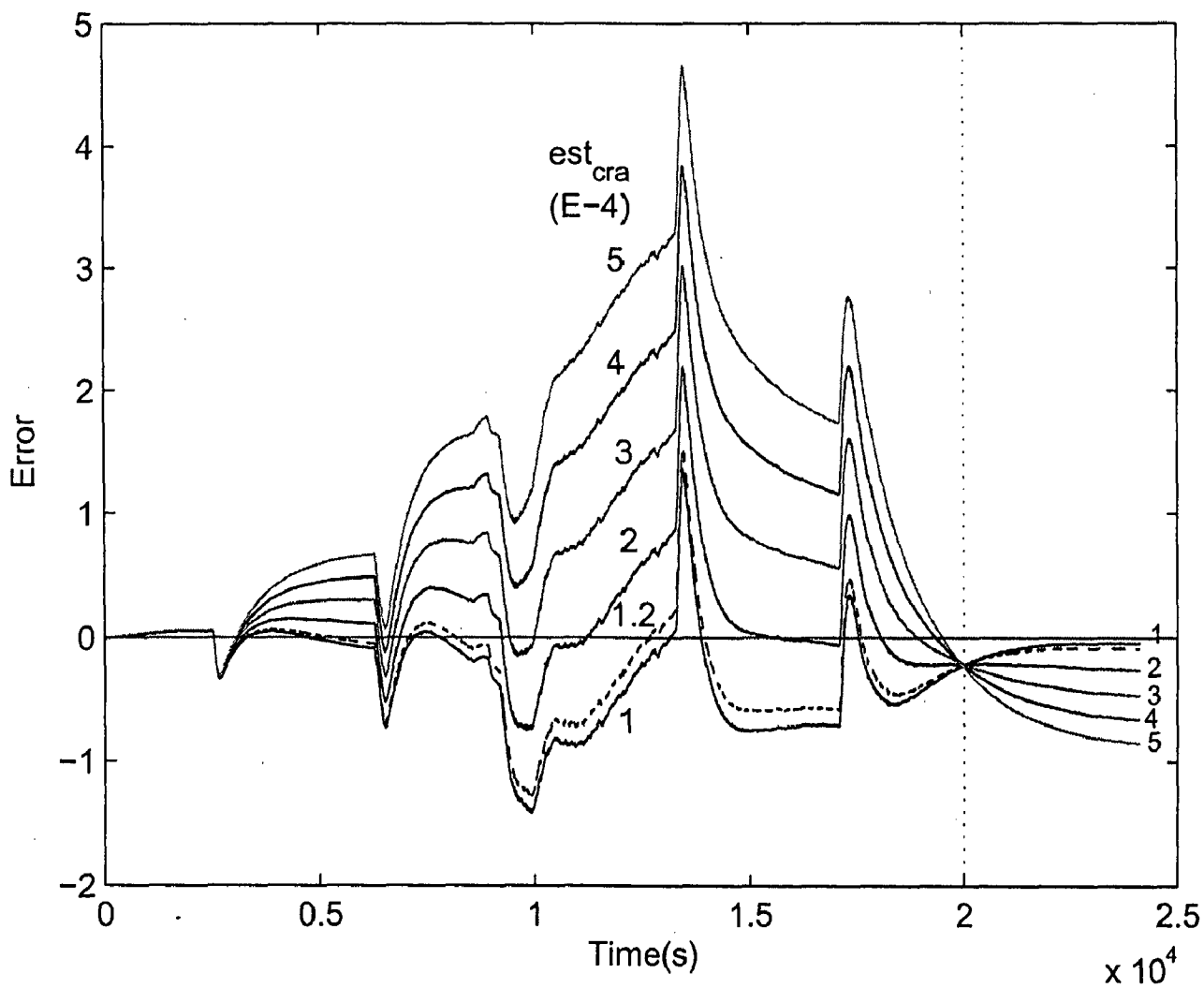


Figure 6.9: This graph shows the difference of the experimental temperature trajectory and the temperature trajectories obtained by the model at different values of the product of the heat transfer coefficient and the area of heat exchange between reactor liquid and ambient air (est_{cra}).

Factor of the heat transfer coefficient

The factor of the heat transfer coefficient (est_α) is used for adjusting the heat transfer coefficient between the bath fluid in the tempering jacket and the surrounding tank wall. Although different equations are used for the heat transfer for the shell part of the tempering jacket and the bottom part of the tempering jacket but the same est_α is assumed in both equations.

The effect of est_α on the temperature trajectory is shown in figure 6.10. The graph shows that the higher the value of est_α the higher will be the heating as well as cooling effect, means est_α will always increase the rate of heat transfer irrespective of the direction of the heat transfer.

The deviation of the temperature trajectories obtained by the mathematical model from the experimental temperature trajectory is shown in figure 6.11. The graph shows that the mathematical model at 2.0 (estimated) value of est_α shows the best agreement with the experimental result.

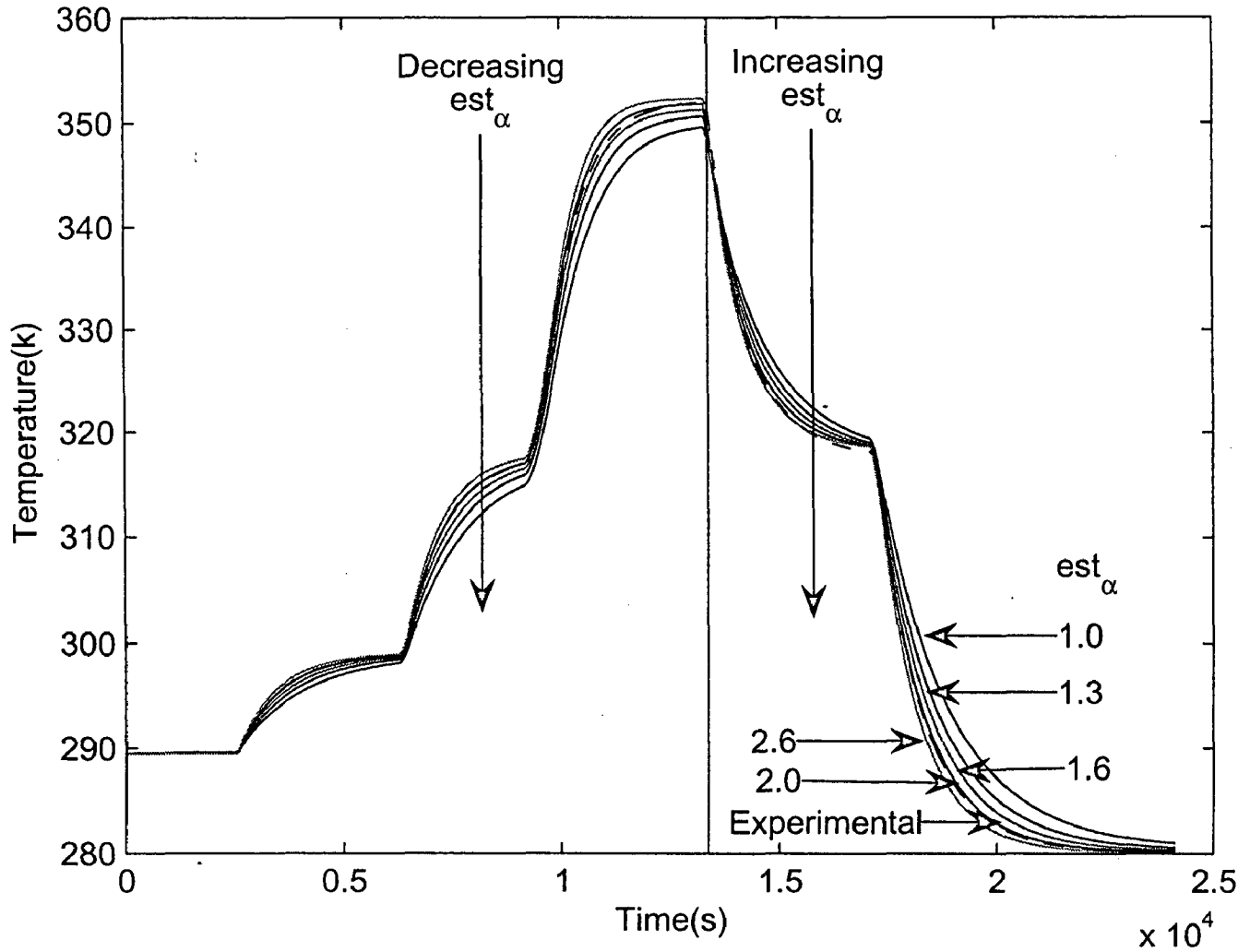


Figure 6.10: This graph shows the effect of the factor for the heat transfer coefficient between the bath fluid in the bottom and shell part of the tempering jacket and the surrounding tank walls (est_{α}) on the reactor temperature trajectory.

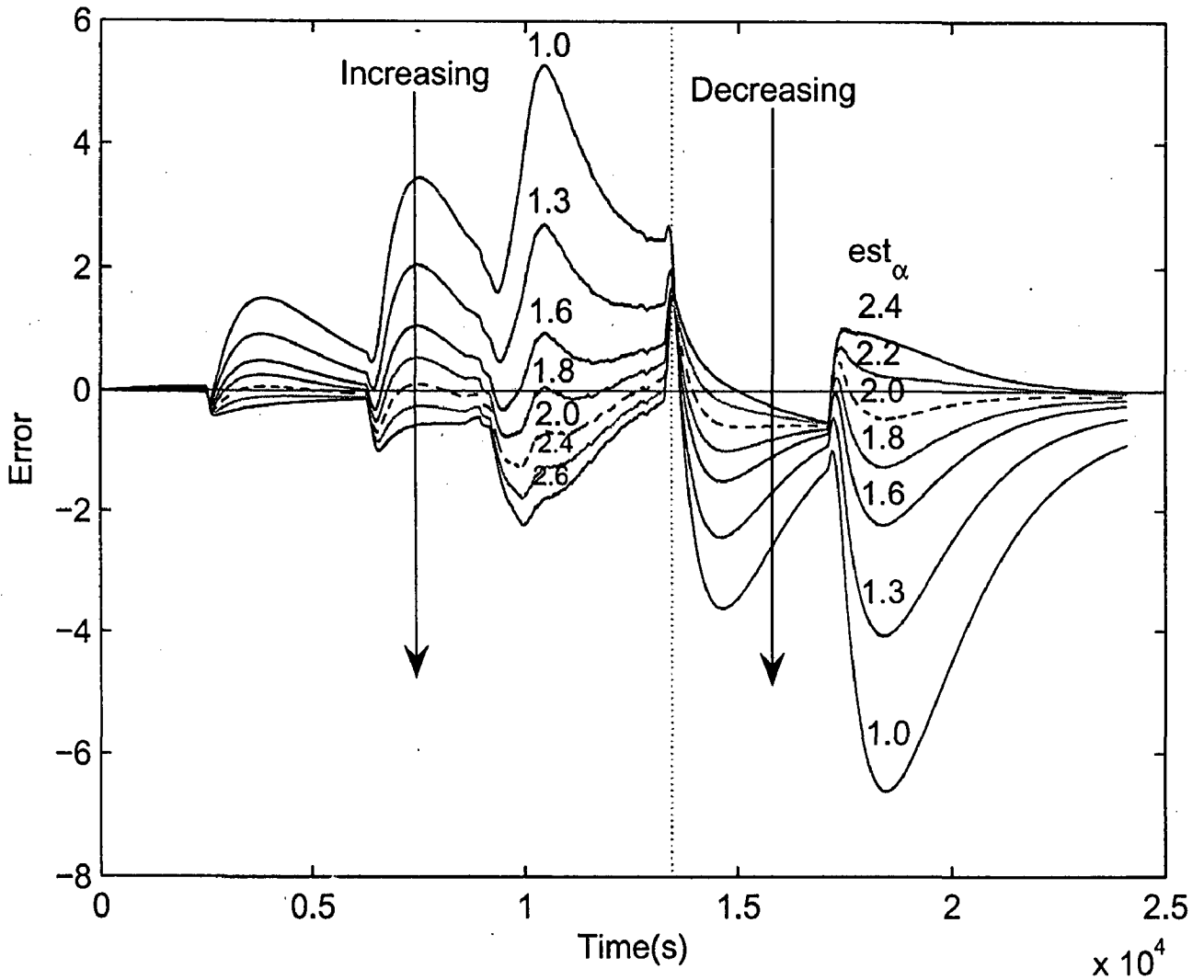


Figure 6.11: This graph shows the difference of the experimental temperature trajectory and the temperature trajectories obtained by the model at different values of the factor for the heat transfer coefficient between the bath fluid in the bottom and shell part of the tempering jacket and the surrounding tank walls (est_α)

Factor of heat conductivity

The effect of the factor of the heat conductivity of the inner and outer tank wall of the reactor (est_λ) on the temperature trajectory is shown in figure 6.12. The graph shows that higher the value of est_λ the higher will be heating as well as cooling effect. The effect of the est_λ is higher at higher temperatures in compare to lower temperatures.

The deviation of the mathematical model from the experimental result is shown in figure 6.13. On increasing the value of est_λ the reactor temperature increases in the heating zone while it decreases in cooling zone. The graph shows that the mathematical model shows the best agreement with the experimental result at the est_λ value of 0.7 (estimated value).

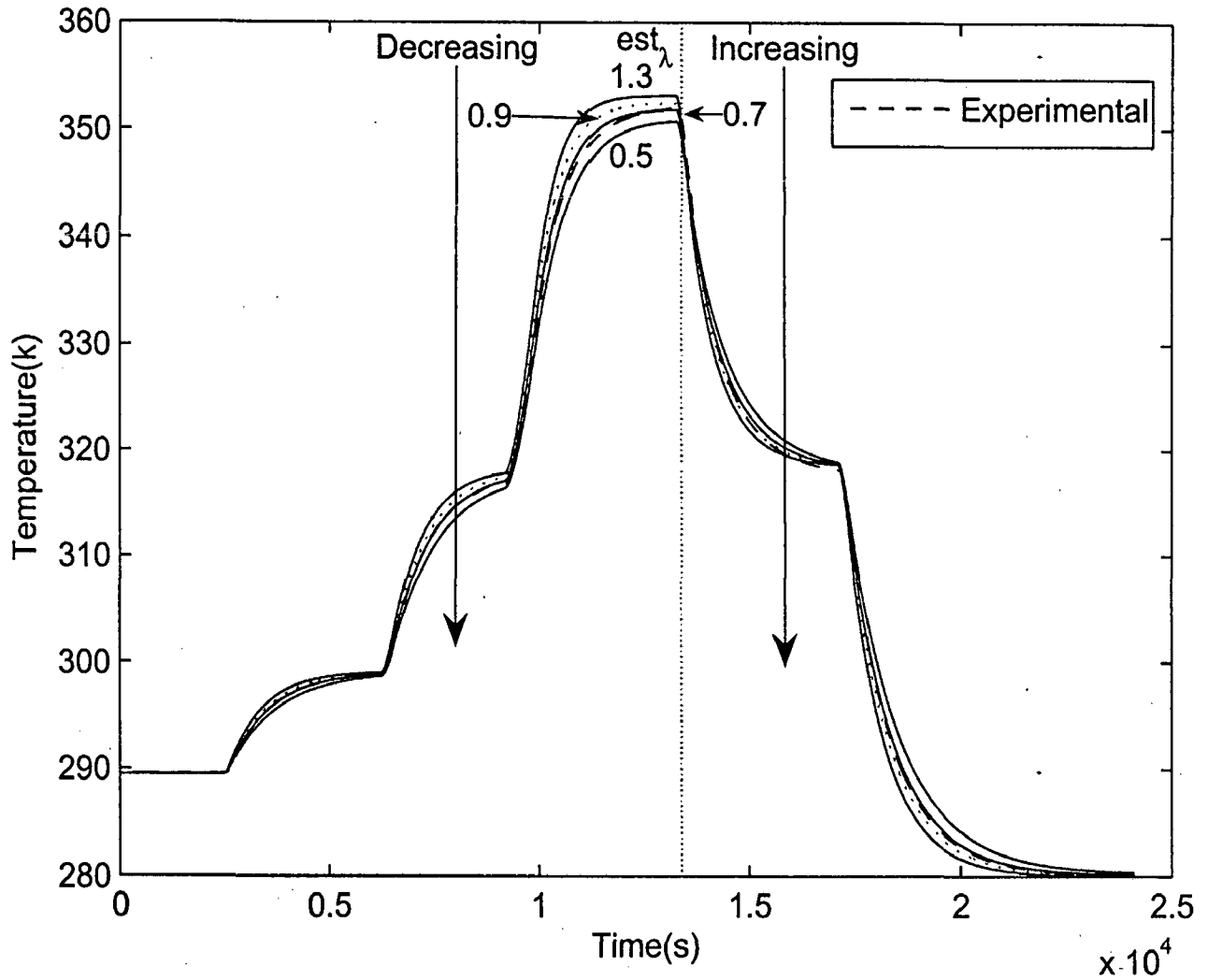


Figure 6.12: This graph shows the effect of the factor of heat conductivity of inner and outer tank wall (est_{λ}) on the reactor temperature trajectory.

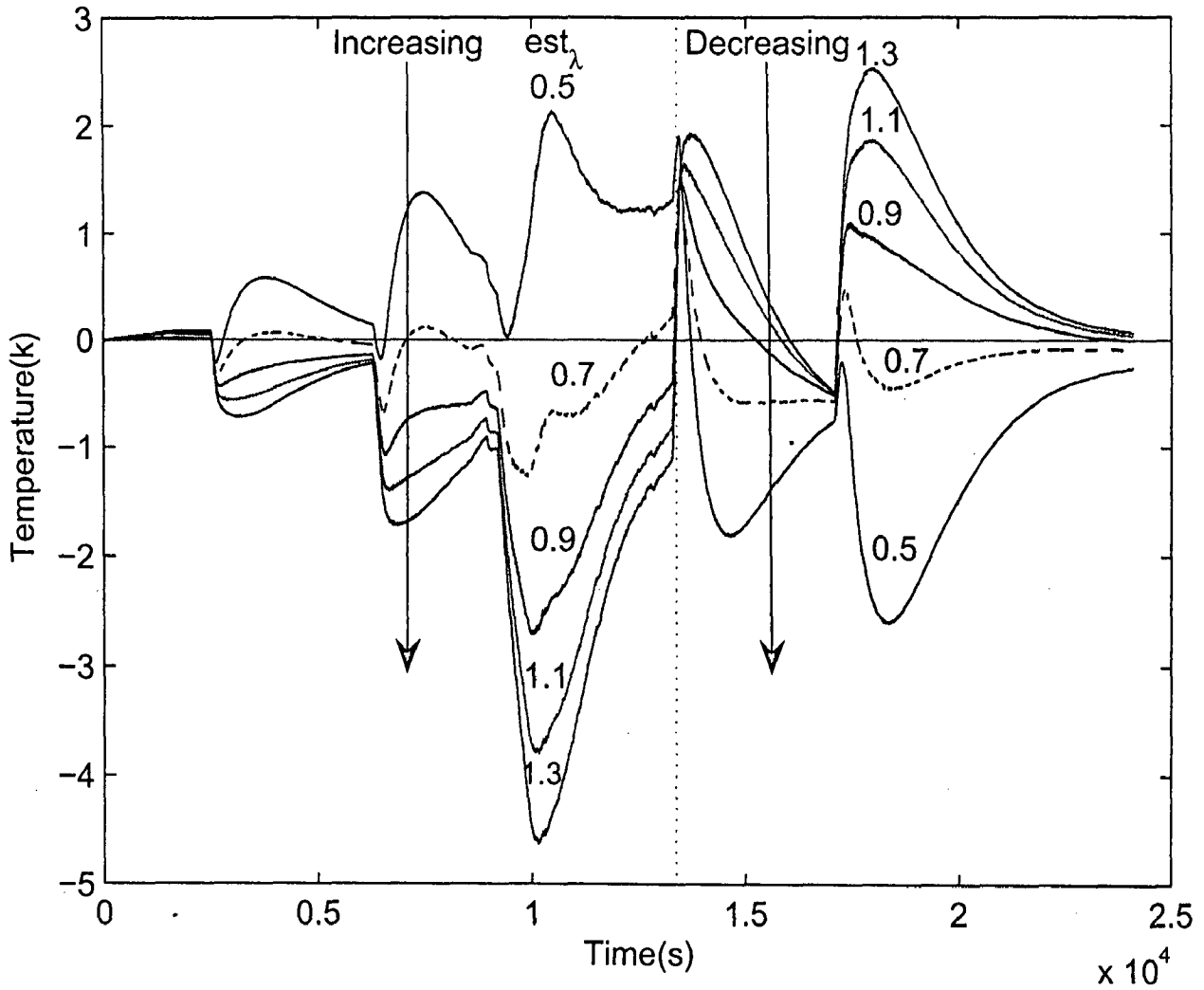


Figure 6.13: This graph shows the difference of the experimental temperature trajectory and the temperature trajectories obtained by the model at different values of the factor of heat conductivity of the inner and outer tank wall (est_λ).

Factor of heat capacity

The factor of heat capacity (est_{cp}) is added to adjust the value of the heat capacity of the glass. The inner tank wall, the bottom part of the outer tank wall and the shell part of the outer tank wall have separate factors for the heat capacity. The factors of the heat capacities does not have a major effect on the temperature trajectory in the reactor. The effect of the factor of heat capacity of the bottom and shell part of the outer tank wall is also negligible. The effect of the factor of heat capacity of the inner tank wall is small and no differences can be seen in the temperature trajectory plot but the differences can be seen in the error plot as shown in figure 6.14. The graph shows that the factor of heat capacity resists the heat transfer through the glass wall. The more the value of the factor of the heat capacity the less will be the heating as well as cooling effect. The mathematical model shows the best agreement with the experimental result at a est_{cp} value of 0.8.

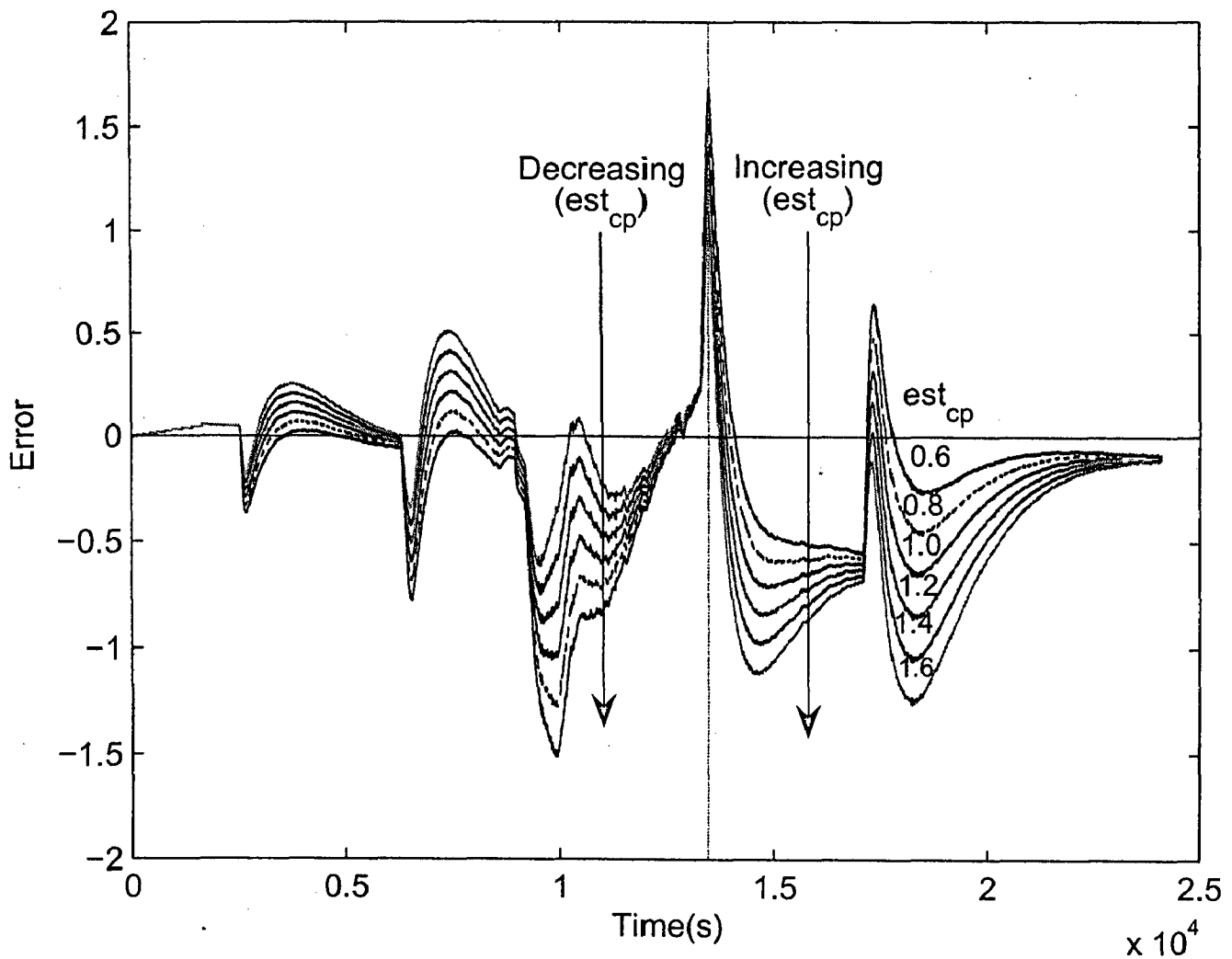


Figure 6.14: This graph shows the difference of the experimental temperature trajectory and the temperature trajectories obtained by the model at different values of the factor of heat capacity of the inner tank wall (est_{cp}).

Minimum cooling coefficient

The minimum cooling coefficient also has very less effect on the temperature trajectory of the reactor but the effect of the minimum cooling coefficient can be seen in the error plot as shown in figure 6.15. The effect of the minimum cooling coefficient is very less at lower temperatures in comparison to a higher temperature of the reactor. The graph shows that the effect of the $Cool_{min}$ is different in the region above ambient temperature to that below ambient temperature. On increasing $cool_{min}$ the reactor temperature will decrease if the reactor temperature is above ambient temperature and it increases if the reactor temperature is below ambient temperature. The mathematical model at $Cool_{min}$ of 0.1 (estimated value) shows the best agreement with the experimental result.

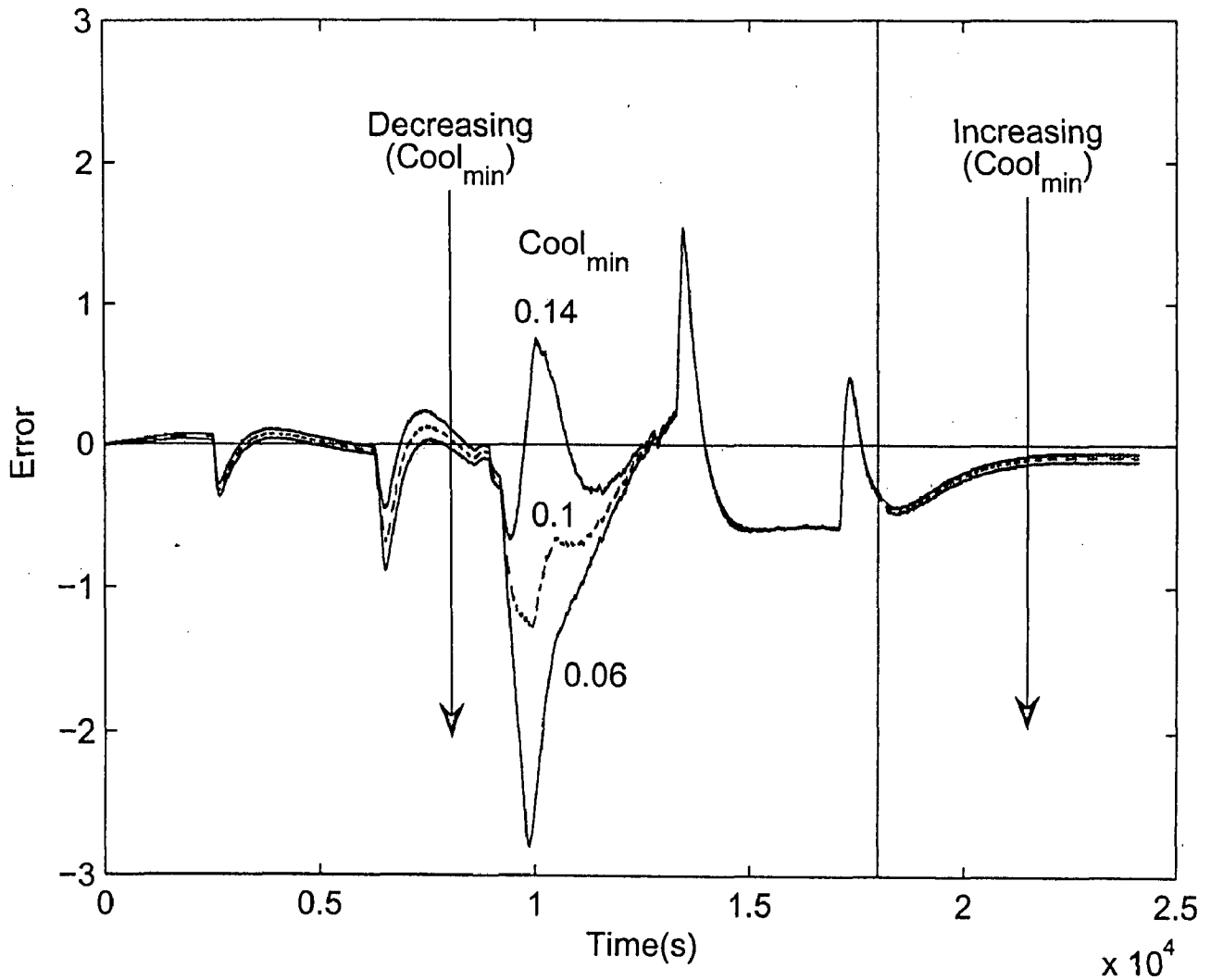


Figure 6.15: This graph shows the difference of the experimental temperature trajectory and the temperature trajectories obtained by the model at different values of the minimum cooling coefficient ($cool_{min}$).

6.1.3 Control parameters

There are three control parameters in the internal controller, T_n , T_v , and X_p . Appropriate values of these parameters are already specified in the control panel of the system under consideration. Still little readjustment of these control parameters are required in order to achieve the best agreement between the thermostat temperature obtained by the mathematical model and the experimental thermostat temperature. These values of the control parameters are adopted in the model for estimating the rest of the parameters.

The external *PID* controller involves three control parameters, k_c , τ_I and τ_D . For the tuning of these control parameters *ITAE* criteria is used. The following objective function is minimized by gOPT :

$$Obj(ITAE) = \int_0^t t |(T_r - T_{r_{set}})| \quad (6.1)$$

The optimization routine of gOPT is used for getting piecewise constant or piecewise linear variables in the specified intervals, in order to optimize the objective function. We specify the controller parameters as a piece wise constant variable and a single interval. The initial guess values of the parameters required for gOPT are determined by a heuristic method.

6.2 Estimated parameters

Since the control parameters are directly related to the thermostat temperature hence for estimating these parameters the thermostat temperature measured in the experiment is used. The values of the control parameters specified in the control panel of the experiment are taken as the initial value for estimating these parameters. Estimated values of the control parameters are specified in the process section for estimating the rest of the parameters.

All parameters to be estimated are related to each other in the mathematical model. So all parameters should be estimated together for increasing the accuracy of the parameter estimation. In order to get the best agreement between the mathematical model and the system under consideration both reactor and thermostat temperature are taken as a measured variable. If all parameters are estimated together using thermostat

temperature and reactor temperature both as measured variables then the parameter estimation routine of gPROMS has problems such as the estimation time being very high, fails to converge at discontinuities, negative number raised to non integer number etc. The problems associated with the parameter estimation routine of gPROMS are mainly due to a large number of experimental data, inaccurate values of the initial guesses and lower bounds and upper bounds of the parameters to be estimated. So in order to make possible the parameter estimation in gPROMS with high accuracy of estimated parameters following strategy is used:

1. In the first phase approximated values of all unknown parameters are estimated together by using both reactor temperature and thermostat temperature as measured variable. In order to reduce the number of experimental data, interval of data measurement increases. In the system under consideration, experimental data for the reactor temperature and the thermostat temperature are measured in a time interval of about 2 seconds. For parameter estimation data only in about 100 seconds interval are taken. In order to handle discontinuities, more experimental data are taken at discontinuities. So for the parameter estimation only about $(1/50)^{th}$ of the experimental data are taken in the time span of 6.67 hours, which can be easily handled by the parameter estimation routine of gPROMS. Estimated values of the parameters are used for the second phase of parameter estimation.
2. The temperature trajectory obtained by the mathematical model at the approximated values of the estimated parameters in step 1 is compared with the experimental temperature trajectory. For the second phase of the parameter estimation the same data set for the measured variables as used in the stem 1 are taken but more experimental data are taken in the time spans where the mathematical model shows more deviation from the system under consideration. All unknown parameters are estimated together using reactor temperature and thermostat temperature both as measured variables. Approximated values of the parameters obtained in step 1 are specified as initial guess values and also in the process section for the second phase parameter estimation. The lower bound and the upper bound of the parameters to be estimated are also adjusted accordingly. The estimated values of the parameters are used for the third phase parameter

estimation.

3. The temperature trajectory obtained by the mathematical model at the values of the parameters obtained in the second phase is compared with the experimental temperature trajectory. The deviation of the mathematical model from the system under consideration is reduced significantly in comparison to the mathematical model obtained in phase 1. In this phase only system dependent parameters are estimated together using the reactor temperature as the measured variable but the whole experimental data of reactor temperature are taken for the parameter estimation instead of using reduced data set as used in the first and the second phase. The estimated values of the parameters in the second phase are specified in the process section. The values of the system dependent parameters obtained in the second phase are specified as initial guess. The lower bounds and the upper bounds of the parameters to be estimated are adjusted accordingly. Estimated values of the parameters are used for estimating the adjusting parameters in the 4th phase of parameter estimation.
4. In this phase the adjusting parameters est_g , est_α , est_λ and $cool_{min}$ are estimated together using the whole experimental data of the reactor temperature. The values of the parameters obtained in the 3rd phase are specified in the process section. The initial guess, the lower bounds and the upper bounds of the parameters to be estimated are also specified accordingly.
5. In this phase the remaining adjusting parameters $iest_{cp}$, $obest_{cp}$, $osest_{cp}$ and cool coefficients are estimated together using the reactor temperature as the measured variable. The parameters estimated in the 4th phase are specified in the process section and other parameters remain unchanged. The initial guess, the lower bounds and the upper bounds of the parameters to be estimated in this phase are also specified accordingly.

All the parameters estimated by the parameter estimation routine of gPROMS by using the above strategy are given in table 6.1

The comparison of the mathematical model with the system under consideration is shown in figures 6.16 and 6.17.

Table 6.1: *Estimated parameters*

Parameter type	Name	Symble	Estimated value
Internal Controller parameters	Proportional gain	X_p	3
	Integral time	T_n	80010
	Differential time	T_v	7
External Controller parameters	Proportional constant	K_c	1.31
	Integral time	T_I	4
	Differential time	T_d	1
System dependent parameters	Power dissipated through the agitator	P	0.002 kw
	Volumetric flow rate through the pump in the thermostat	V_{dod}	0.00012
Adjusting parameters	Factor of the mass transfer coefficient at the surface of the reactor liquid	est_g	0.5
	Factor of the heat transfer coefficient between the bath fluid in the bottom and shell part of the tempering jacket and the surrounding tank walls	est_α	2
	Factor for the heat conductivity of the inner and outer tank wall of the reactor	est_λ	0.7
	Factor for the heat capacity of the inner tank wall	$iest_{cp}$	0.8
	Factor for the heat capacity of bottom part of outer tank wall	$obest_{cp}$	1.6
	Factor for the heat capacity of shell part of outer tank wall	$osest_{cp}$	1.6
	Minimum cooling coefficient	$cool_{min}$	0.1

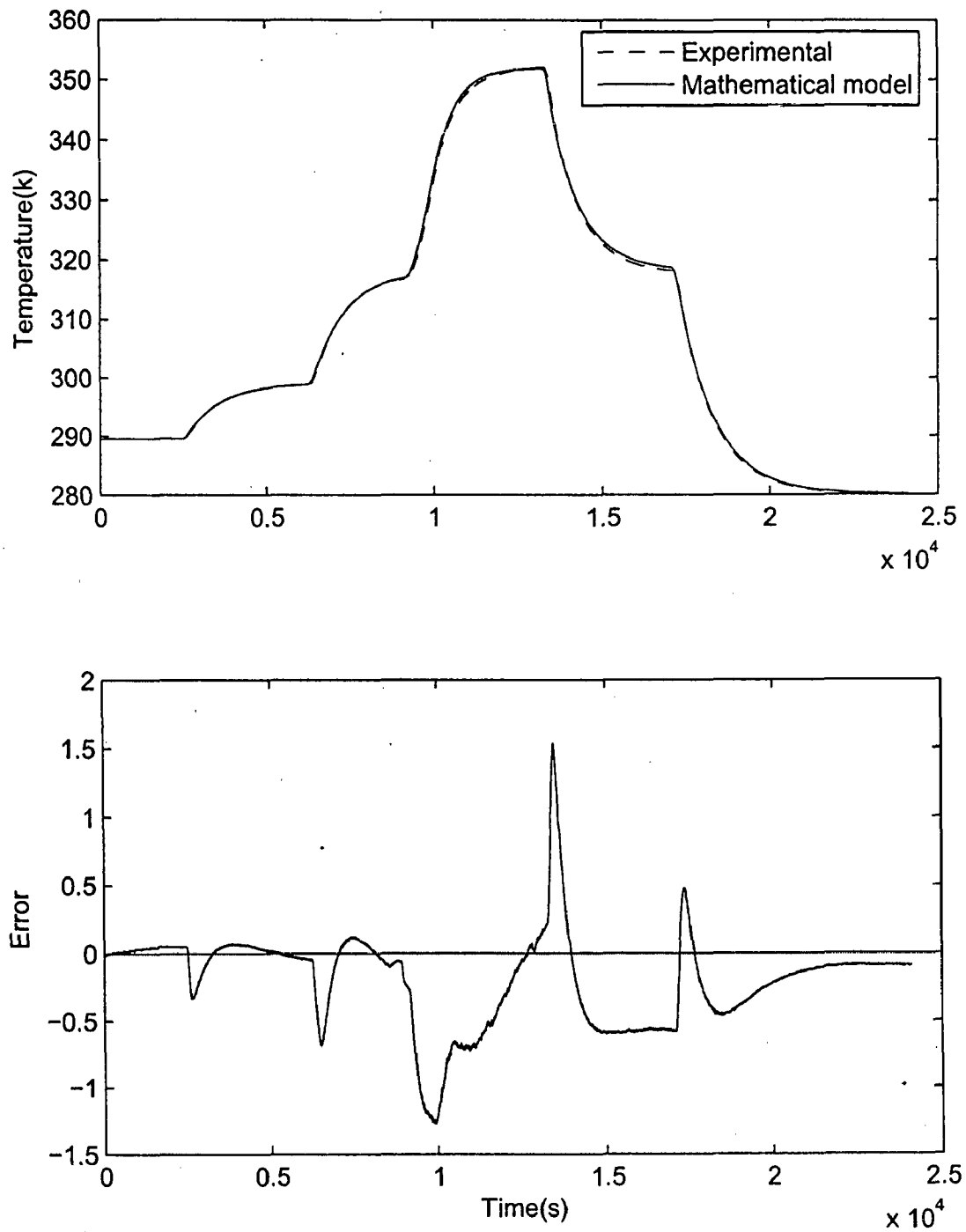


Figure 6.16: The first graph shows the experimental temperature trajectory of the reactor and the reactor temperature trajectory obtained by the mathematical model at the estimated values of the parameters and the second graph shows the difference of the experimental reactor temperature trajectory and the temperature trajectories obtained by the mathematical model

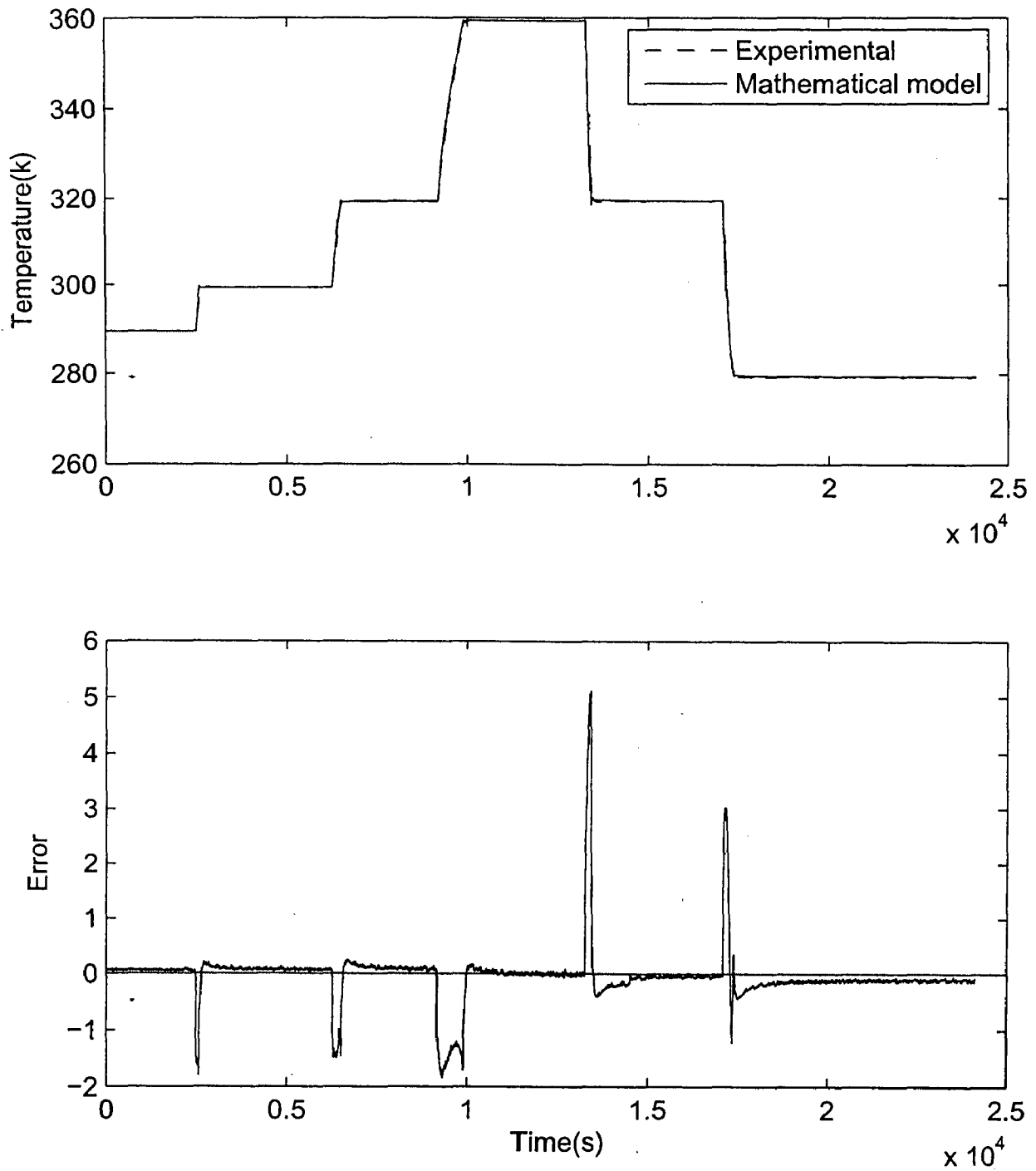


Figure 6.17: The first graph shows the experimental temperature trajectory of the thermostat and the thermostat temperature trajectory obtained by the mathematical model at the estimated values of the parameters and the second graph shows the difference of the experimental thermostat temperature trajectory and the temperature trajectories obtained by the mathematical model

6.3 System identification

The experiments are performed at different conditions and for system identification three sets of experimental data are collected. In order to get a more accurate model, the system is identified using two different sets of experimental data and the estimated models are validated with all three experimental data. To ensure that the selected model which gives best agreement with one experiment is also good for other experiments, two estimations are performed.

6.3.1 First estimation

The input output signals as shown in figure 6.18 are taken for system identification. In the beginning the system shows unstable response so the initial data are not suitable for system identification. After removing undesired data the input output signal which are used for system identification are shown in figure 6.19.

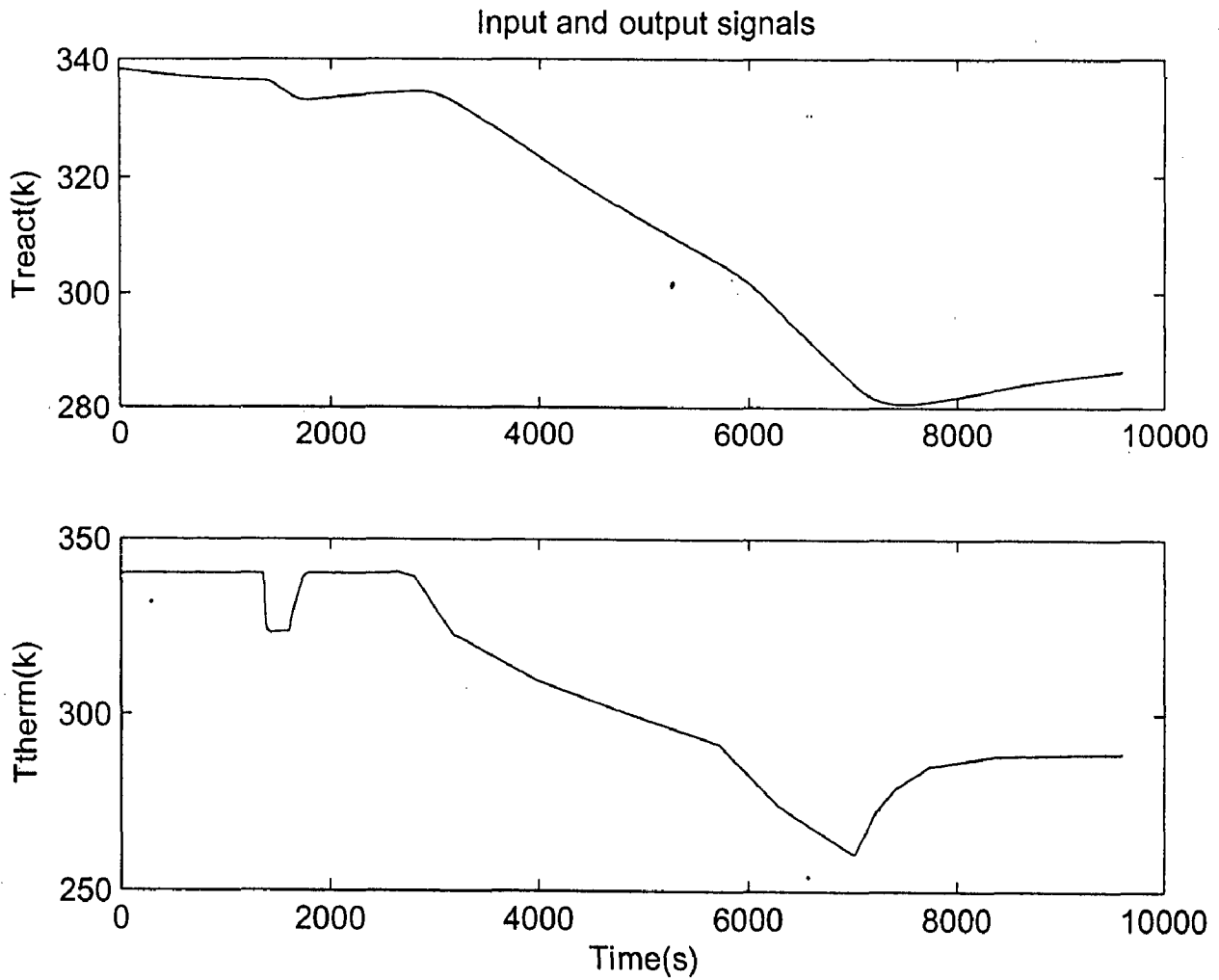


Figure 6.18: *These graphs show the input and output signal used for system identification. The first graph shows the output signal generated by the system and the second graph shows the input signal given to the system.*

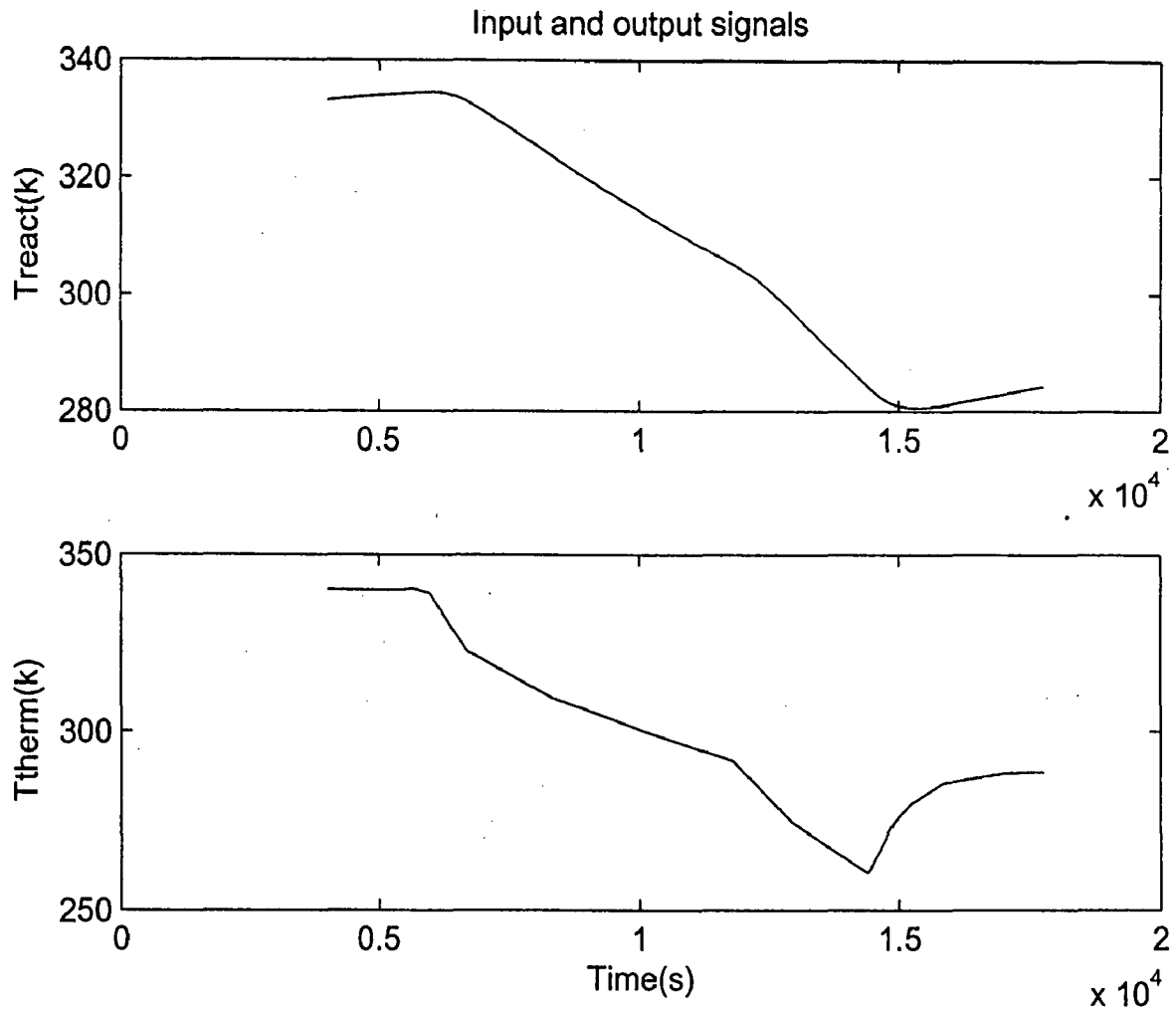


Figure 6.19: *These graphs show the input and output signal used for system identification. The first graph show the output signal generated by the system and the second graph show the input signal given to the system.*

Model selection

The system is identified with ARX, ARMAX, OE, BJ, P2DZ and P3DZ model structure. Three sets of experimental results are used for model validation. The deviation of each estimated model with the experimental result are shown in the figures.

Validation 1

The same data which is used for model estimation is used for model validation. The comparison of the ARX and ARMAX linear model with the system behavior is shown in figure 6.20. The behavior of both linear models are similar. The linear ARX and ARMAX models show more deviation in the initial as well as in the last span of process times. This deviation arises due to the discontinuities present in the model. The linear model tries to fit the larger portion of the temperature trajectory which lies between these two discontinuous points hence beyond these two points there is a comparatively large deviation. The error plot shows that the experimental temperature trajectory deviated from the temperature trajectory obtained by the linear model by -1 to 1.4 K.

The comparison of the OE and BJ linear model with the system is given in figure 6.21. The figure shows that the OE linear model has the best agreement with the system. The experimental temperature trajectory is deviated from the linear model only by -0.3 to 0.5 K which is the least value compared to other linear models. The BJ linear model shows the little more deviation from the system in comparison to the OE model but still less deviation in comparison to other linear models. The loss function and the FPE of the OE and BJ linear models are very high compared to the ARX and ARMAX linear models (refer table 6.2) hence these models may not always reflect the true behavior of the system.

The linear process models P2DZ and P3DZ are compared with the system in figure 6.22. The process models also show better agreement with the system in comparison to the ARX and ARMAX linear models but poor agreement in comparison to the OE and BJ linear models in all other points except the initial time where sudden large deviation is found. The loss function and the FPE of the P2DZ linear model are highest among the linear models. The loss function and the FPE of the P3DZ model is little less in comparison to the P2DZ and the OE linear model but still very high in

comparison to the *ARX* and *ARMAX* linear model. Hence the *ARX* and *ARMAX* may shows the system behavior better in comparison to the process models.

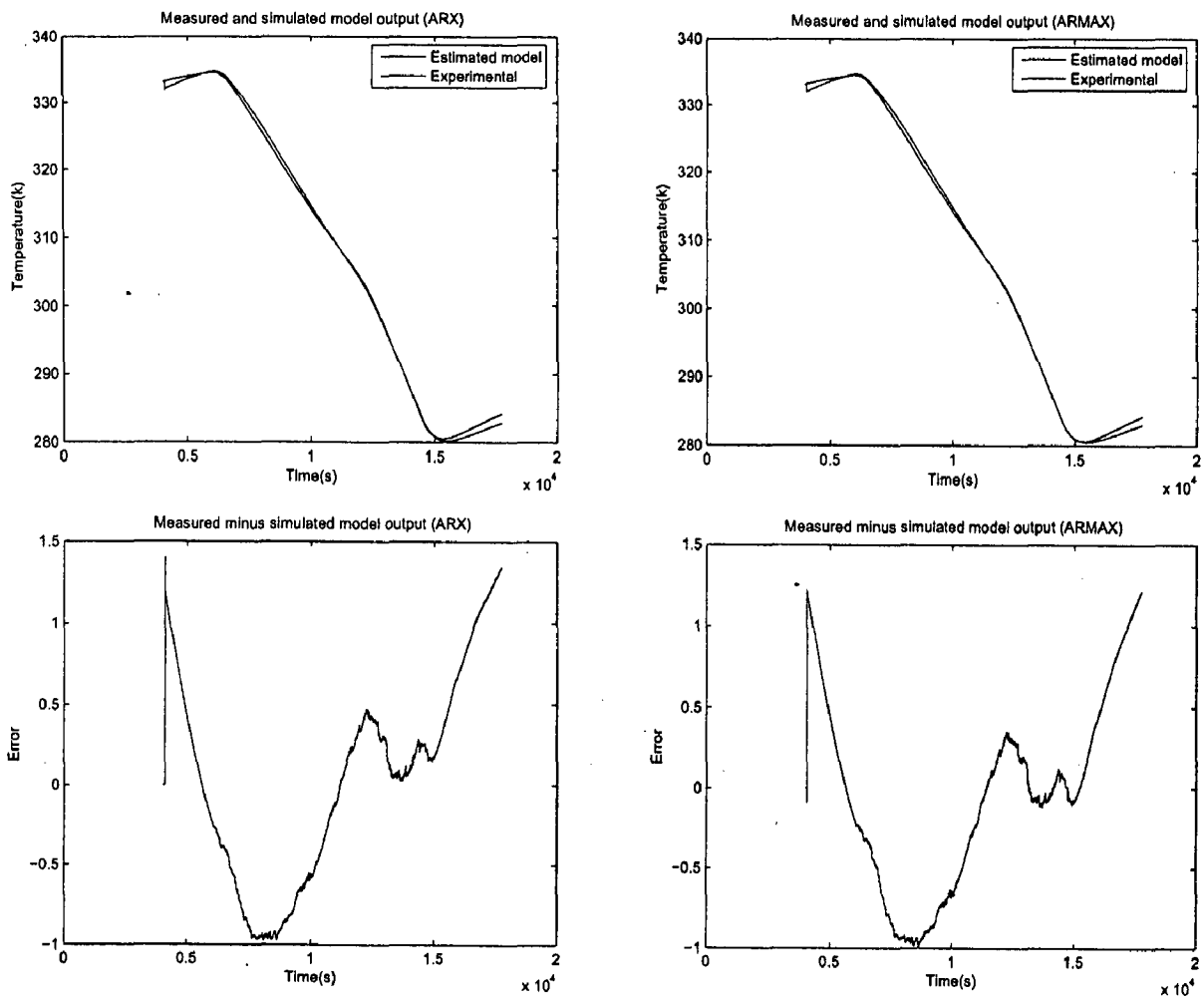
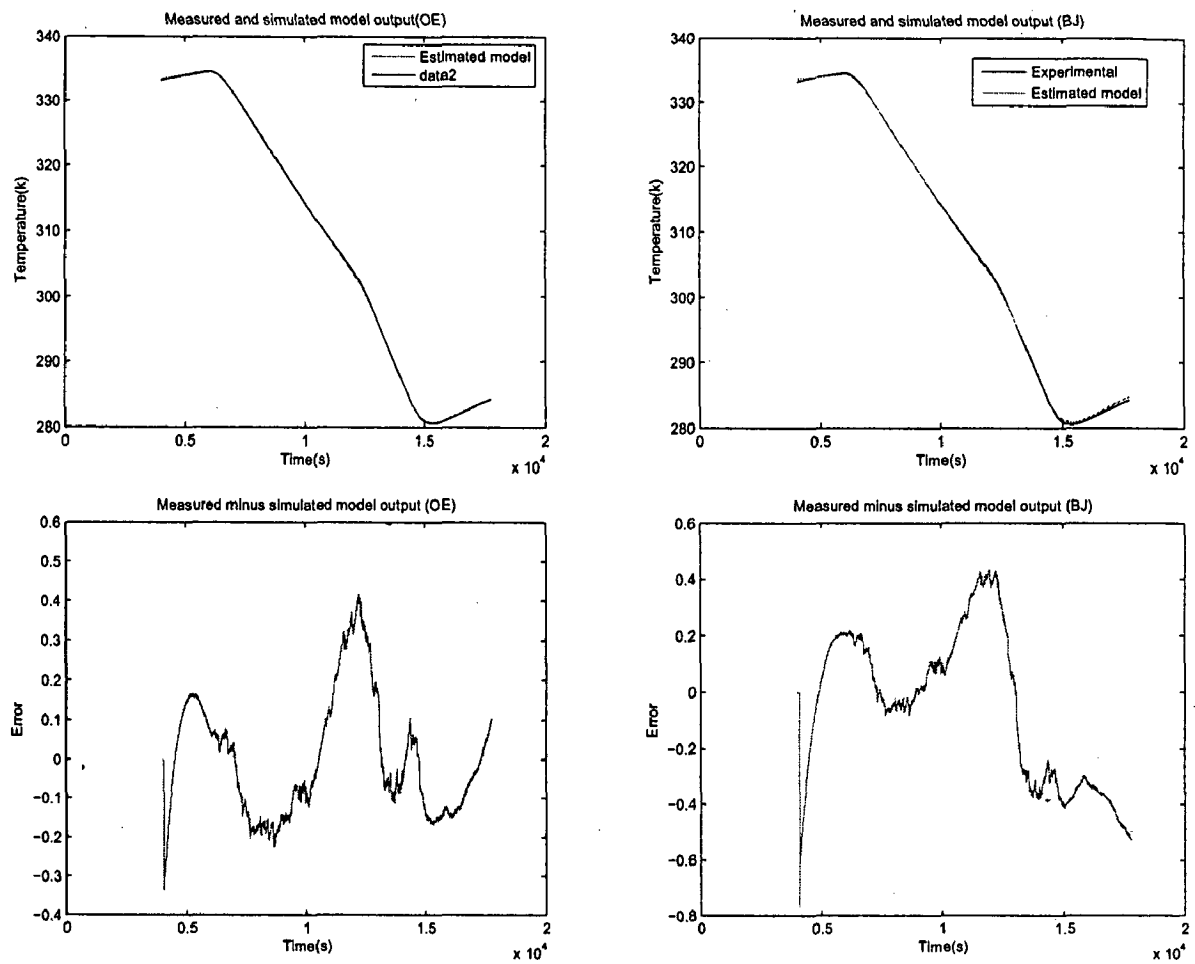


Figure 6.20: Validation 1 for *ARX* and *ARMAX* model.

Figure 6.21: Validation 1 for *OE* and *BJ* model.

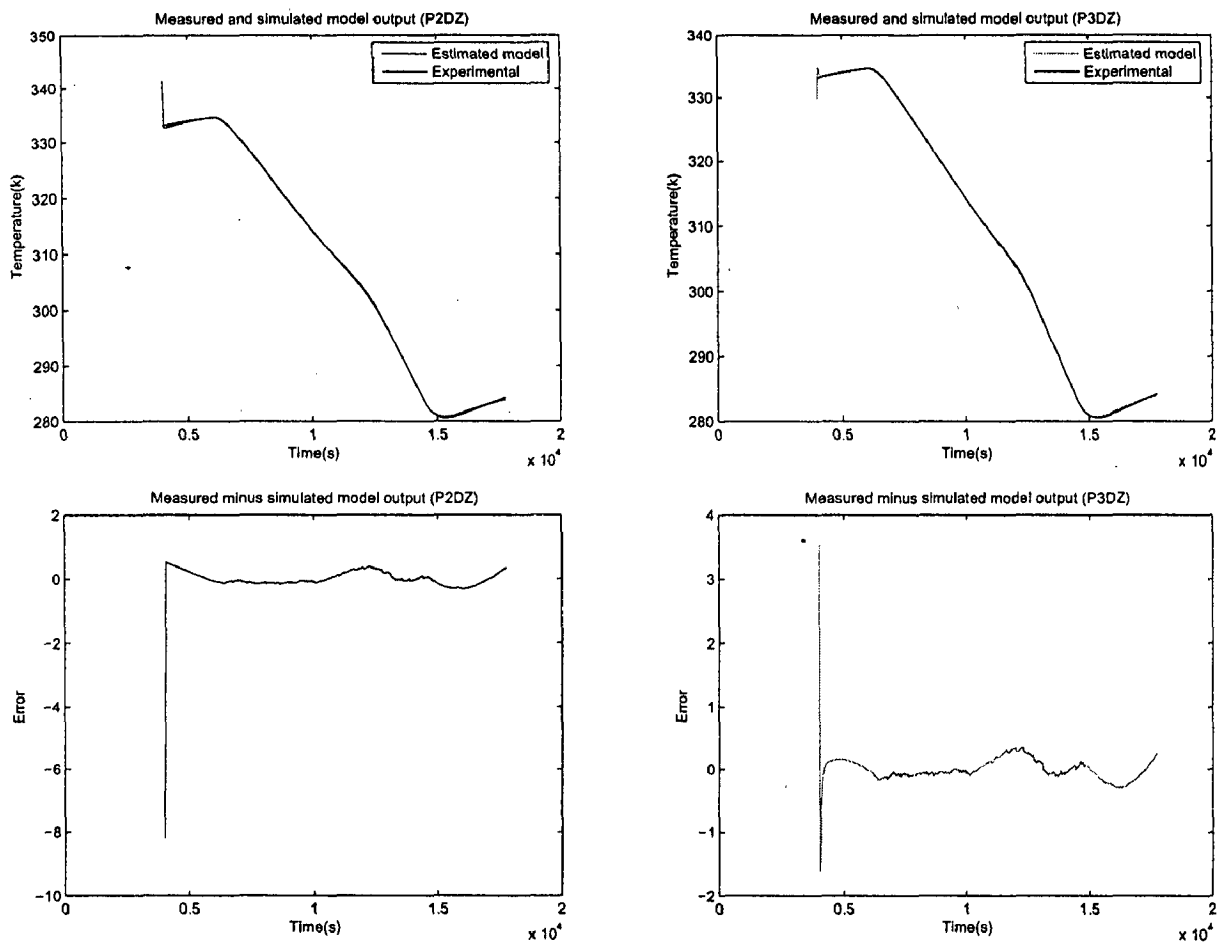


Figure 6.22: Validation 1 for *P2DZ* and *P3DZ* model.

Validation2

Validation data is different to that of the estimation data. The same linear models which are estimated in the subsection, first estimation are validated with the other set of the experimental data. The input output signal used for the model validation are shown in figure 6.23. For this input signal the output signal is calculated by each estimated linear model and these output signals calculated by the linear models are compared with the output signal obtained by the experiment for the same input signal. With this validation data the process models, $P2DZ$ and $P3DZ$ show very large deviation from the system behavior. Hence the process models should not be used for the system under consideration.

The behavior of the ARX and the $ARMAX$ linear models are compared with the system behavior in figure 6.24. The behavior of the both models are similar. As shown in figure, these linear models follow the system behavior but not exactly track the system behavior. One of the possible reason of this deviation may be that the set of the data used for the linear model estimation and the set of the data used for the model validation are collected from the experiment at different initial conditions. The deviation of the experimental temperature trajectory from the ARX and $ARMAX$ linear models temperature trajectory lies between -2 to 5 K which is quite large.

The comparison of the OE and BJ linear model with the system is shown in figure 6.25. The BJ linear model shows better agreement with the system behavior compared to OE linear model while in validation 1, the OE model was showing better agreement. The experimental temperature trajectory deviated from the OE linear model temperature trajectory from -0.75 to 2.8 K and from the BJ linear model from -1.4 to 0.5 K.

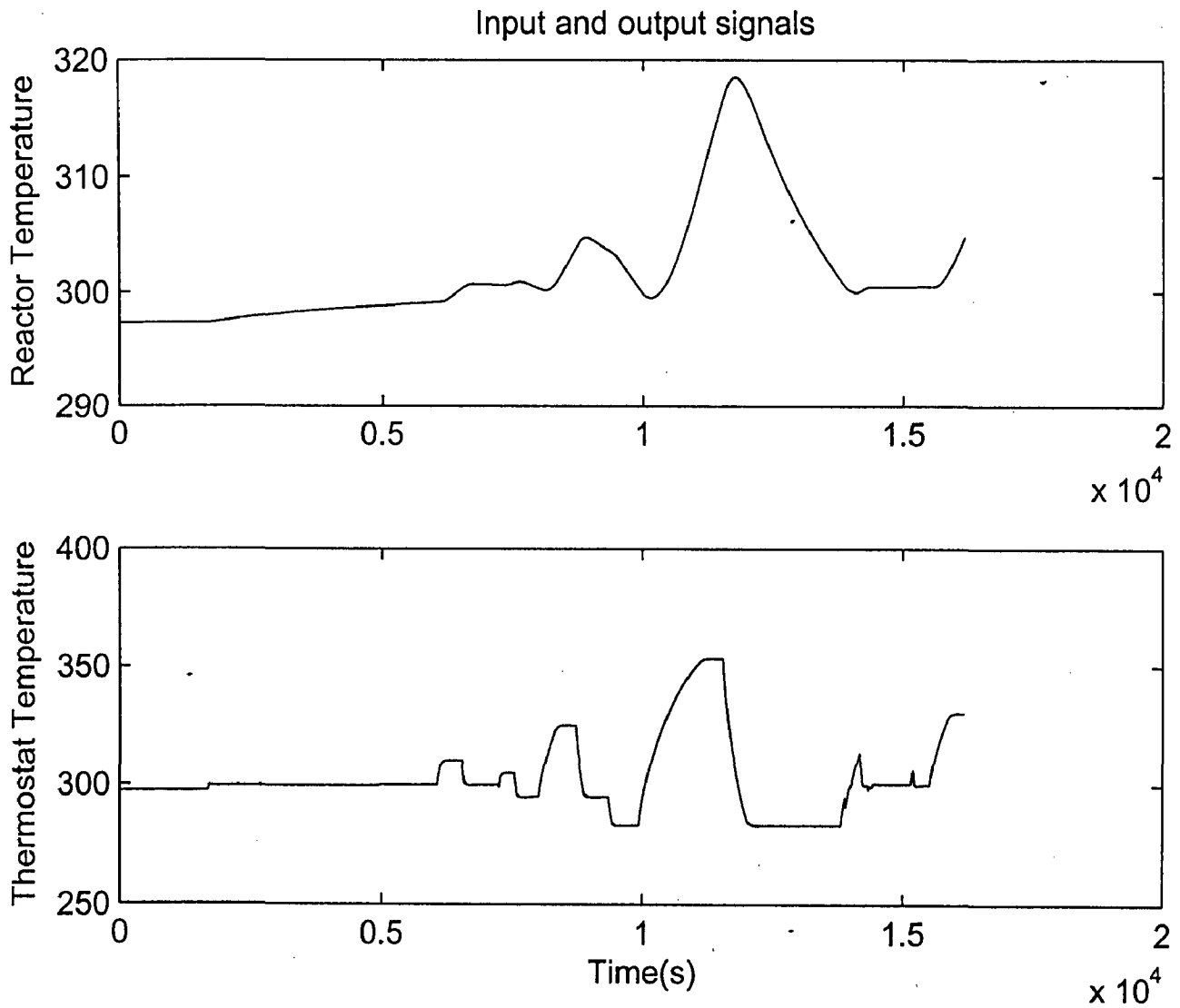


Figure 6.23: *These graphs show the input and output signal used for model validation. The first graph shows the output signal generated by the system and the second graph shows the input signal given to the system.*

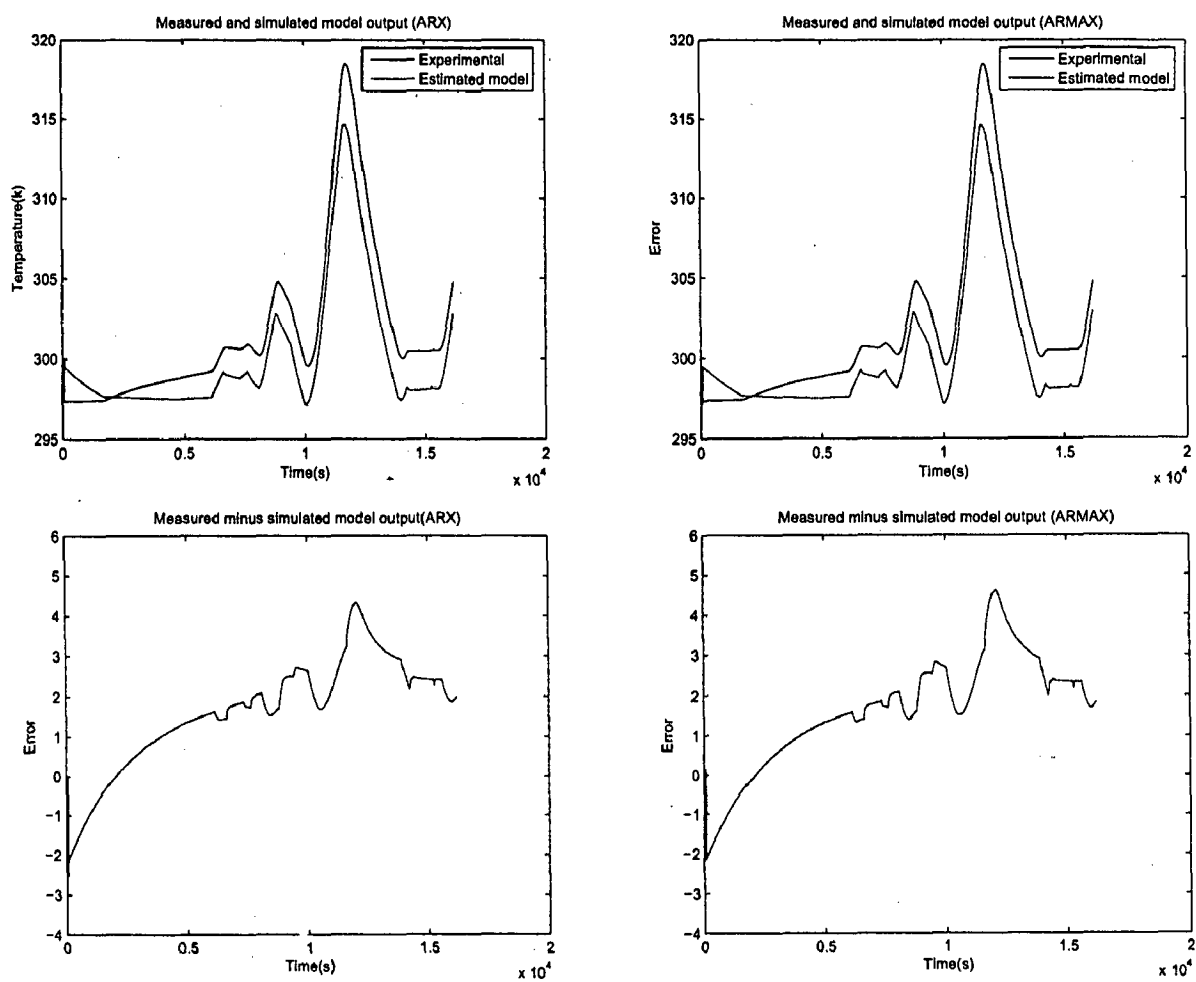


Figure 6.24: Validation 2 for ARX and ARMAX model.

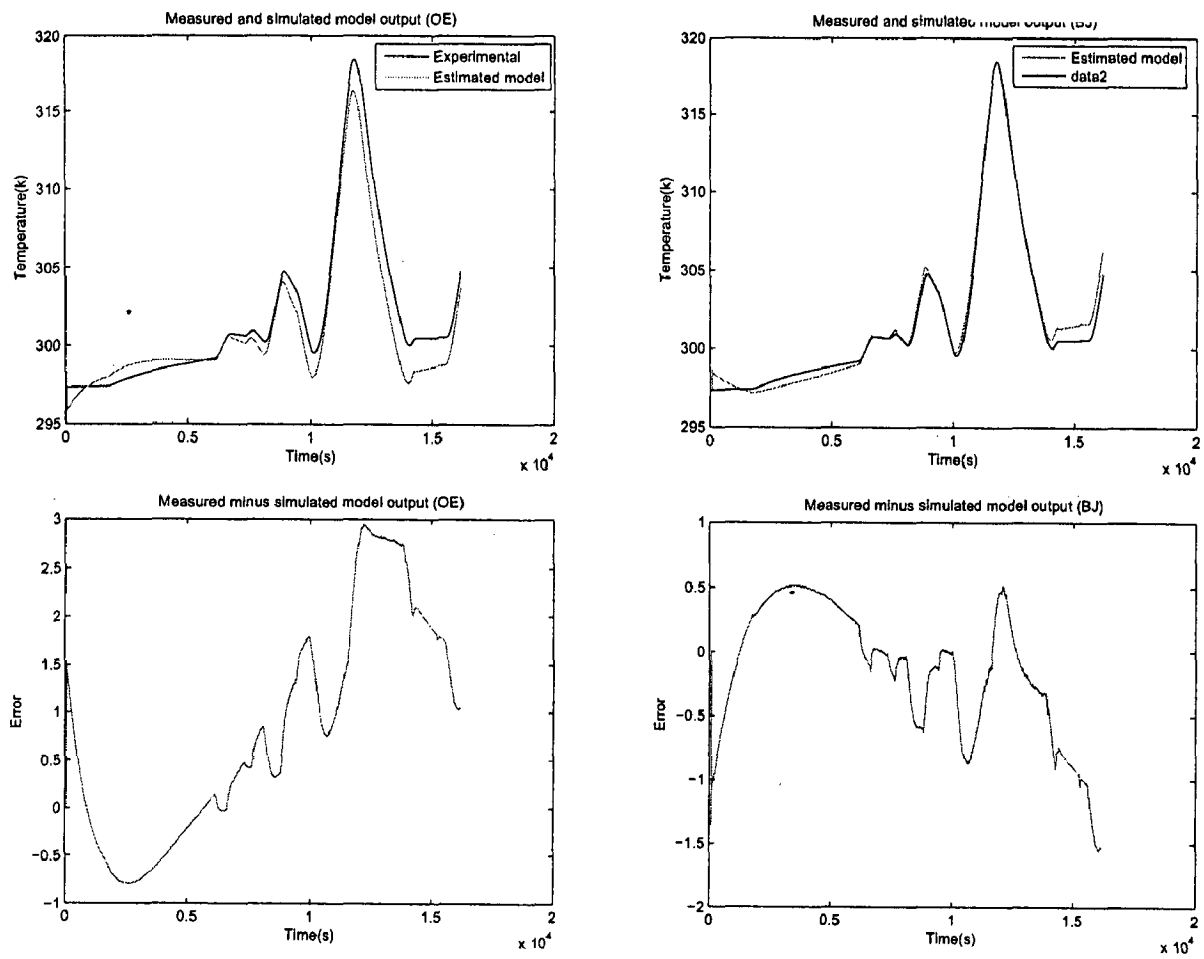


Figure 6.25: Validation 2 for *OE* and *BJ* model.

Validation3

The same linear models which are estimated in the subsection, first estimation are validated with another set of the experimental data. The input output signal used for the model validation are shown in figure 6.26. For this input signal the output signal is calculated by each estimated linear models and these output signals calculated by the linear models are compared with the output signal obtained by the experiment for the same input signal. With this validation data the process models, $P2DZ$ and $P3DZ$ also show very large deviation from the system behavior. Hence the process models should not be used for the system under consideration.

The comparison of the ARX and $ARMAX$ linear models with the system behavior for this set of the validation data is given in figure 6.27. For this set of validation data the ARX and the $ARMAX$ model show a better fit with the experimental result in comparison to validation 2. The linear deviation of the ARX , $ARMAX$ model from the system is also present in this case as in validation 2 due to the same reason but for this set of the validation data the deviation is less it varied from -2 to 3 . The negative deviation is only in the initial unstable region while in the rest span of the time there are only positive deviations.

The comparison of the OE and the BJ linear models with the system behavior for this set of data is shown in figure 6.28. In this validation the OE model is showing better fit with the experimental result in compared to validation 2. However BJ model is showing the little better fit in compared to OE model.

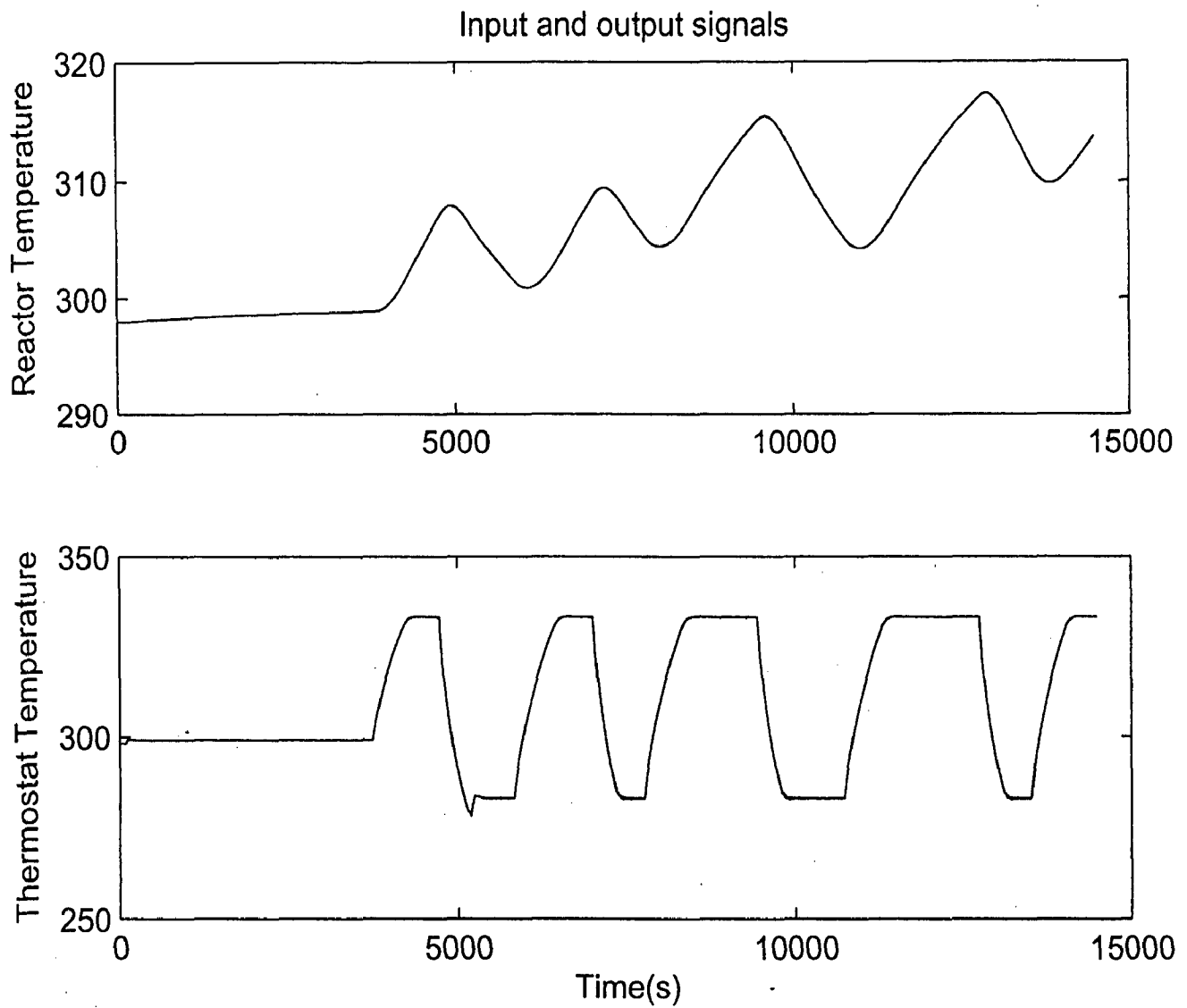


Figure 6.26: *These graphs show the input and output signal used for model validation. The first graph shows the output signal generated by the system and the second graph shows the input signal given to the system.*

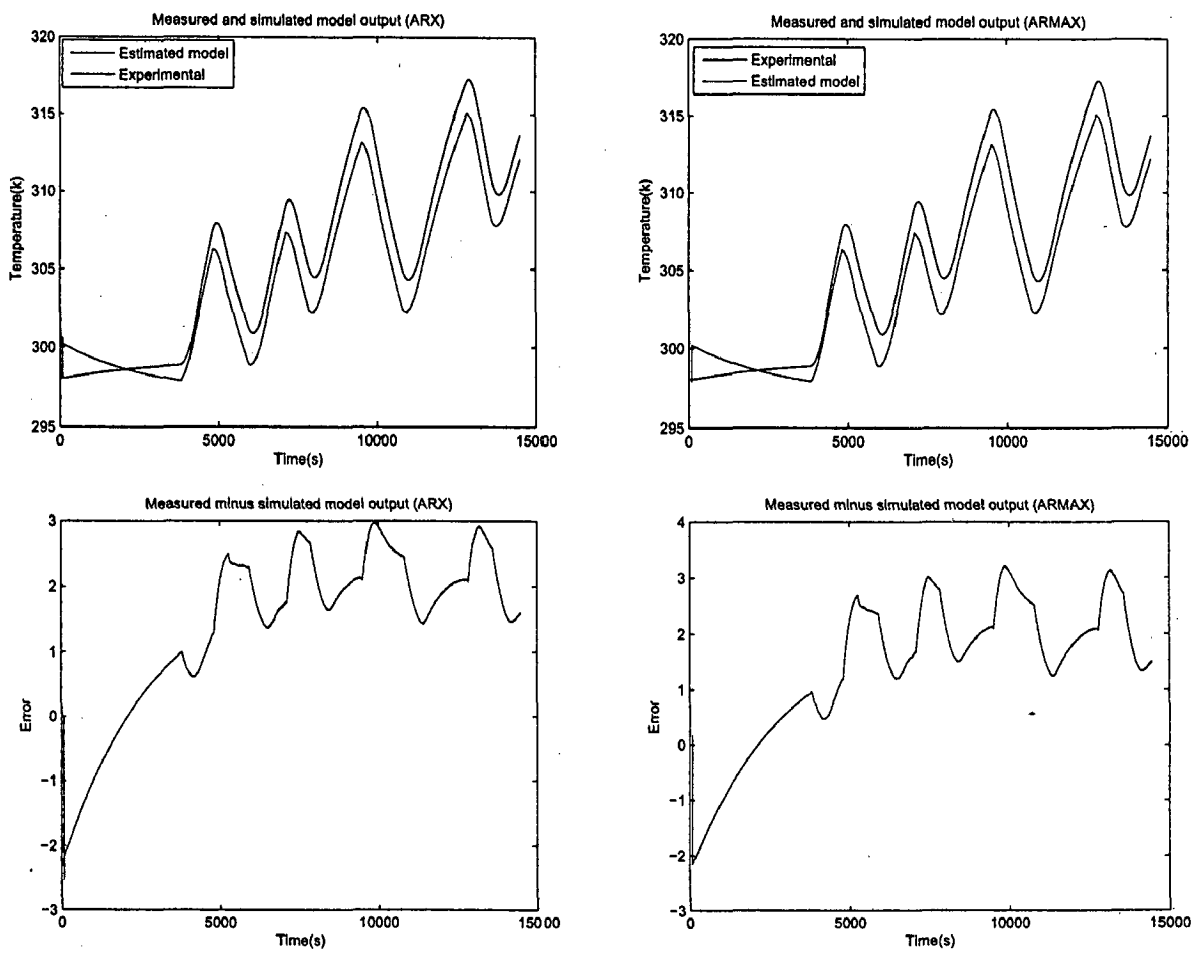
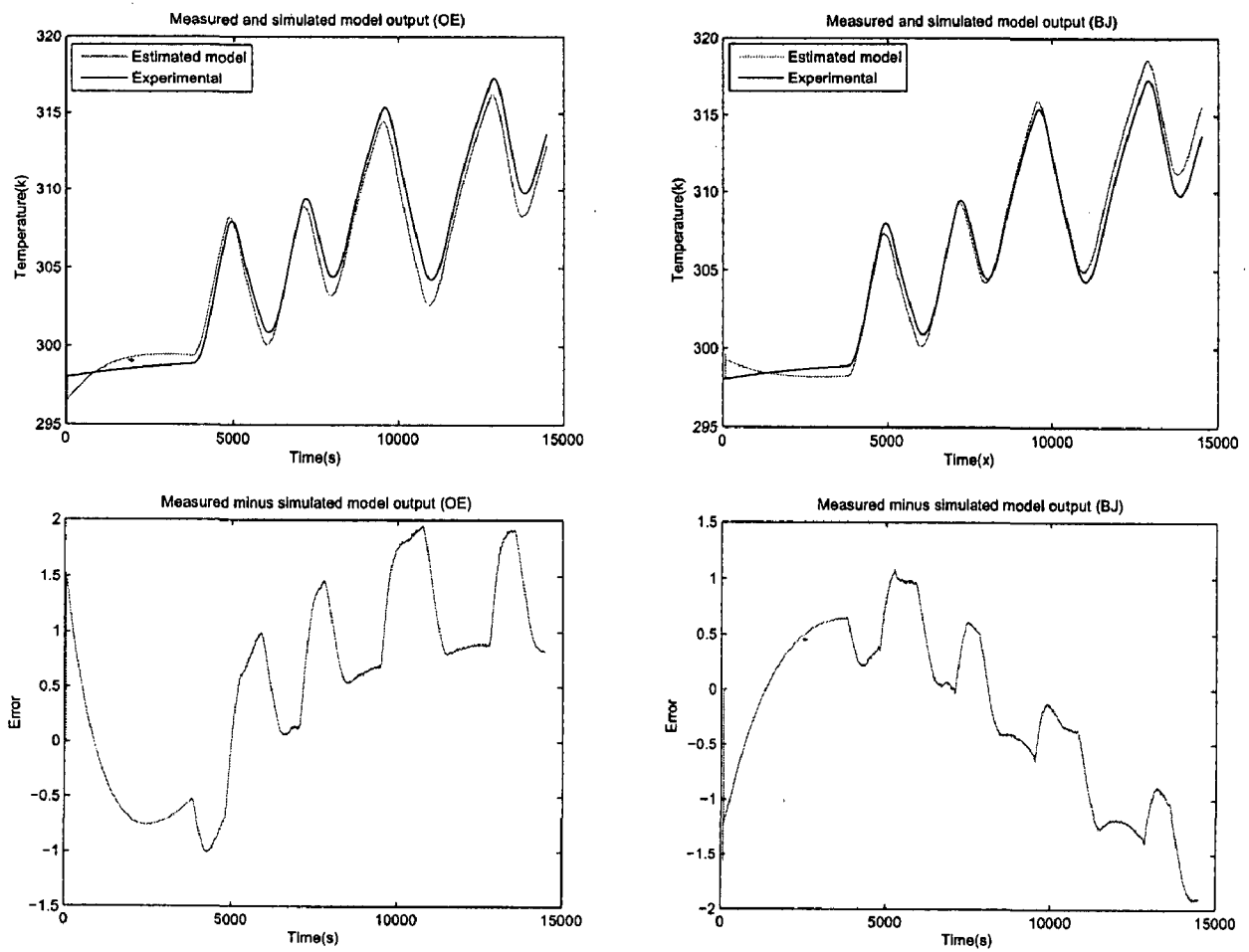


Figure 6.27: Validation 3 for ARX and ARMAX model.

Figure 6.28: Validation 3 for *OE* and *BJ* model.

6.3.2 Second Estimation

In this estimation the linear models are estimated by using another set of estimated data, the input output signal of which are shown in figure 6.26. The estimated models are validated with another 2 set of the experimental data and with the estimation data itself.

Validation 1

The input output signal used for validating the estimated model are shown in figure 6.19. The figure 6.29 compared the *ARX* and *ARMAX* linear models with the system behavior. At the initial point the linear models show large deviation because the estimation data are measured from the initial time while the initial values of the validation data are not included. The *ARX* and the *ARMAX* model show good agreement with the experimental result.

The comparison of the *OE* and *BJ* linear models with the system behavior is shown in figure 6.30. There is very little improvement in the fits of *OE* and *BJ* models in comparison to the *ARX* and *ARMAX* model but the loss function and the *FPE* of the *OE* and *BJ* models are still very high compared to the *ARX* and *ARMAX* models refer table 6.2.

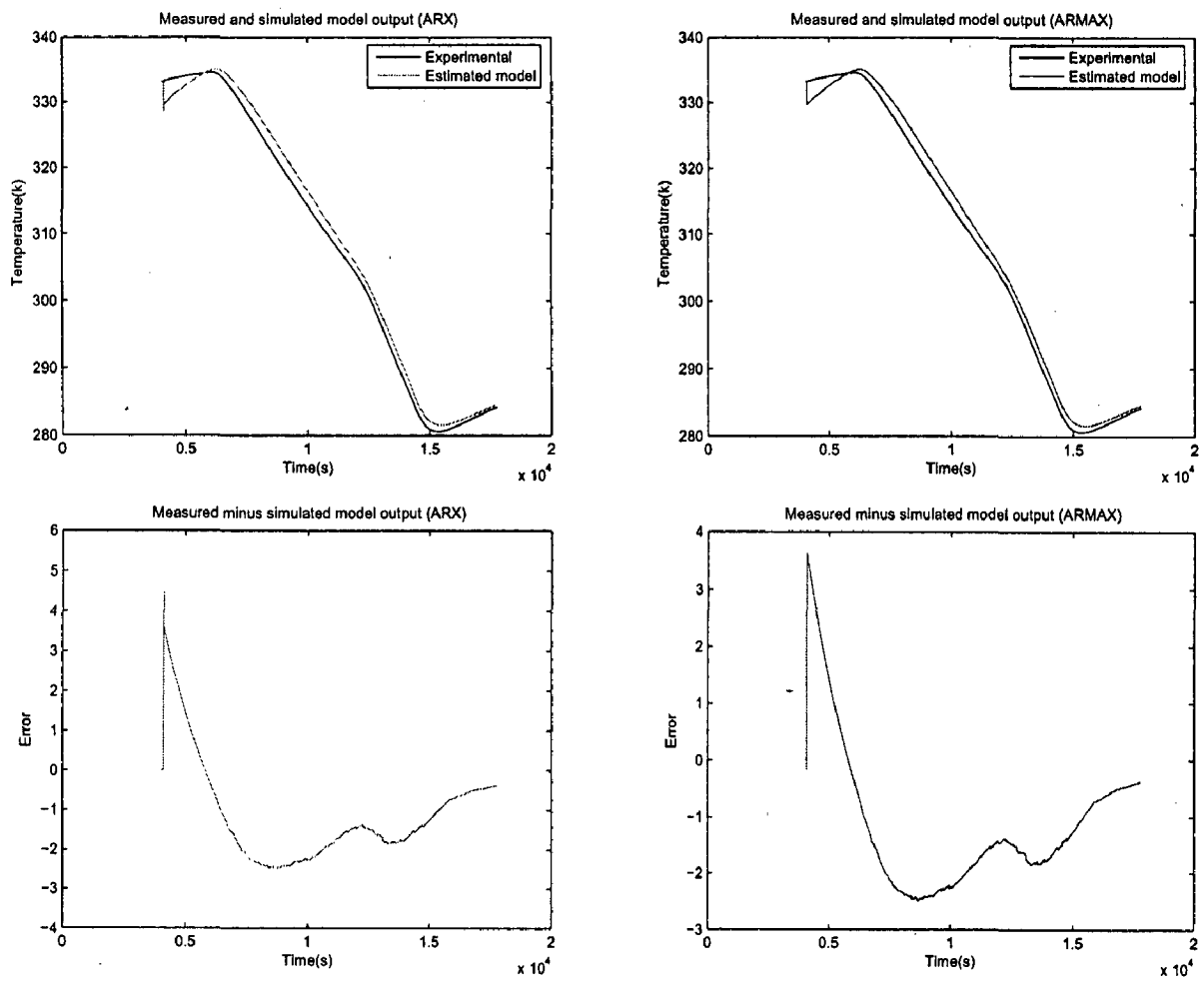
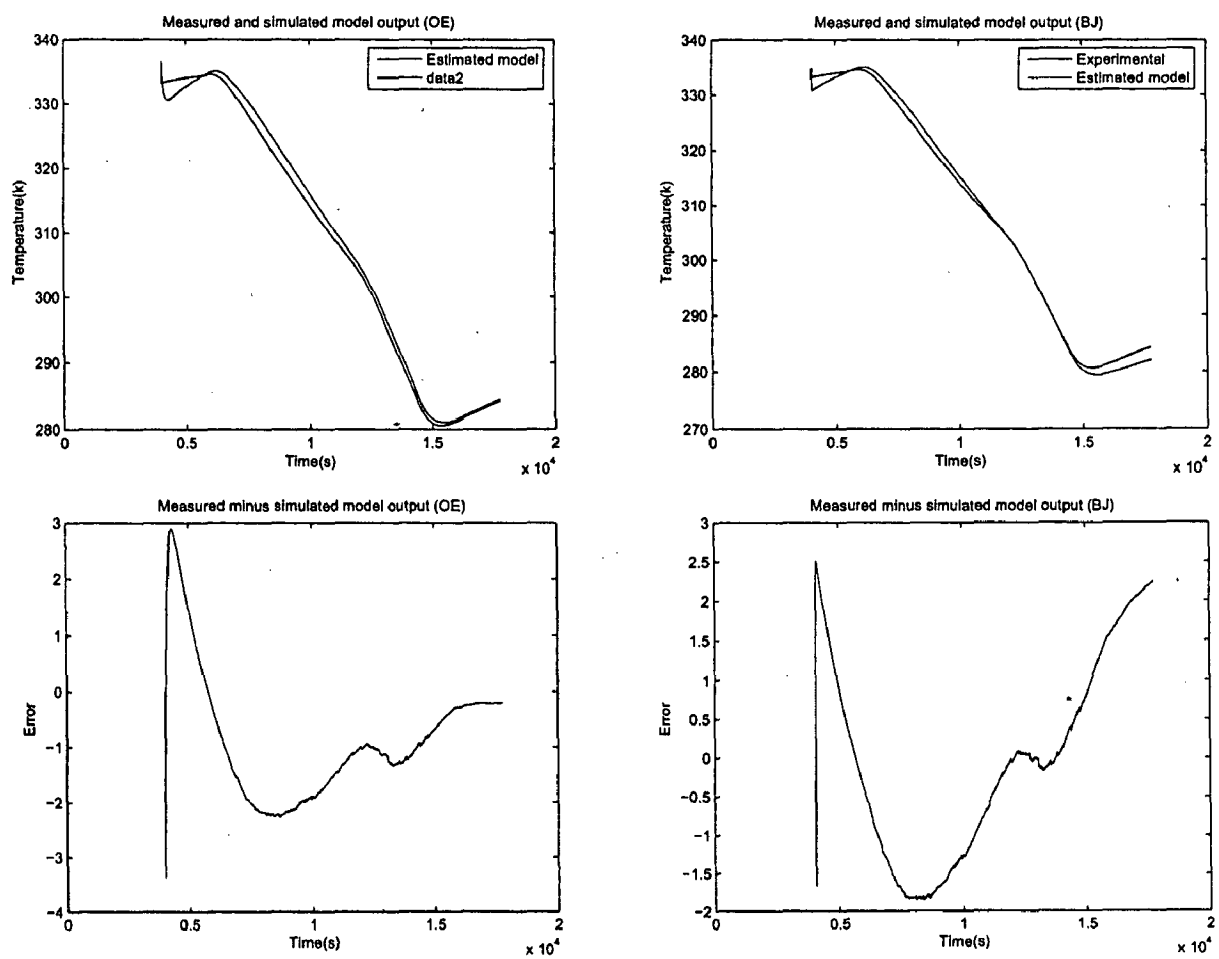


Figure 6.29: Validation 1 for ARX and ARMAX model.

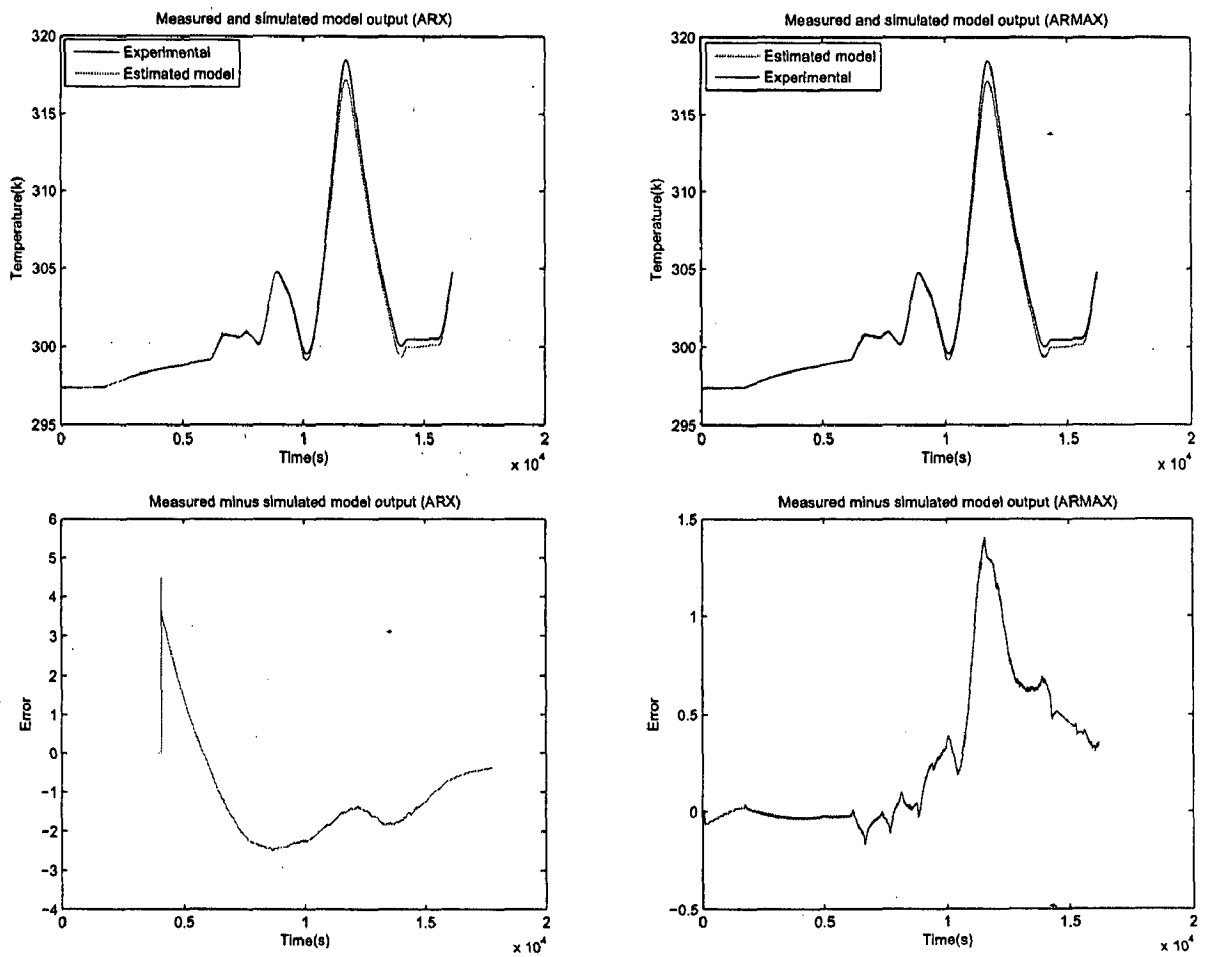
Figure 6.30: Validation 1 for *OE* and *BJ* model.

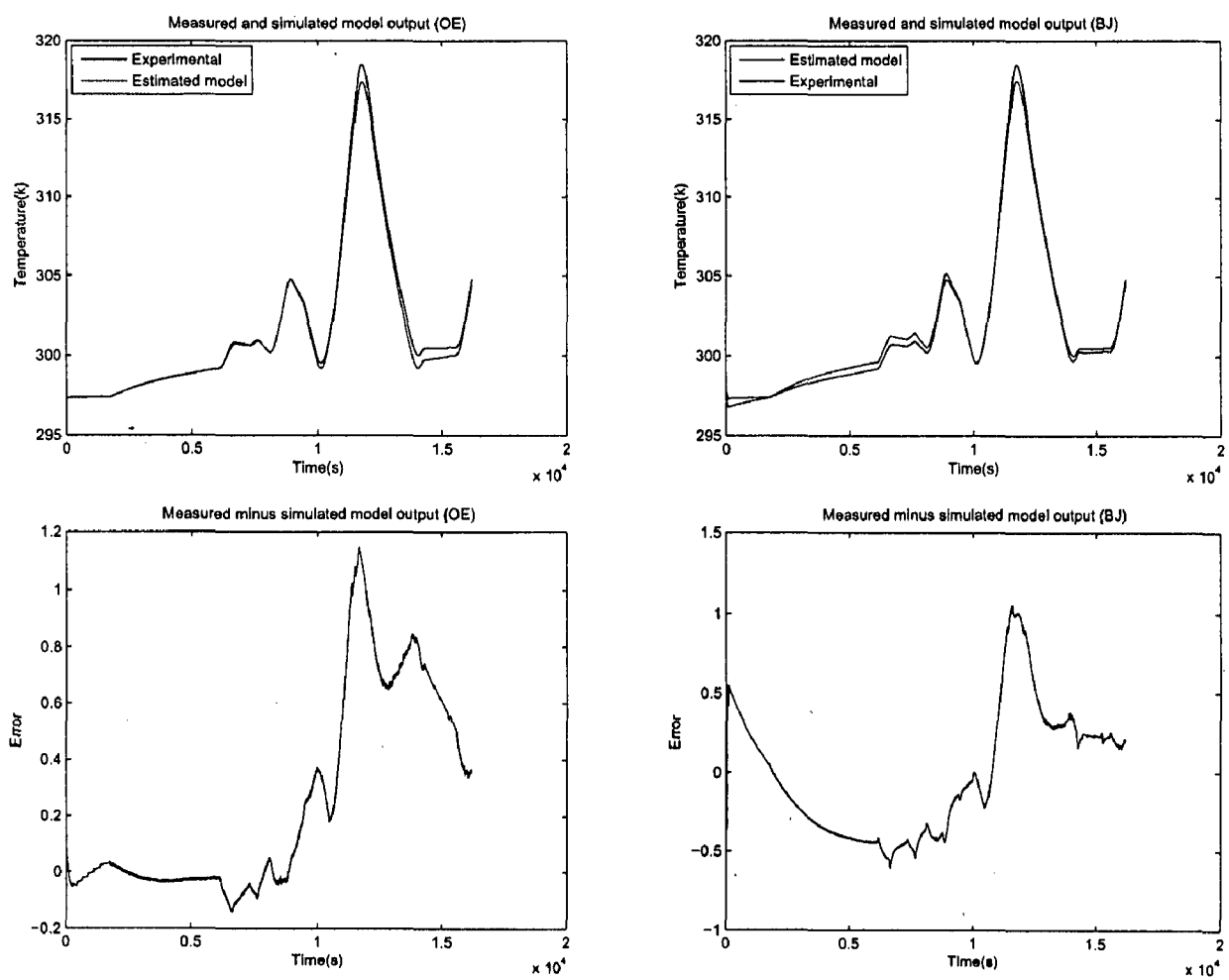
Validation 2

The input output signal used for validation 2 are shown in figure 6.23. This validation data is different to that of estimation data.

Figure 6.31 compared the behavior of the *ARX* and *ARMAX* linear model with the system behavior for this set of validation data. The figure shows that the *ARX* and *ARMAX* models have good agreement with the experimental results, even though the estimation and the validation data are not same. Hence the *ARX* and *ARMAX* linear models reflect the true behavior of the system.

The comparison of the *OE* and the *BJ* linear models with the system behavior is shown in figure 6.32. On comparison the figures 6.31 and 6.32 it is clear that *ARX* and *ARMAX* models are fitting better compared to the *OE* and *BJ* models.

Figure 6.31: Validation 2 for *ARX* and *ARMAX* model.

Figure 6.32: Validation 2 for *OE* and *BJ* model.

Validation 3

The input output signal used for this validation are shown in figure 6.26. This validation data is the same to that of the estimation data.

The figure 6.33 shows the comparison of the *ARX* and *ARMAX* linear model with the system behavior. The graph shows good agreement between linear models (*ARX* and *ARMAX*) and the system.

The comparison of the *OE* and *BJ* linear models with the system behavior are shown in figure 6.34. On comparing the figure 6.33 and 6.34 it is clear that the *ARX* and *ARMAX* models are fitting as good as *OE* and *BJ* model.

For the accuracy measurement of the estimated model different terms are used (e.g loss function, FPE, Fit). The values of these terms for the different models are given in table 6.2.

Validation 3

The input output signal used for this validation are shown in figure 6.26. This validation data is the same to that of the estimation data.

The figure 6.33 shows the comparison of the *ARX* and *ARMAX* linear model with the system behavior. The graph shows good agreement between linear models (*ARX* and *ARMAX*) and the system.

The comparison of the *OE* and *BJ* linear models with the system behavior are shown in figure 6.34. On comparing the figure 6.33 and 6.34 it is clear that the *ARX* and *ARMAX* models are fitting as good as *OE* and *BJ* model.

For the accuracy measurement of the estimated model different terms are used (e.g loss function, FPE, Fit). The values of these terms for the different models are given in table 6.2.

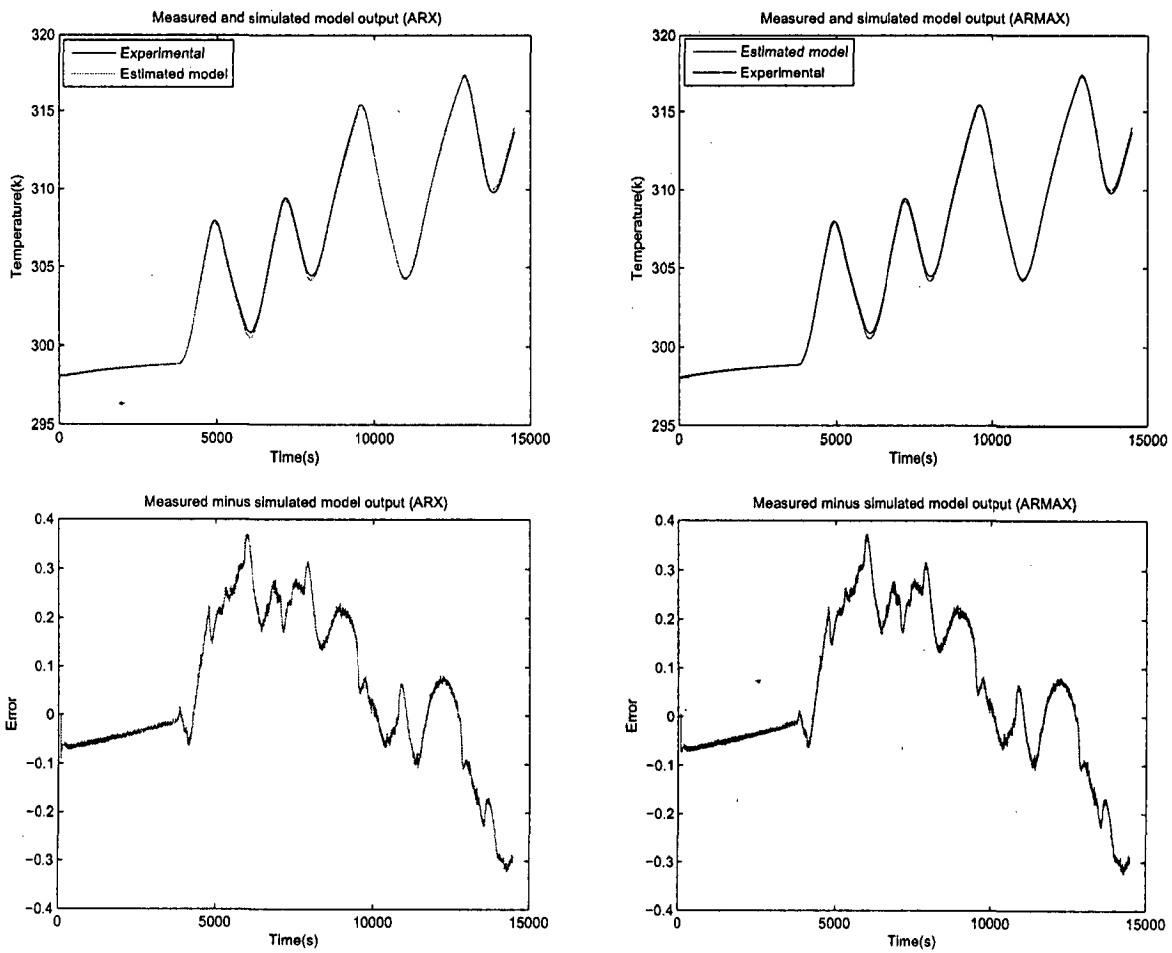


Figure 6.33: Validation 3 for *ARX* and *ARMAX* model.

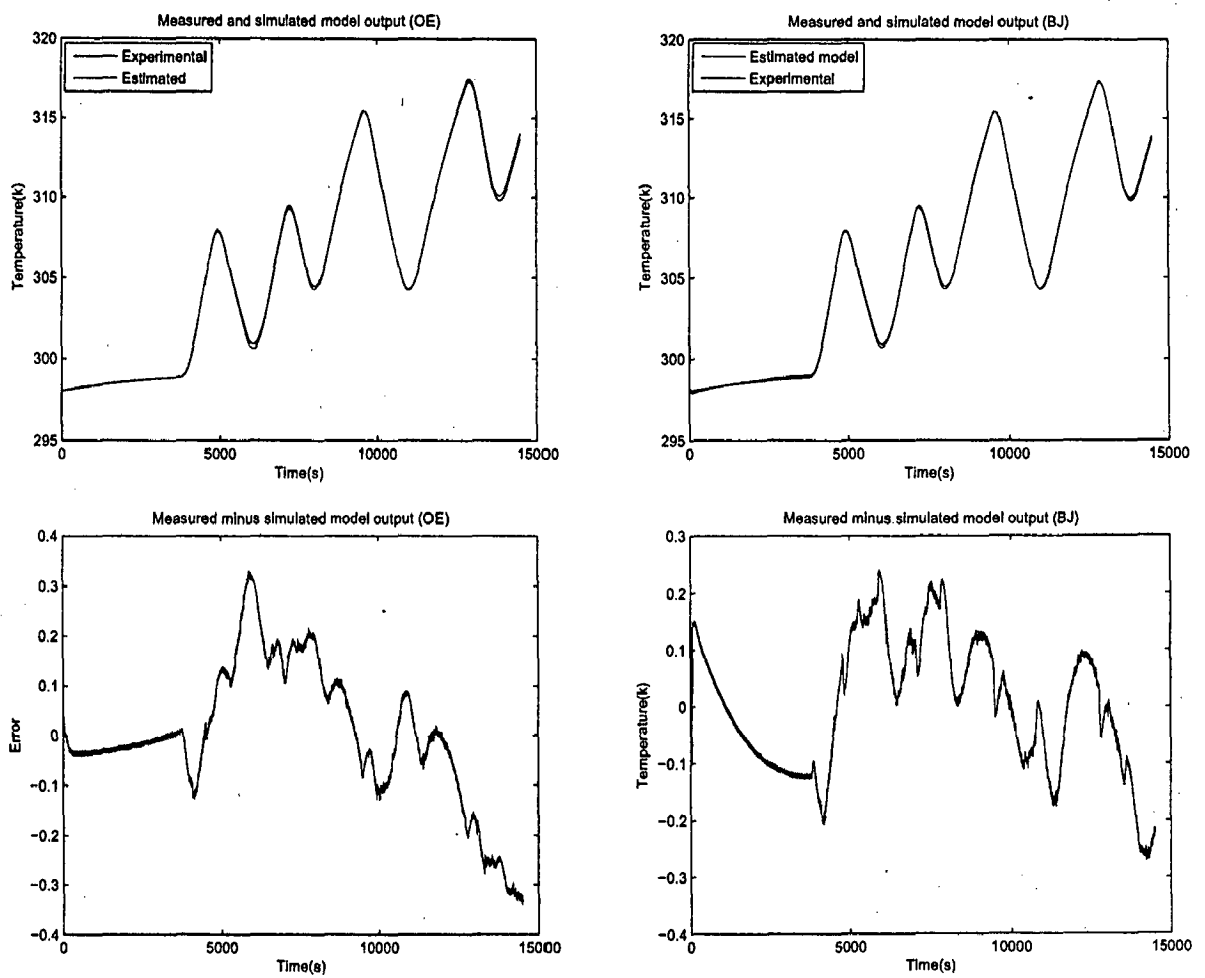
Figure 6.34: Validation 3 for *OE* and *BJ* model.

Table 6.2: Comparison of the system identification methods

Model	Estimation from experiment1					Estimation from experiment2				
	LF	FPE	Fit			LF	FPE	Fit		
			V1	V2	V3			V1	V2	V3
	10^{-5}	10^{-5}				10^{-5}	10^{-5}			
<i>ARX</i> [2240]	2.82863	2.83192	96.82	57.5	68.45	1.87367	1.87574	91.53	90.91	97.28
<i>ARMAX</i> [22140]	2.81107	2.8489	97.05	57.4	68.05	1.80165	1.82467	91.54	90.91	97.23
<i>OE</i> [2218] [2215]	2357.89	2373.71	99.23	71.83	82.88	1903.6	1914.13	92.89	91.3	97.64
<i>BJ</i> [222240]	59.9107	60.8053	98.63	89.42	86.57	36.425	36.7883	93.68	91.94	98.01
<i>P2DZ</i>	2613.7	2617.5	98.18	53.22	66.29	3173.15	1177.53	92.66	89.9	Low
<i>P3DZ</i>	2012.82	2016.33	99.07	53.71	66.6	2003.05	2006.37	94.82	90.8	Low

6.4 Linear model of the system

The table 6.2 show that the *ARX* model have lowest value of the loss function and *FPE* and it also fit good to the experimental result hence this model is taken for further consideration. The linear model is given as:

$$\frac{d^2y}{dt^2} + a\frac{dy}{dt} + by = c\frac{du}{dt} + du \quad (6.2)$$

Where *u*, and *y* represents the input and output signal respectively. In the system under consideration *u* is the thermostat setpoint temperature and *y* is the reactor temperature. coefficients *a*, *b*, *c*, *d* are given in the appendix A.2

6.5 Temperature trajectory optimization

6.5.1 Optimization alone

The thermostat setpoint temperature profile is obtained by the minimization of the area between the desired reactor temperature profile and the actual reactor temperature profile, using the dynamic optimization routine of gPROMS. In the linear model the optimized reactor temperature profile shows good agreement with the desired reactor temperature profile, which is shown in figure 6.35. The difference of the optimized reactor temperature trajectory and the desired reactor temperature trajectory is shown in figure 6.36.

The experiment is performed using an optimized setpoint temperature profile of the thermostat and the obtained reactor temperature profile is shown in figure 6.37. The experimental reactor temperature profile is not showing good agreement with the desired reactor temperature profile. In figure 6.37 it can be seen that the reactor temperature deviates more during the start of the cooling of the reactor fluid, may be in this region the linear model does not fit the system very well.

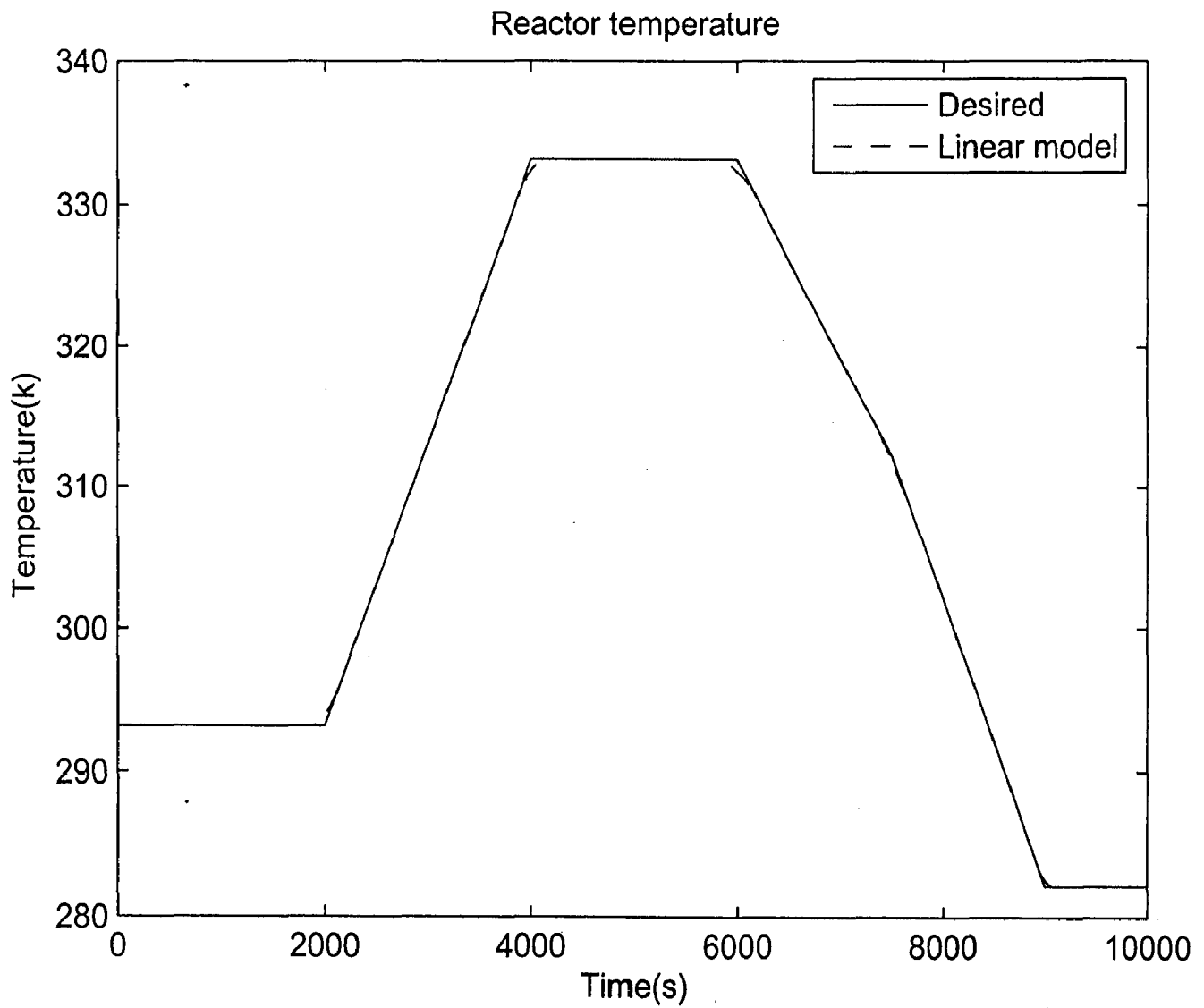


Figure 6.35: *Deviation of optimize reactor temperature trajectory from the desired reactor temperature in the linear model*

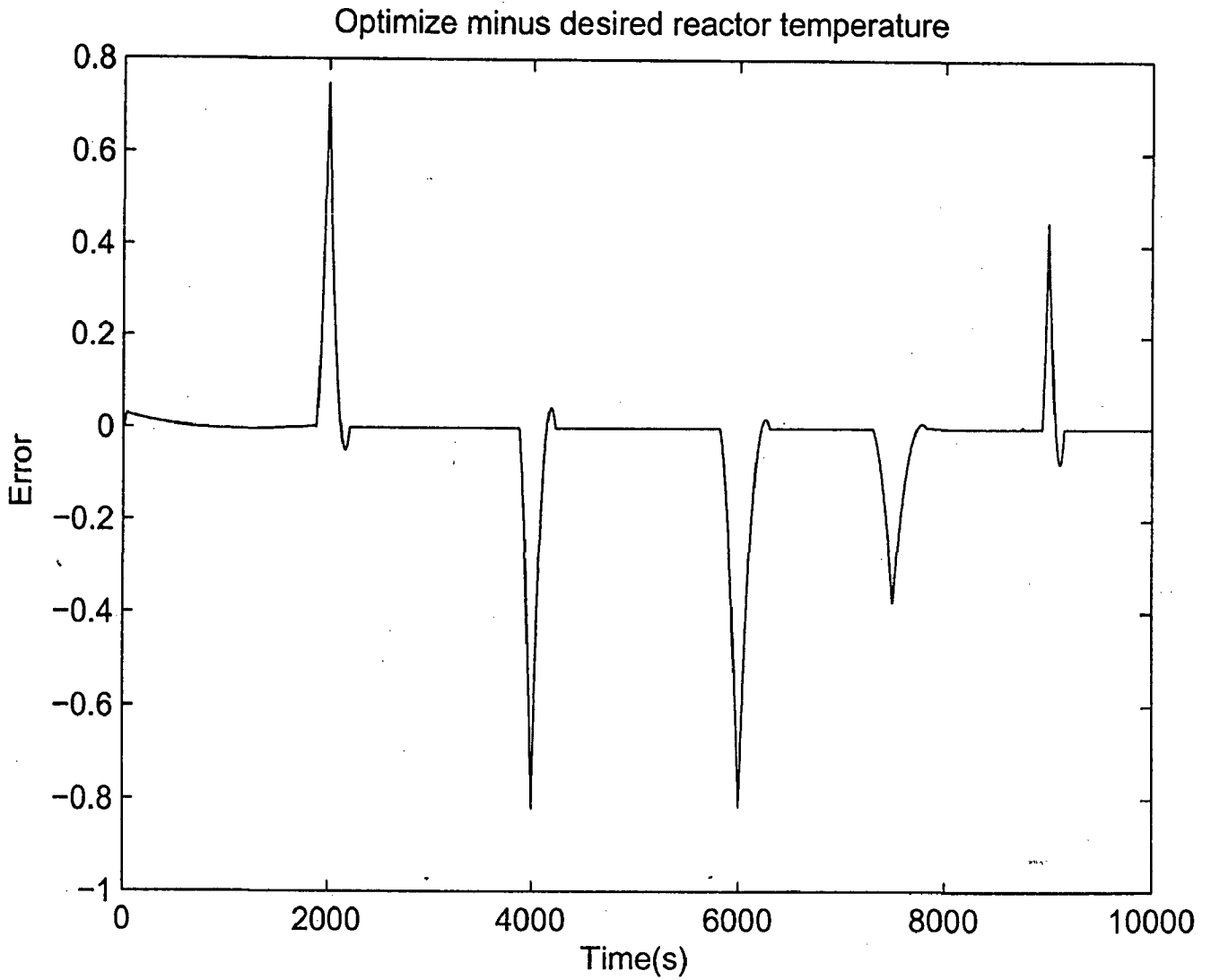


Figure 6.36: *Difference of the the optimize reactor temperature trajectory in the linear model and desired reactor temperature trajectory*

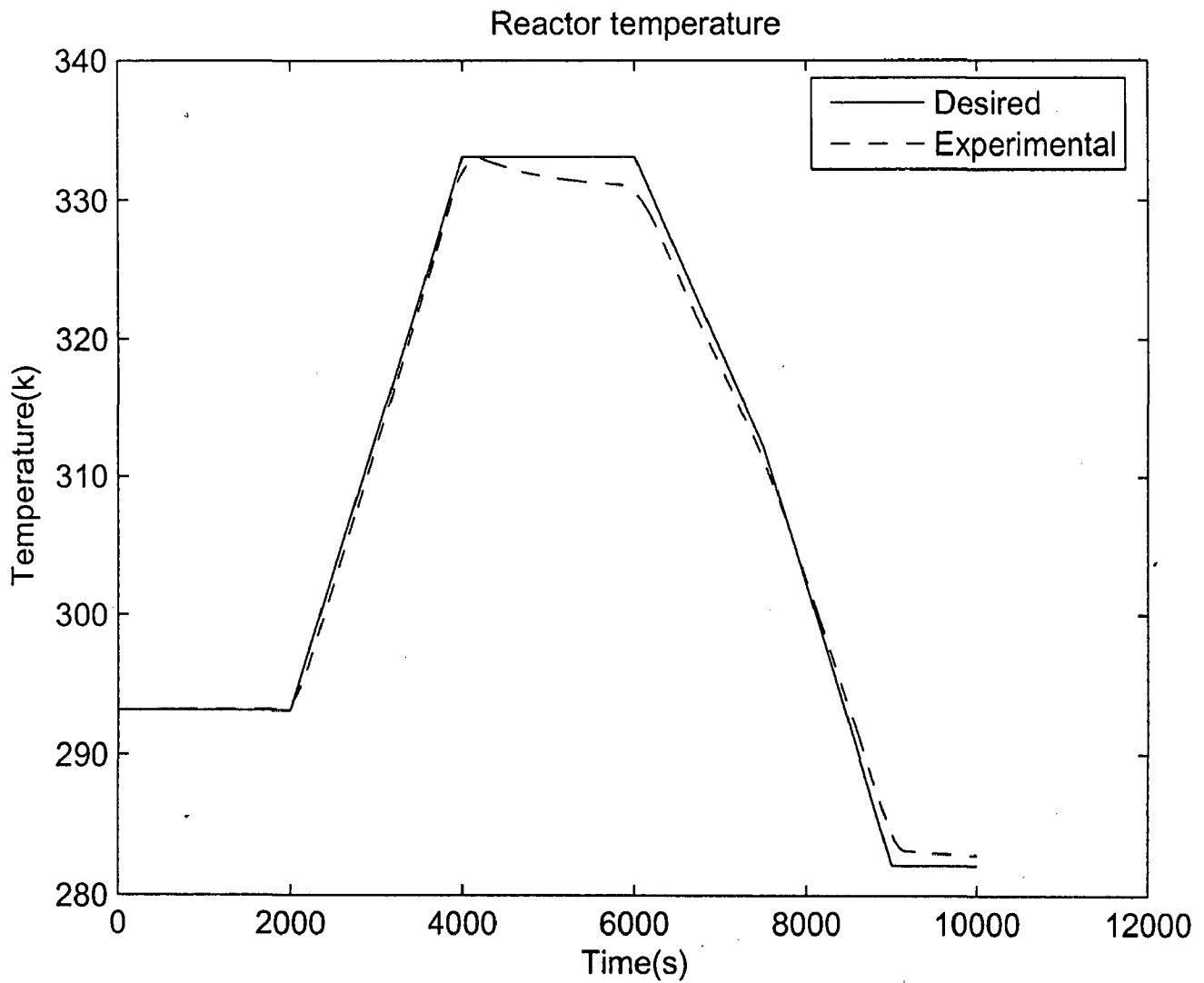


Figure 6.37: Deviation of the experimental reactor temperature trajectory from the desired reactor temperature trajectory

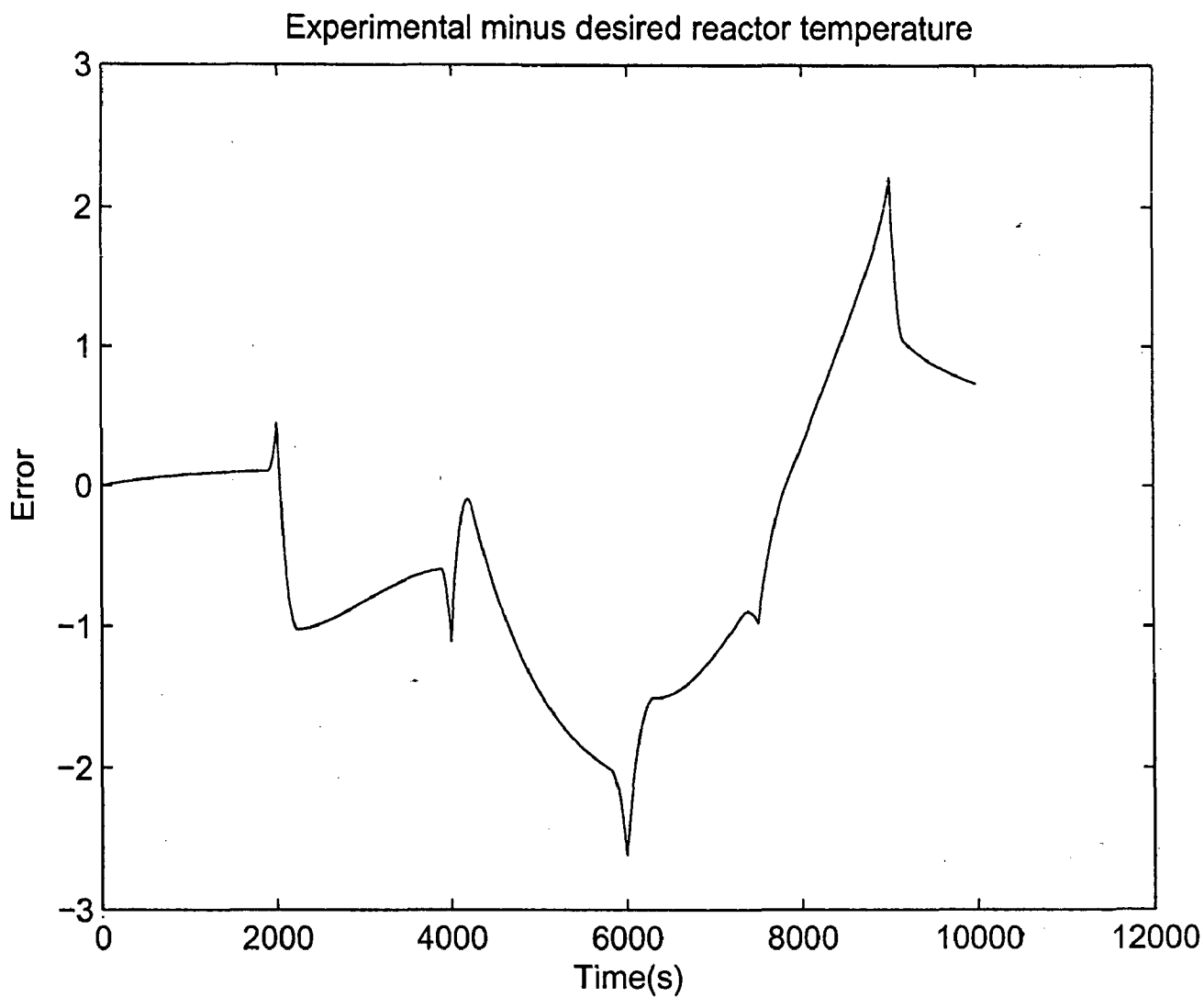


Figure 6.38: *Difference of the experimental reactor temperature trajectory and desired reactor temperature trajectory*

6.5.2 Optimization with addition *PID*

The result of the desired reactor temperature tracking by optimization is very sensitive towards ambient temperature, system conditions, system identification error. To accommodate these factors during the experiment and to ensure the exact tracking of the prespecified reactor temperature profile online adjustment of the optimized setpoint temperature of the thermostat is needed. The external *PID* controller is used to adjust the prespecified setpoint temperature of the thermostat (setpoint temperature of the internal controller). In order to achieve the desired reactor temperature trajectory, the setpoint temperature trajectory of the internal controller is adjusted online which is shown in figure 6.39.

The external *PID* controller is implemented in the model. The experimental reactor temperature trajectory obtained by using optimization and an additional *PID* controller both is compared with that obtained by the mathematical model in figure 6.40. A good agreement between the experimental result and the mathematical model is shown. The difference of the experimental and mathematical model's result can be seen in figure 6.41 which is negligible.

The *ITAE* criteria is used for the tuning of the controller parameters. *gOPT* is used as an optimization tool. Due to the complexity of the model the optimization time is about 30 hours which is impracticable. In order to tune the controller parameters with *gOPT*, the same external *PID* controller is also implemented in the linear model. The external *PID* controller in the linear model is also showing good agreement with the experimental result which can be seen in figure 6.42. The difference of the experimental and the linear model result is shown in figure 6.43.

The experimental reactor temperature trajectory obtained by using optimization and *PID* controller both is compared with the desired reactor temperature profile in figure 6.44. The figure shows that the reactor temperature tracks the prespecified reactor temperature profile very well. The difference of the experimental reactor temperature trajectory and the prespecified temperature trajectory is shown in figure 6.45. The difference is so less that it can be tolerated.

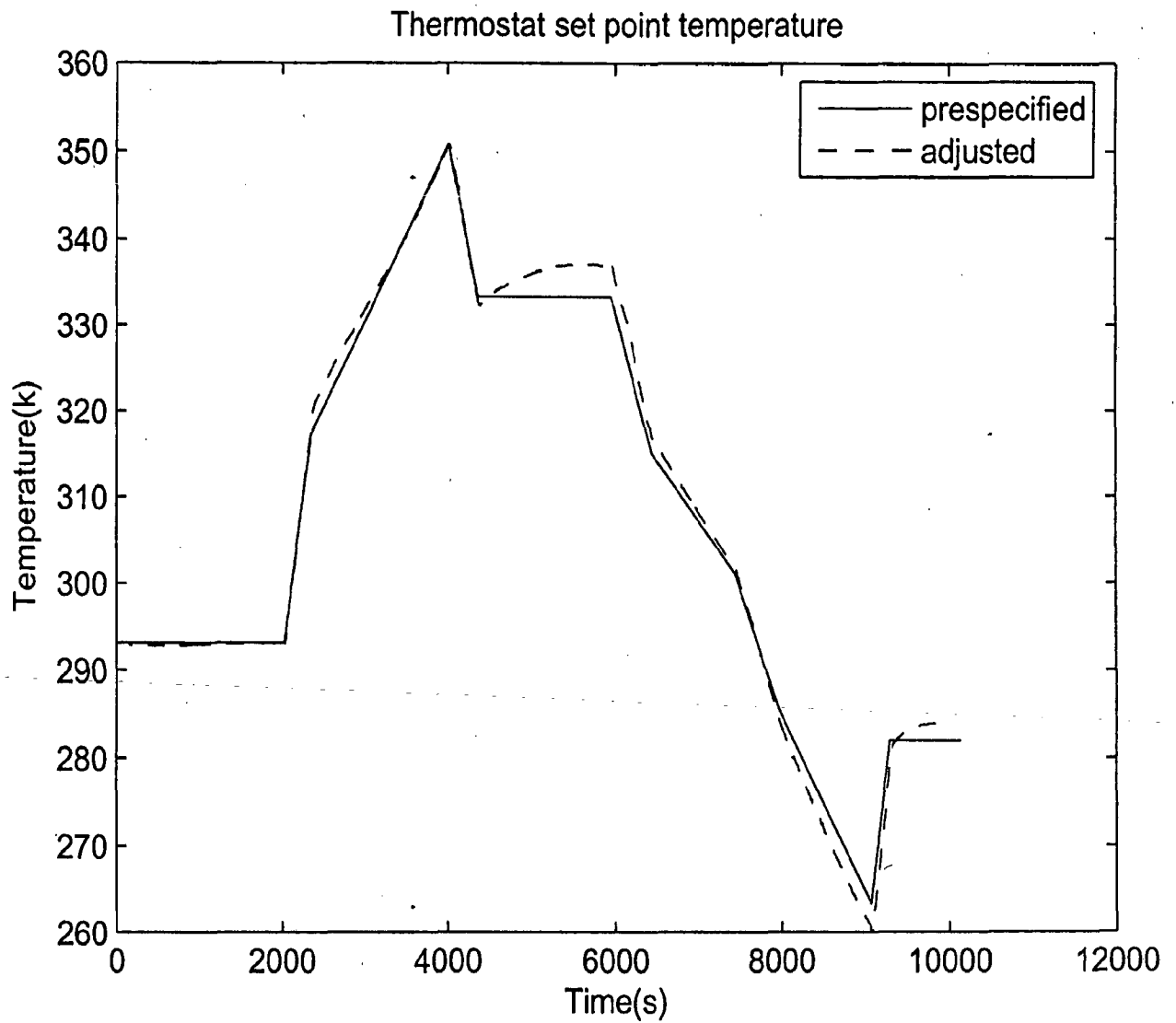


Figure 6.39: *Online adjusted and prespecified setpoint temperature trajectory of internal controller*

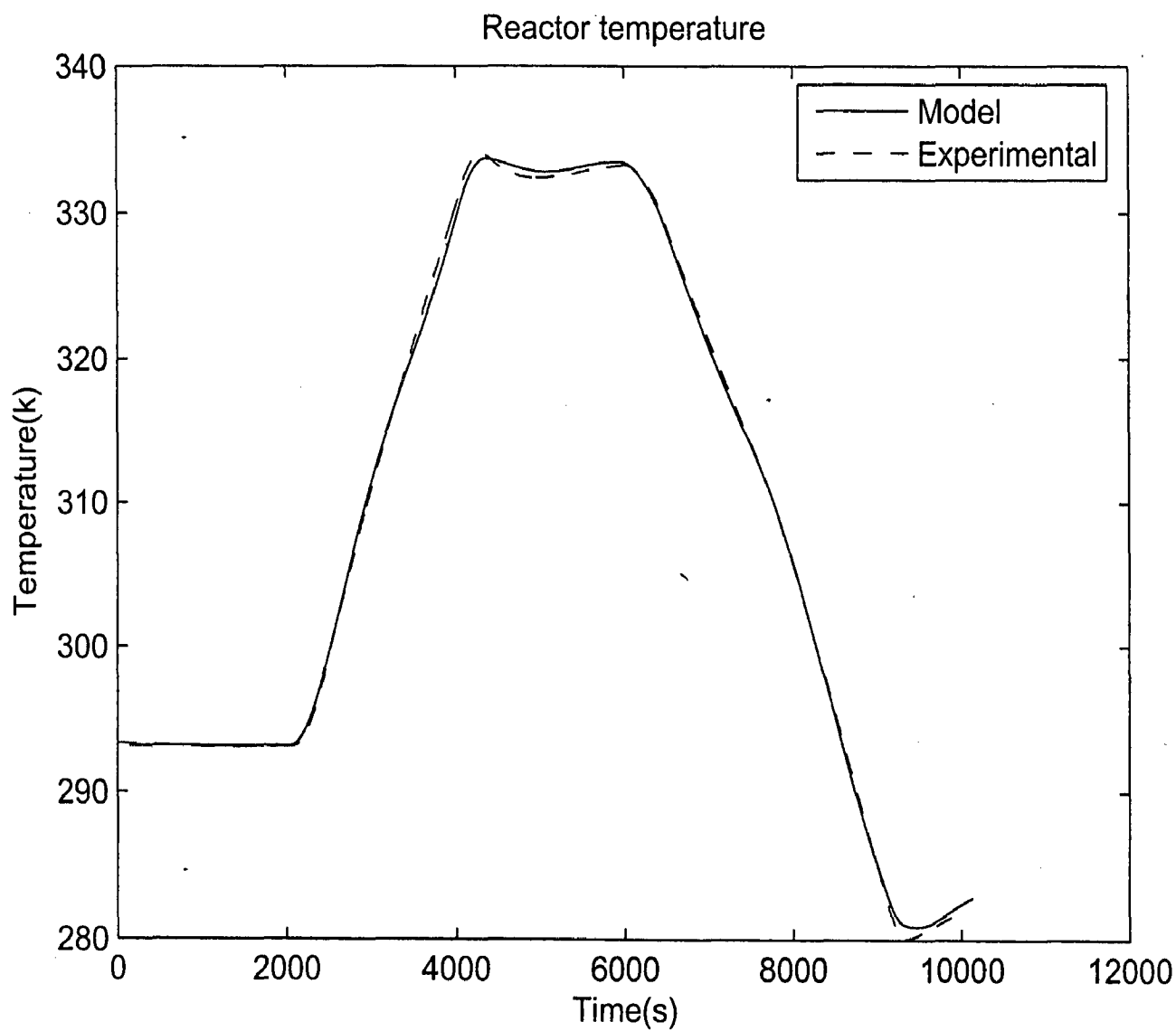


Figure 6.40: *Deviation of experimental reactor temperature trajectory from the model*

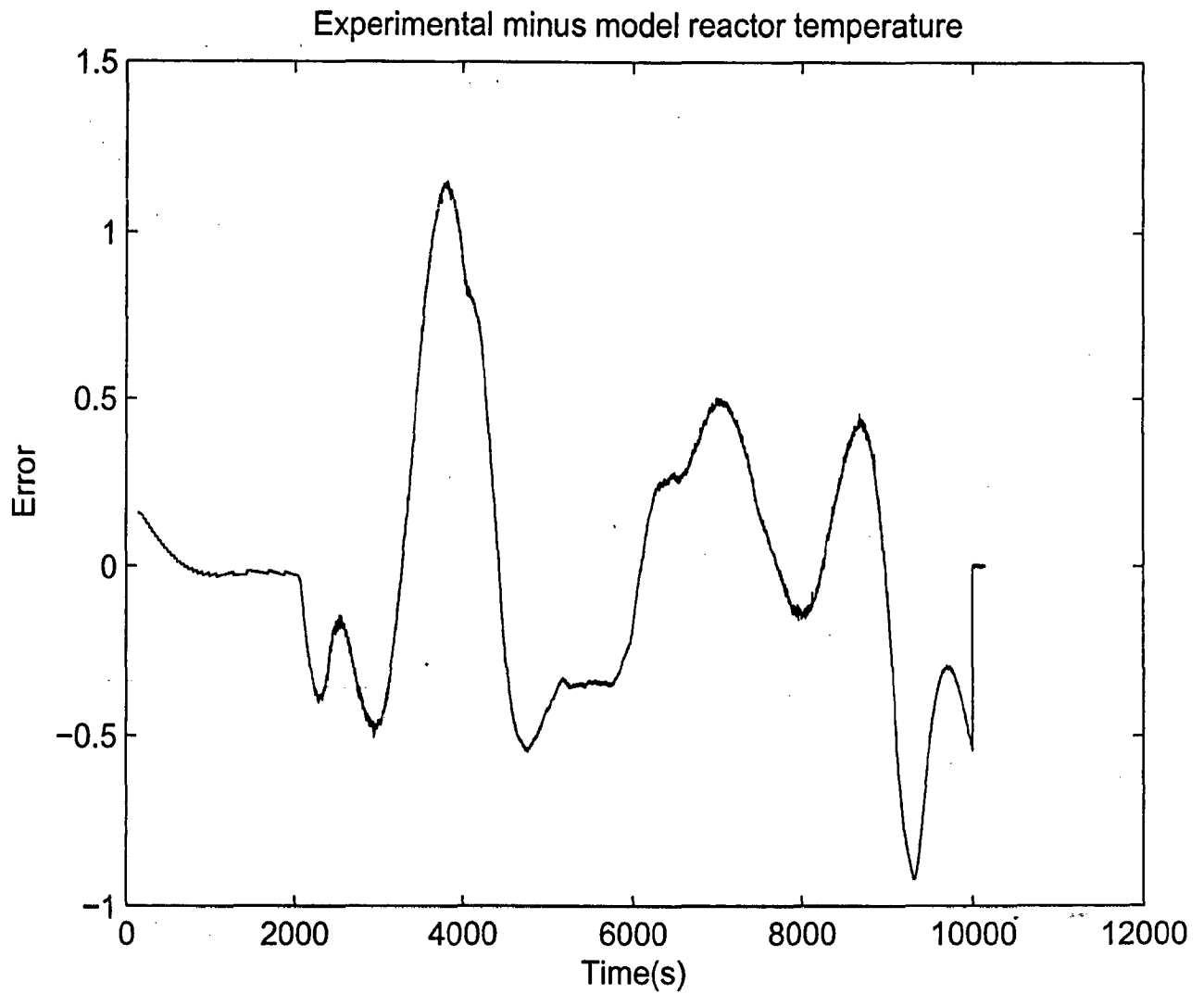


Figure 6.41: *Difference of the the experimental reactor temperature trajectory and the modeled reactor temperature trajectory*

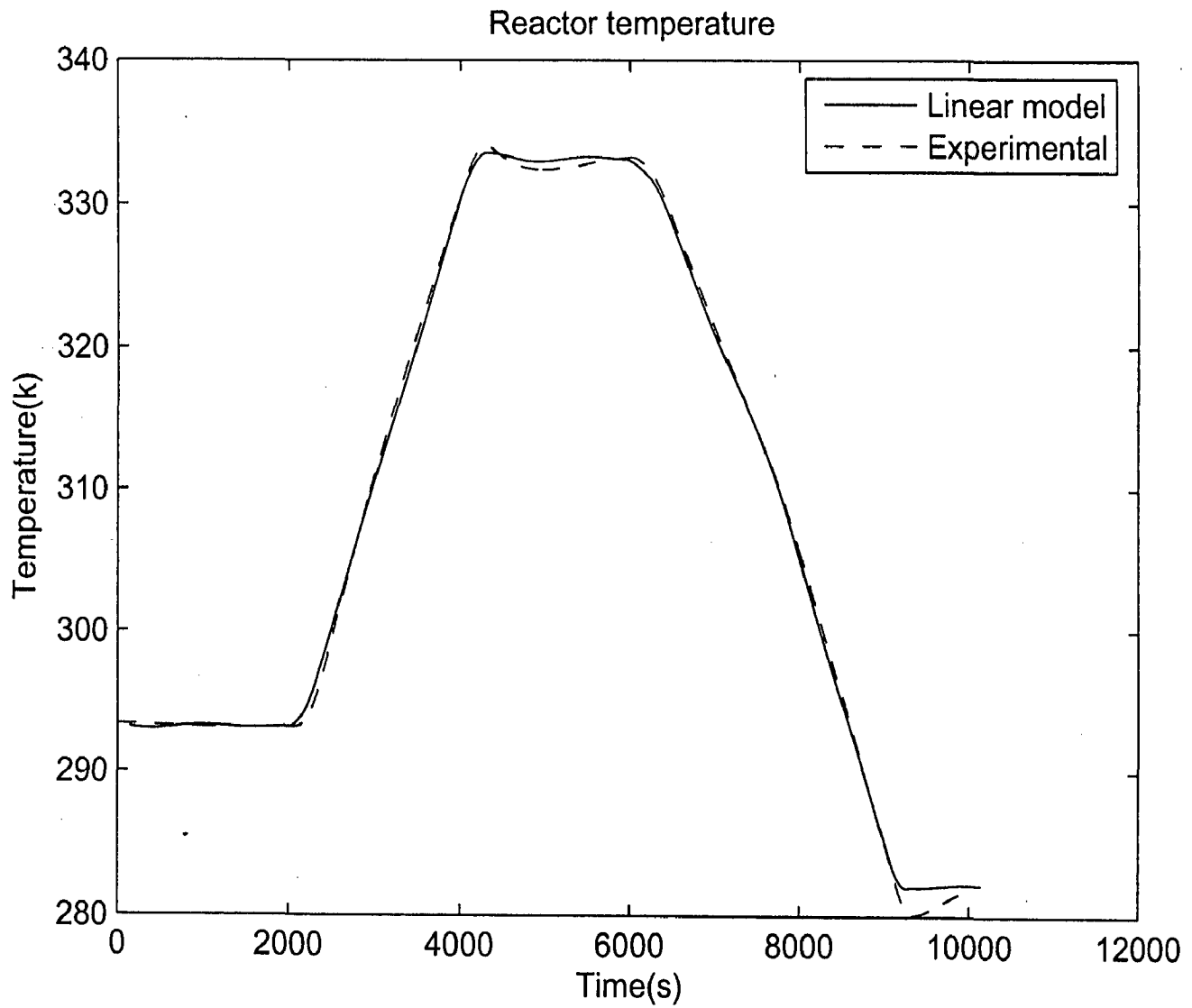


Figure 6.42: *Deviation of the experimental reactor temperature trajectory from the linear model*

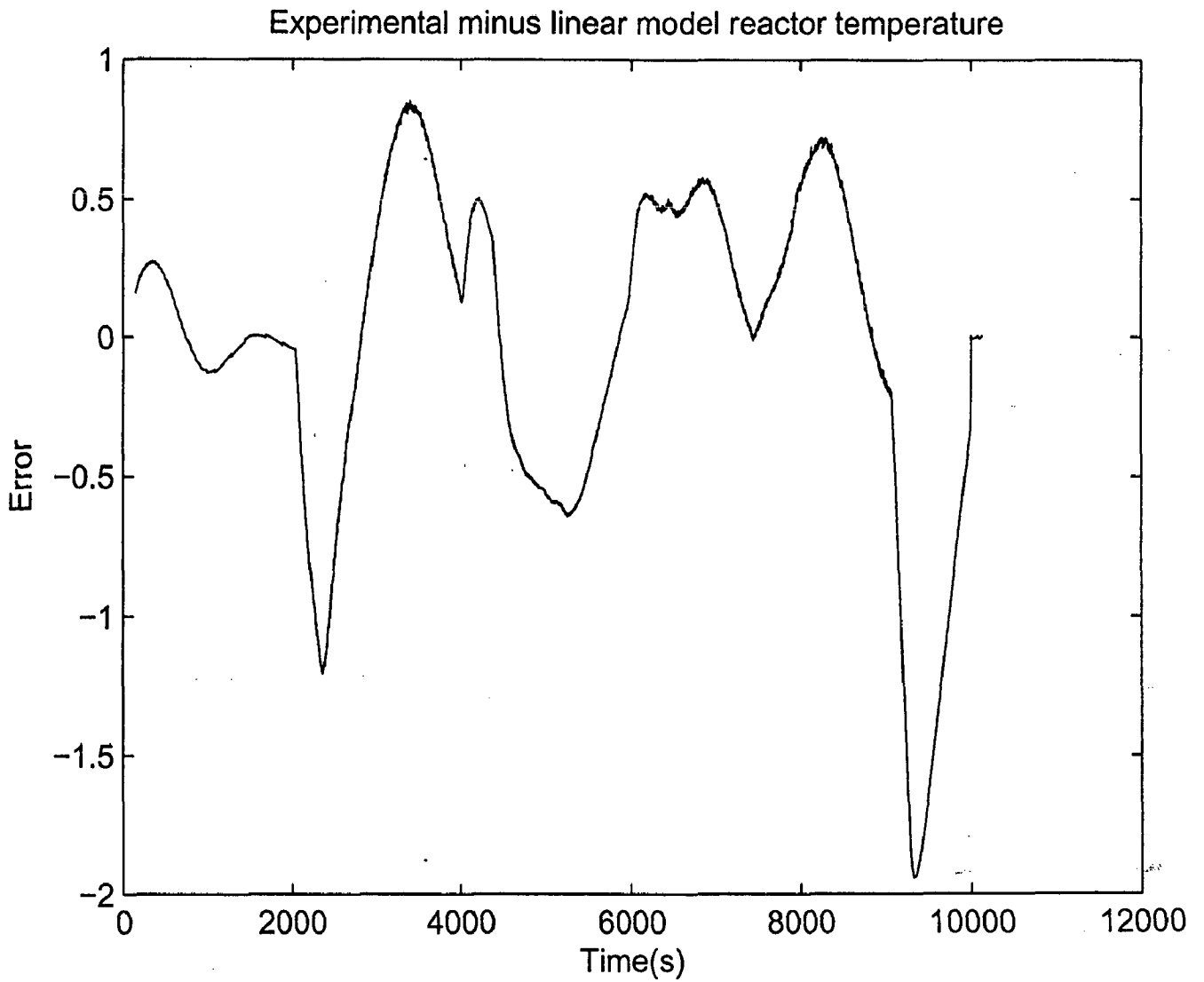


Figure 6.43: *Difference of the experimental reactor temperature trajectory and the linear model reactor temperature trajectory*

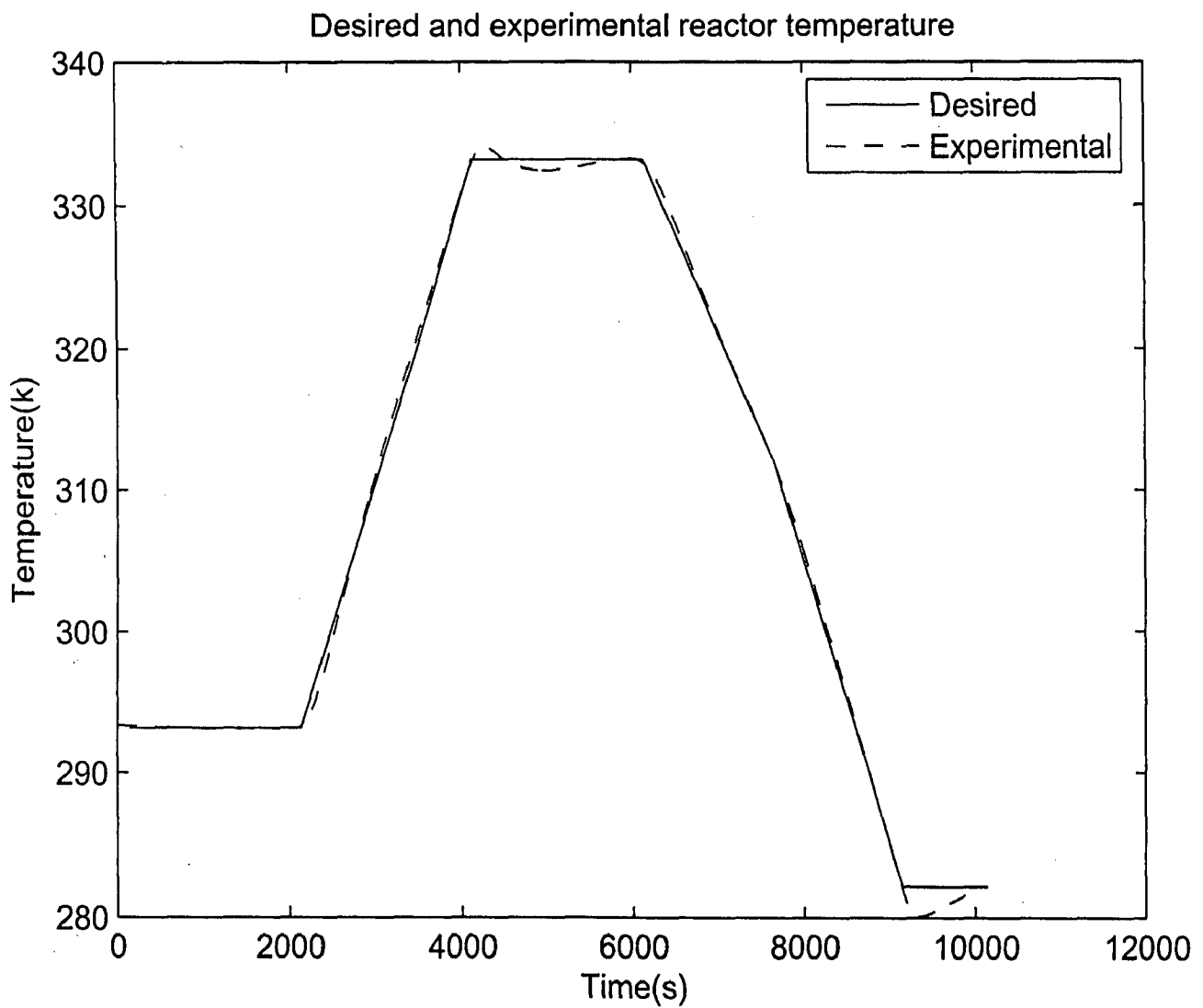


Figure 6.44: *Deviation of the experimental reactor temperature trajectory from the desired reactor temperature trajectory*

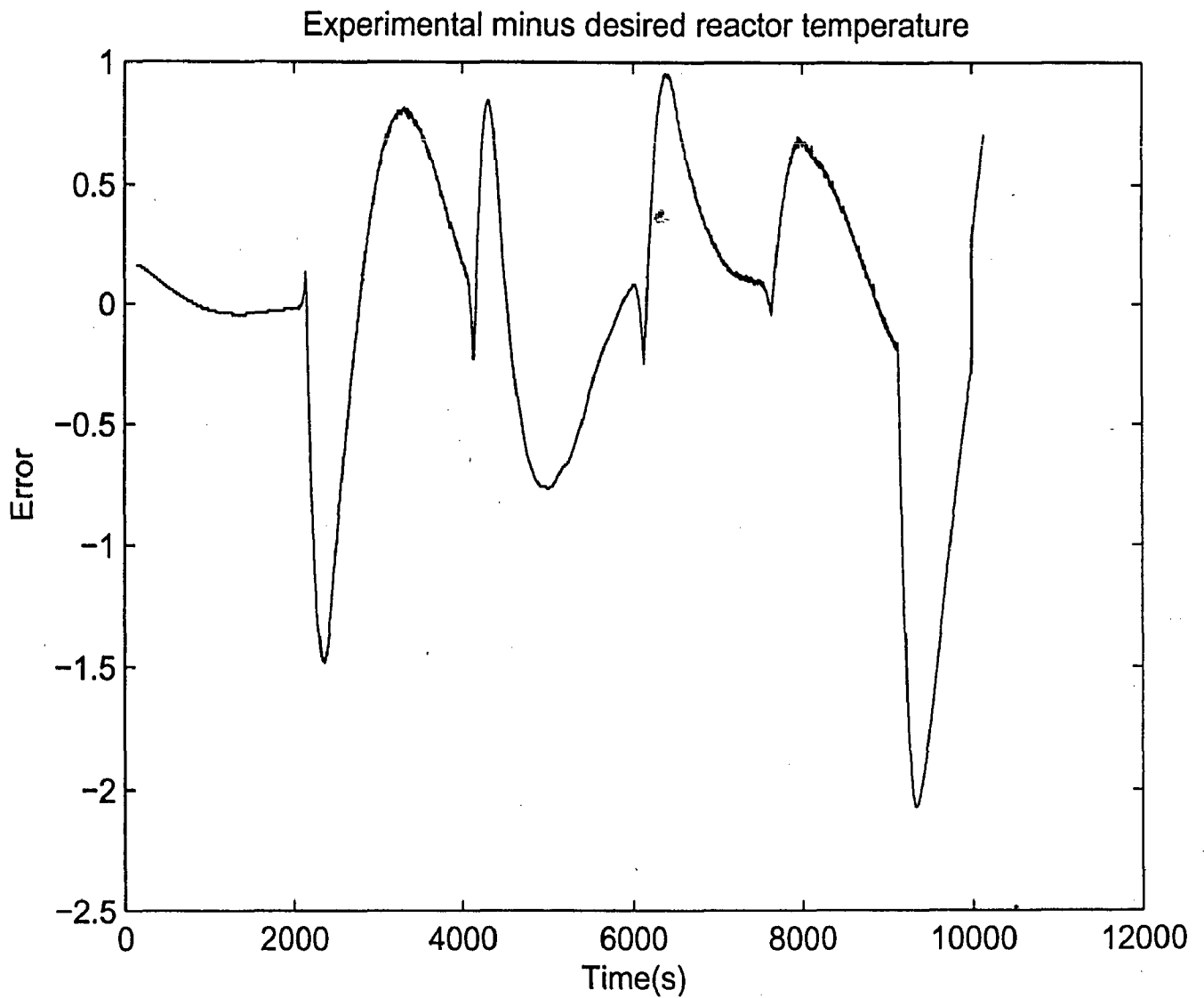


Figure 6.45: *Difference of the the experimental reactor temperature trajectory and the desired reactor temperature trajectory*

6.5.3 Controller alone

In order to show the importance of temperature trajectory optimization, an experiment is performed without optimization. The setpoint of the thermostat temperature is fixed as a constant value and the external *PID* controller is allowed to adjust the thermostat setpoint temperature in order to track the prespecified reactor temperature trajectory. The experimental result is shown in figure 6.46. The figure shows a large deviation of the experimental reactor trajectory from the desired reactor trajectory hence temperature trajectory optimization is essential for exact tracking of the desired reactor temperature.

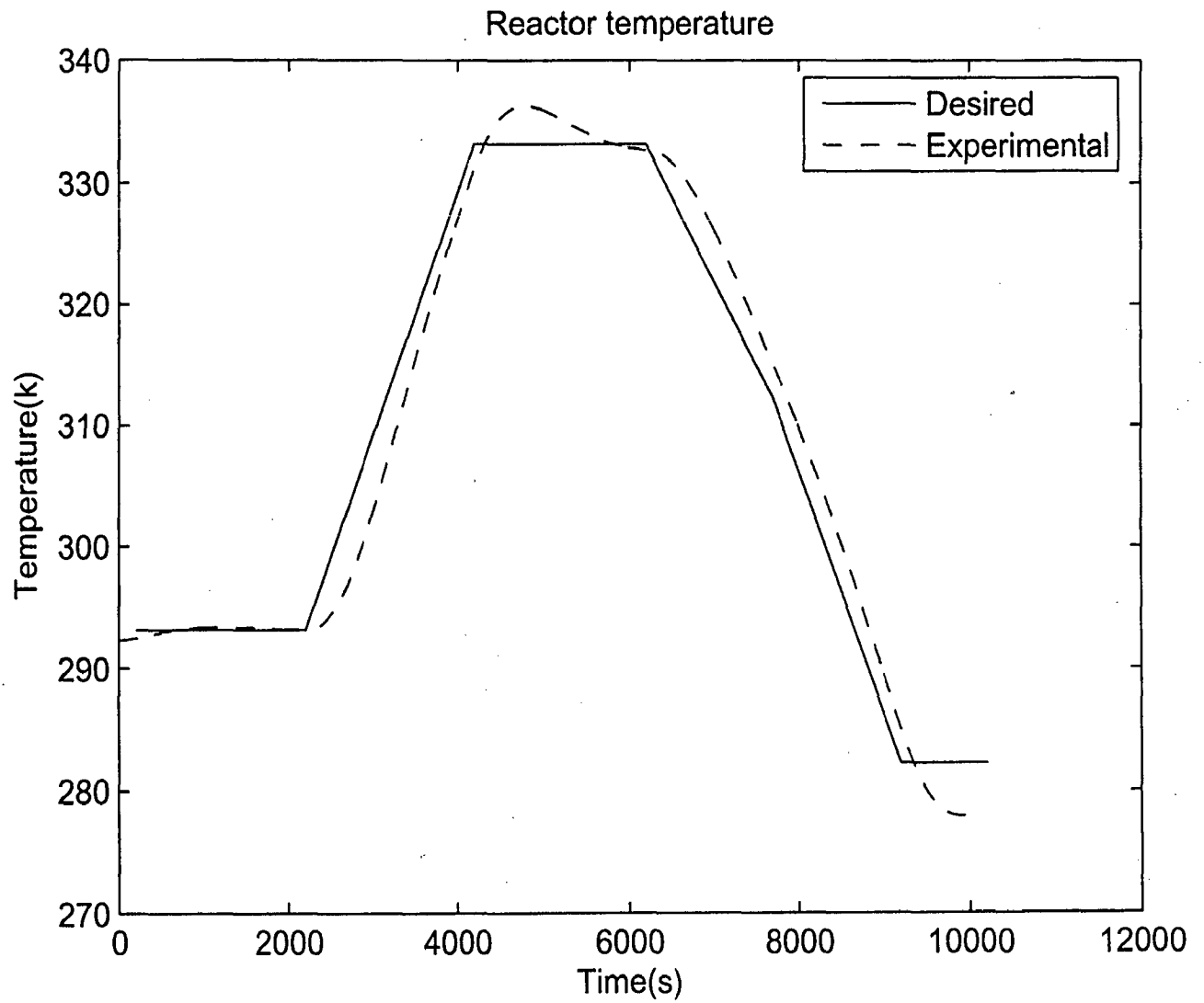


Figure 6.46: Deviation of the experimental reactor temperature trajectory from the desired reactor temperature trajectory

Chapter 7

Case study

A case study is performed to show the transformation of α form of L-Glutamic acid to the β form.

7.1 Model

There are two phases, the solid crystalline phase and the solution phase. The α form is dissolving in the solution phase while β form is crystallizing. The change in the mole of the solution is governed by the following equation:

$$\frac{dM_f}{dt} = M_f \cdot Y \quad (7.1)$$

Where M_f is the total mole of the solution, Y is a variable given as:

$$Y = -0.5 \frac{\rho_\alpha}{\rho} \cdot A_{\alpha_s} \cdot (G_\alpha - D_\alpha) - \frac{\rho_\alpha}{\rho} \cdot K_v \cdot Ln_\alpha^3 \cdot B_\alpha - 0.5 \frac{\rho_\beta}{\rho} \cdot A_{\beta_s} \cdot (G_\beta - D_\beta) - \frac{\rho_\beta}{\rho} \cdot K_v \cdot Ln_\beta^3 \cdot B_\beta \quad (7.2)$$

Where G is the crystal growth rate, B is the nucleation rate, D is the dissolution rate. ρ , ρ_α and ρ_β are molar density of the solution, α form and the β form respectively. A_{α_s} and A_{β_s} are specific surface area of the α and the β form which are given as:

$$A_{\alpha_s} = \frac{A_\alpha}{V} \quad (7.3)$$

$$A_{\beta_s} = \frac{A_\beta}{V} \quad (7.4)$$

Where V is the magma volume. A_α and A_β are the total surface area of the α and β form respectively.

Growth rate

The growth rate of the α form is given as:

$$G_{\alpha} = k_{g\alpha} \cdot S_{\alpha}^g \quad (7.5)$$

Where $k_{g\alpha}$ is the growth rate constant of α form and S_{α} is the supersaturation of α form.

The growth rate of the β form is given as:

$$G_{\beta} = k_{g\beta} \cdot S_{\beta}^g \quad (7.6)$$

Where $k_{g\beta}$ is the growth rate constant of β form and S_{β} is the supersaturation of β form.

Nucleation rate

The nucleation rate of the α form is given as:

$$B_{\alpha} = k_{n\alpha} \cdot S_{\alpha}^n \quad (7.7)$$

Where $k_{n\alpha}$ is the nucleation rate constant of α and n is the nucleation order.

The nucleation rate of the β form is given as:

$$B_{\beta} = k_{n\beta} \cdot S_{\beta}^n \quad (7.8)$$

Where $k_{n\beta}$ is the nucleation rate constant of β

Dissolution rate

Dissolution rate of the α form is given as:

$$D_{\alpha} = k_{d\alpha} \cdot S_{\alpha}^d \quad (7.9)$$

$$D_{\beta} = k_{d\beta} \cdot S_{\beta}^d \quad (7.10)$$

Where $k_{d\alpha}$ and $k_{d\beta}$ is the dissolution rate constant of α and β form and d is the dissolution order.

Supersaturation

The supersaturation of the α form is given as:

- If $M_\alpha > 0$

$$S_\alpha = \frac{-(x - x_{\alpha_{sat}})}{x_{\alpha_{sat}}} \quad (7.11)$$

- If $M_\alpha \leq 0$

$$S_\alpha = 0 \quad (7.12)$$

The supersaturation of the β form is given as:

- If $x > x_{\beta_{sat}}$

$$S_\beta = \frac{(x - x_{\beta_{sat}})}{x_{\beta_{sat}}} \quad (7.13)$$

- If $x \leq x_{\beta_{sat}}$

$$S_\beta = 0 \quad (7.14)$$

Where x is the mole fraction of solute in the solution, $x_{\alpha_{sat}}$ and $x_{\beta_{sat}}$ are the mole fraction of the α and β form in the solution at the saturation.

The mole fraction is related with the concentration by following equations:

$$x_{\alpha_{sat}} \cdot (18 \cdot (C_{\alpha_{sat}} + C_{\beta_{sat}}) + 147.13(100 - C_{\alpha_{sat}} - C_{\beta_{sat}})) = 18 \cdot C_{\alpha_{sat}} \quad (7.15)$$

$$x_{\beta_{sat}} \cdot (18 \cdot (C_{\alpha_{sat}} + C_{\beta_{sat}}) + 147.13(100 - C_{\alpha_{sat}} - C_{\beta_{sat}})) = 18 \cdot C_{\beta_{sat}} \quad (7.16)$$

Where $C_{\alpha_{sat}}$ and $C_{\beta_{sat}}$ are the mass concentration of the α and β form at the saturation which are governed by the following equations:

$$C_{\alpha_{sat}} = a_\alpha \cdot \text{EXP}(b_\alpha \cdot (T_r - 273.15)) \quad (7.17)$$

$$C_{\beta_{sat}} = a_\beta \cdot \text{EXP}(b_\beta \cdot (T_r - 273.15)) \quad (7.18)$$

Where T_r is the reactor temperature. Coefficients a_α , b_α , a_β , b_β are taken from the published literature [OtHJ04] and given in appendix E.

The mole fraction of the solute in the solution is given as:

$$\frac{dx}{dt} = Y \cdot (1 - x) \quad (7.19)$$

The mole fraction of the solvent in the solution is given as:

$$x_w = 1 - x \quad (7.20)$$

Total number of crystals

Number of the α and β form of the crystals are governed by the following equations:

$$\frac{dN_\alpha}{dt} = \frac{m_f}{\rho} \cdot B_\alpha \quad (7.21)$$

$$\frac{dN_\beta}{dt} = \frac{m_f}{\rho} \cdot B_\beta \quad (7.22)$$

Crystal size

Total length of the α and β form of the crystals are governed by the following equations:

$$\frac{dL_\alpha}{dt} = N_\alpha \cdot (L_{\alpha_n} + G_\alpha - D_\alpha) \quad (7.23)$$

$$\frac{dL_\beta}{dt} = N_\beta \cdot (L_{\beta_n} + G_\beta - D_\beta) \quad (7.24)$$

The average size of the α and β is given by following equations:

$$L_{\alpha_{avg}} = \frac{L_\alpha}{N_\alpha} \quad (7.25)$$

$$L_{\beta_{avg}} = \frac{L_\beta}{N_\beta} \quad (7.26)$$

Total surface area of the crystals

Surface area of the α and β form of the crystals are governed by the following equations:

$$\frac{dA_\alpha}{dt} = K_a \cdot N_\alpha \cdot (L_{\alpha_n})^2 + 2 \cdot L_\alpha \cdot (G_\alpha - D_\alpha) \quad (7.27)$$

$$\frac{dA_\beta}{dt} = K_a \cdot N_\beta \cdot (L_{\beta_n})^2 + 2 \cdot L_\beta \cdot (G_\beta - D_\beta) \quad (7.28)$$

Mole balance of the crystal polymorph

The change in the mole of the α and β form in the crystalline phase is governed by the following equations:

$$\frac{dM_\alpha}{dt} = \rho_\alpha \cdot k_v \cdot N_\alpha \cdot L_{\alpha_n}^3 + 3 \cdot \frac{A_\alpha}{k_a} (G_\alpha - D_\alpha) \quad (7.29)$$

$$\frac{dM_\beta}{dt} = \rho_\beta \cdot k_v \cdot N_\beta \cdot L_{\beta_n}^3 + 3 \cdot \frac{A_\beta}{k_a} (G_\beta - D_\beta) \quad (7.30)$$

7.2 Result

This model is implemented in the gPROMS. The value of the parameters, and initial conditions are given in appendix *E*. The simulation results shows good agreement with the published result in the literature [SN03]. In order to study the effect of seeding in the crystallization, the model is implemented for unseeded and seeded crystallization both.

Unseeded crystallization

In this case it is assume that no seed of the β form is present in the magma. The growth rate of the α form is also assumed to be negligible in compared to it's dissolution rate. Figure 7.1 shows the decrease in mole of α form in the solid crystalline phase. This figure also show the effect of, ratio of growth of β form and dissolution of α form on the molar change of α form in the solid crystalline phase. The change in mole of the β form is shown in figure 7.2 for the same ration of growth and dissolution rate constant. The change in supersaturation of β form is shown in figure 7.3

Seeded crystallization

In this case it is assumed that some seed of the β form is already present in the magma . Figure 7.4 shows the decrease in mole of α form in the solid crystalline phase. This figure also show the effect of, ratio of growth of β form and dissolution of α form on the molar change of α form in the solid crystalline phase. The change in mole of the β form is shown in figure 7.5 for the same ratio of growth and dissolution rate constant. The change in supersaturation of β form is shown in figure 7.6. On comparing the seeded crystallization with unseeded crystallization it can be seen that, seeding increases the dissolution rate of α form as well as growth rate of β form.

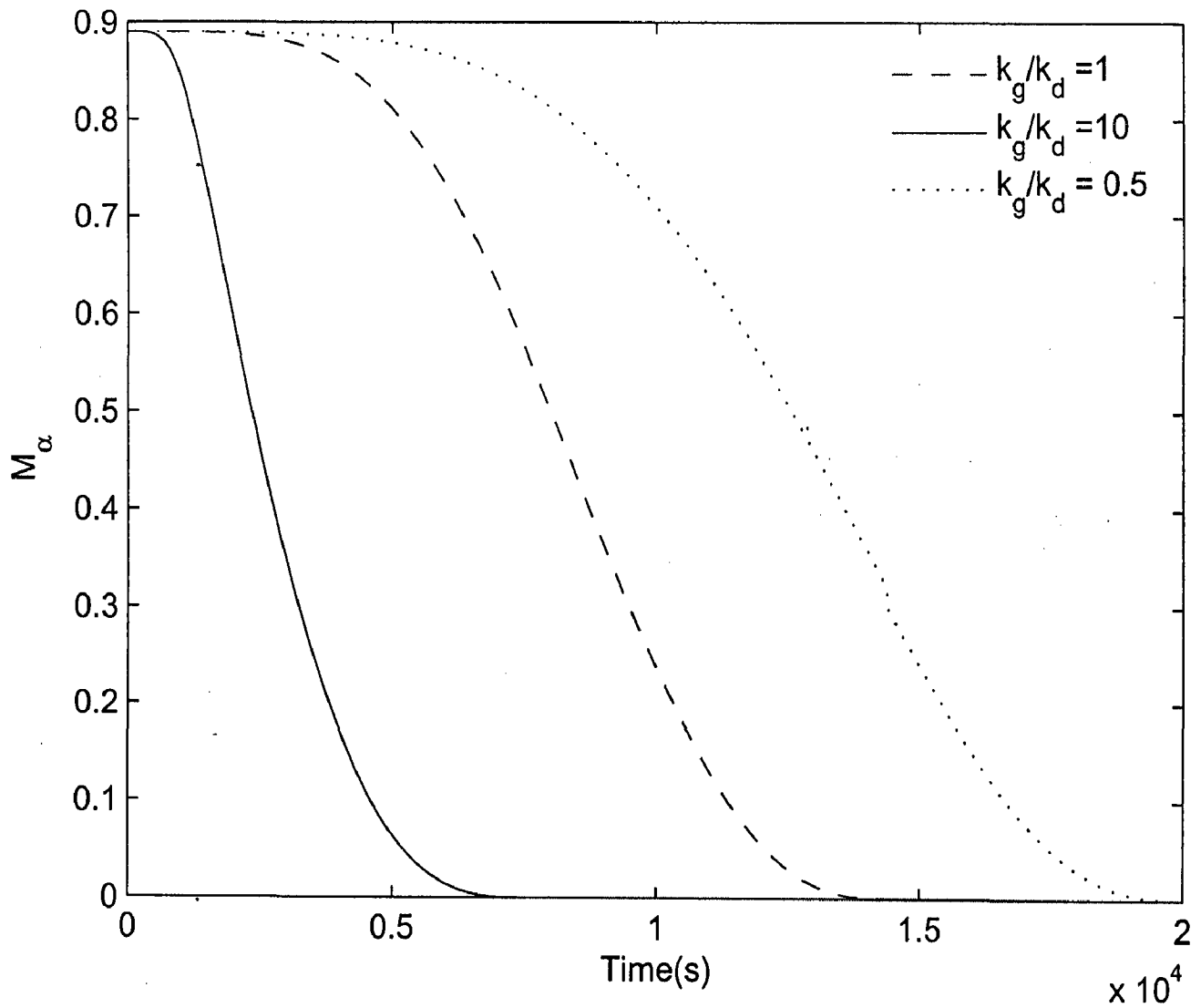


Figure 7.1: This graph shows the change in mole of α form of L-glutamic acid in unseeded crystallization

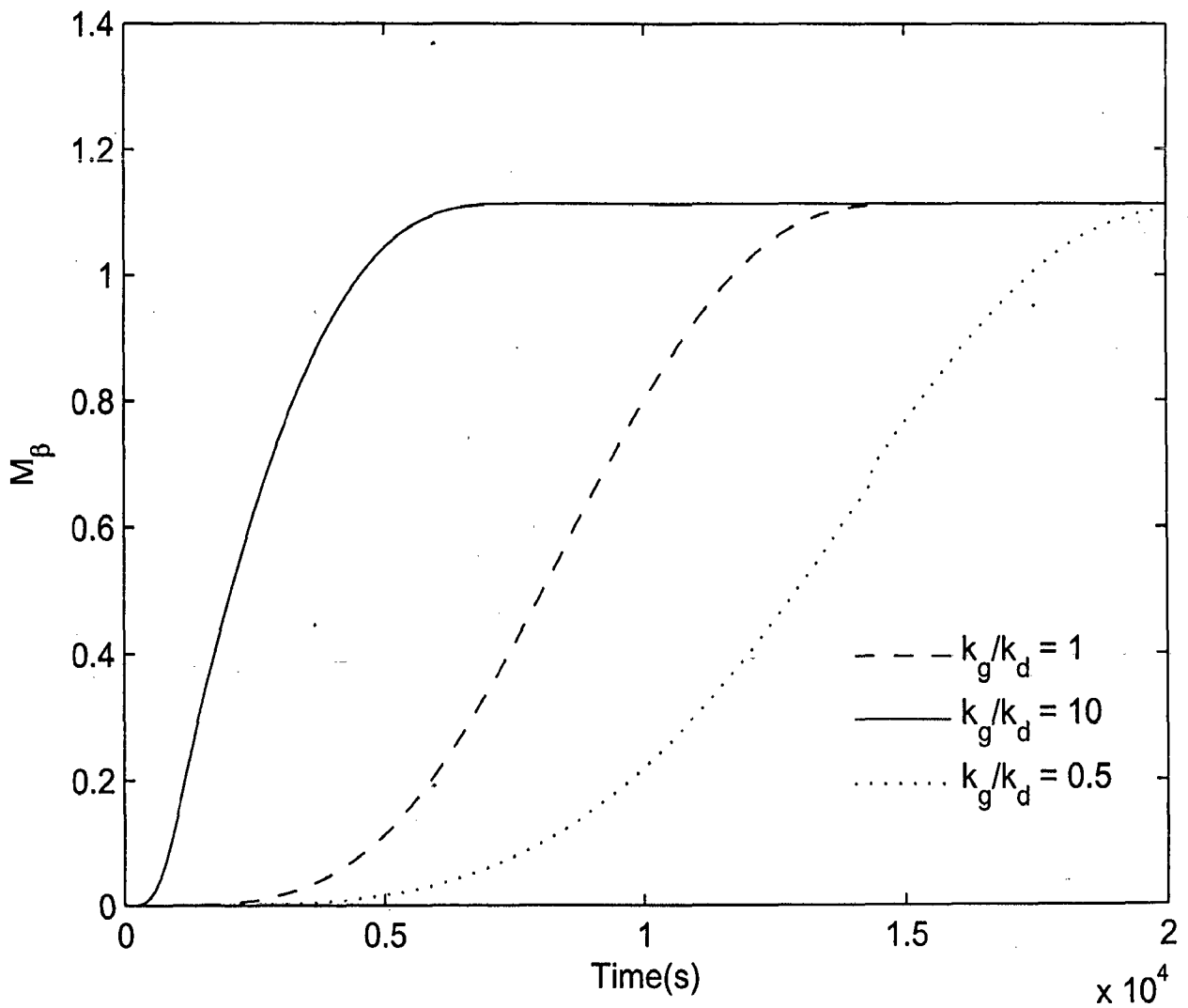


Figure 7.2: This graph shows the change in mole of β form of L-glutamic acid in unseeded crystallization

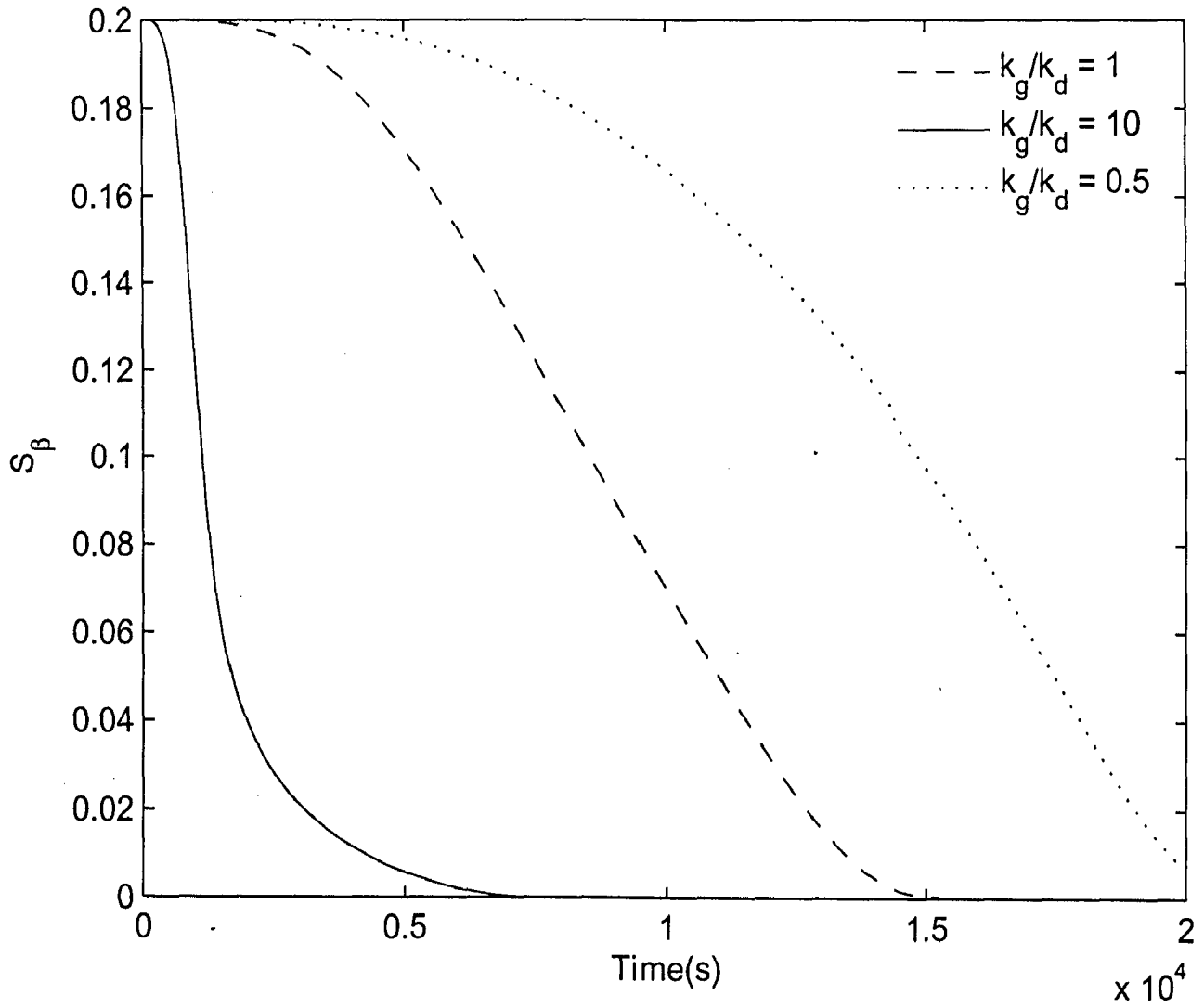


Figure 7.3: *Supersaturation of β form in unseeded crystallization*

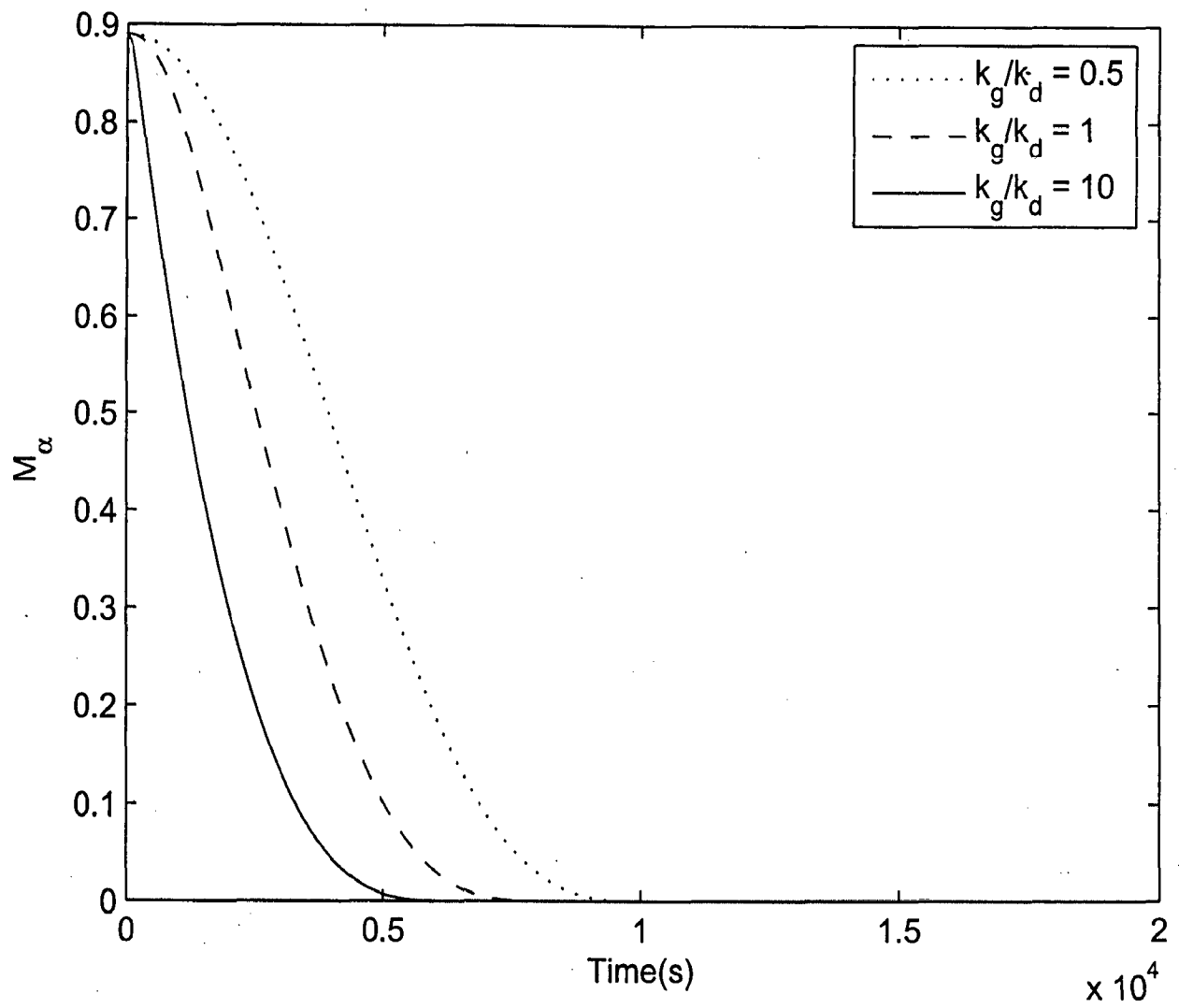


Figure 7.4: This graph shows the change in mole of α form of L-glutamic acid in seeded crystallization

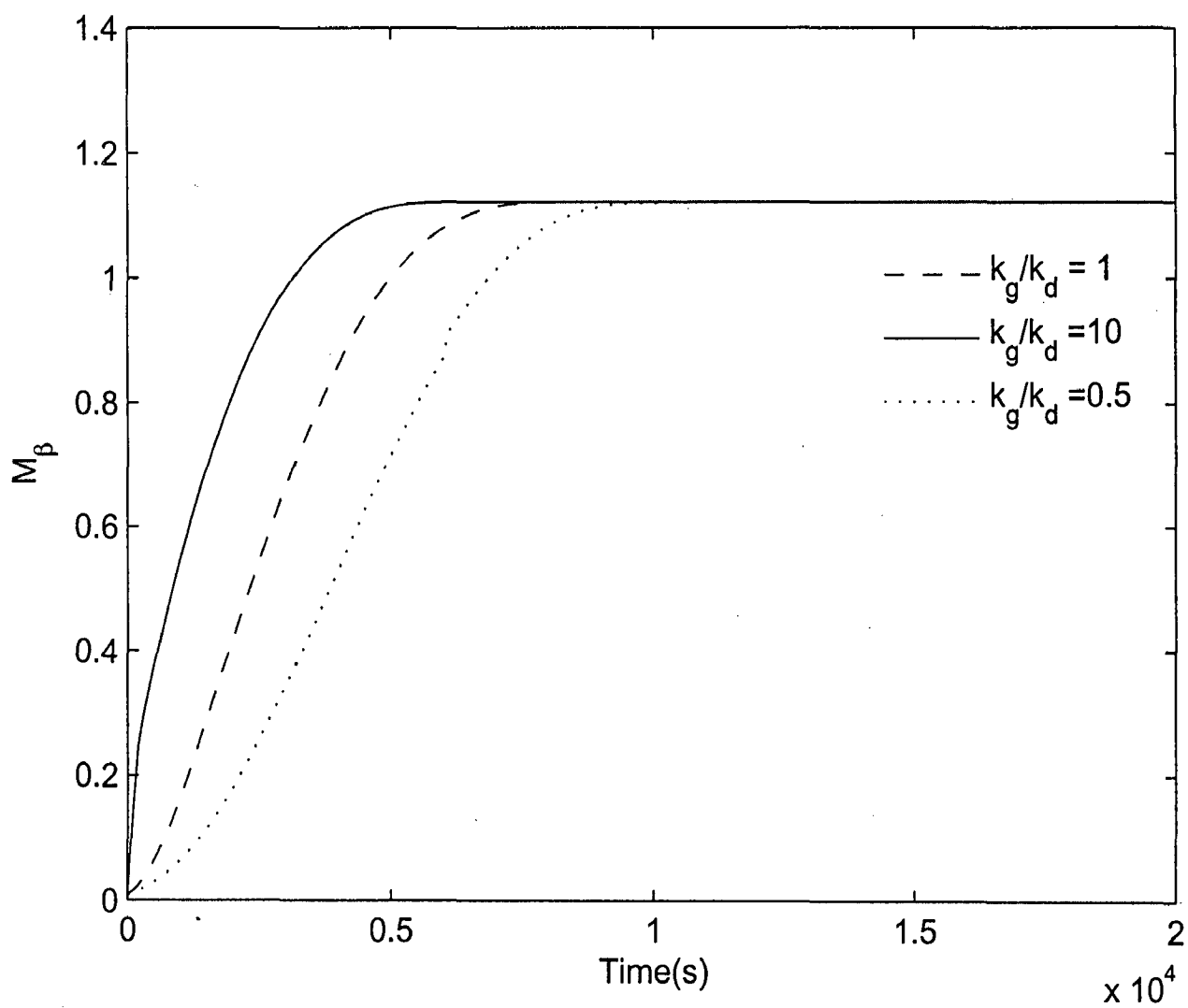


Figure 7.5: *This graph shows the change in mole of β form of L-glutamic acid in seeded crystallization*

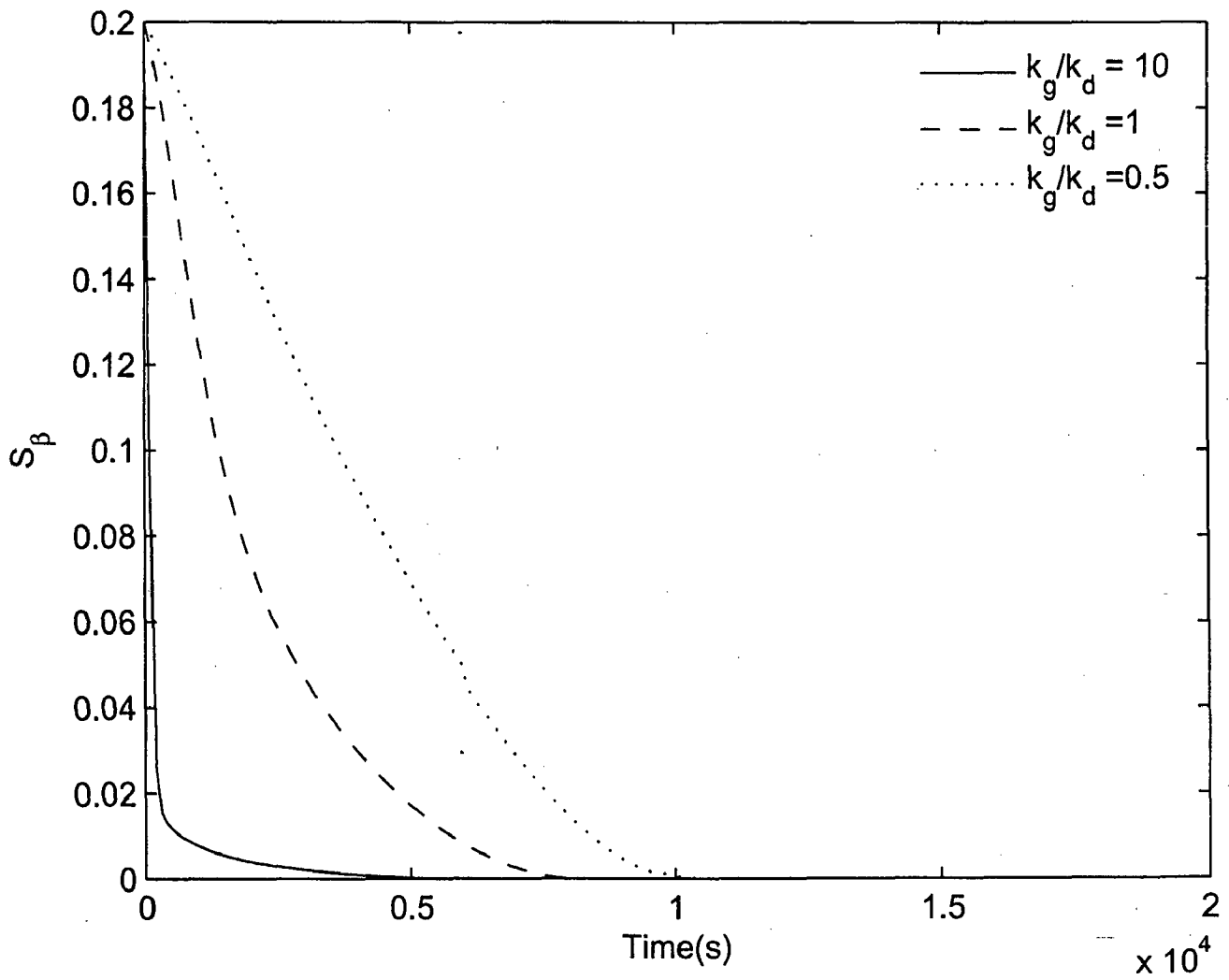


Figure 7.6: *Supersaturation of β form in seeded crystallization*

Chapter 8

Conclusions and recommendations

8.1 Conclusions

In the course of this project an appropriate methodology is developed for controlling the batch reactor temperature. An optimization technique is integrated with the controller for which a mathematical model is implemented in gPROMS. With the experiment it is proved that the mathematical model has a very good agreement with the system under consideration. Furthermore it is also proved that the optimization with an integrated control technique is very efficient for the temperature control of the batch reactor.

The mathematical model involves many unknown parameters which are estimated by the parameter estimation routine of gPROMS. But before that it is proved that the parameter estimation routine of gPROMS is reliable and can be adopted for accurate parameter estimation. The appropriate variance model and the value of the parameters ω and γ which are prerequisite for parameter estimation are also estimated. For making the model more general and flexible to adopt any change in the system, the effect of the parameters are also studied.

In order to reduce the optimization time and hence making the optimization problem more suitable for the experiment purpose a linear model of the system is developed. It is proved that the *ARX* model is best to our system. With the experiment it is proved that the linear model is also behaving as the system under consideration.

The appropriate setpoint temperature trajectory of the thermostat which gives the minimum deviation of the reactor temperature from the prespecified setpoint temper-

ature trajectory of the reactor is determined by optimization. To track the setpoint temperature of the thermostat an internal *PID* controller is implemented. For handling the system disturbances a suitable model is developed for online adjustment of the prespecified thermostat setpoint trajectory. To achieve this an external *PID* controller is implemented. A strategy is developed to use the optimization routine of gPROMS for tuning the controller parameter which is proved to be a very efficient technique for determining the appropriate controller parameters.

8.2 Recommendation for future work

In the course of future work the developed methodology can be used for process control. For example for a crystallization process this technique may be very useful. Some substance show polymorphism, for example L-glutamic acid has two polymorph that are the stable α form and the unstable β form. The formation of these polymorph largely depends on the reactor temperature. It is possible to achieve a fixed composition of α and β form by maintaining the specific temperature profile in the reactor which can be obtained by the optimization. A model for the crystallization of the L-glutamic acid is already implemented in gPROMS which shows good agreement with the published result in the literature [SN03]. In the course of future work this model can be validated by the experiment.

The linear model of the system and the developed temperature trajectory optimization strategy can be used for developing a predictive controller. In the course of this work the optimized temperature trajectory is obtained by off line optimization. In the course of future work the optimization tool can be integrated with the Labview interface and online optimization can be achieved using the already estimated linear model of the system.

Appendix A

Process section

A.1 Model

Specified parameters

```
g := 9.81; # m/s^2,
gravity constant pi := 3.14159265;
#Geometric parameters for the reactor
dn := 0.12;          m, inner diameter of inner tank
di := 0.13;          m, outer diameter of inner tank
da := 0.15;          m, outer diameter of outer tank
d0 := 15E-3;         m, diameter of inlet of tempering jacket
Si := 4E-3;          m, thickness of inner tank wall
So := 5E-3;          m, thickness of outer tank wall
Ls := 0.11;          m, height of tempering jacket shell
delta_jacket := 10E-3; m, width of tempering jacket
d_ag := 0.05;         m, diameter of agitator blade
h_ag := 0.005;        m, height of agitator blade
V_ag := 0.03E-3;      m^3, volume of agitator including baffles
#parameters for thermostat
V_he := 4.53E-3;      m^3, volume of heat exchanger (estimated value)
Q_max := 1.1;         kW, maximum heating duty of heater in thermostat
# parameters for stability of conversion in gPROMS
eps_1 := 1.3;
eps_2 := 200;
# variable parameters (value can differ for each run)
mass_r := 1;         kg, mass of liquid in reactor
p_r := 1;            bar, pressure in reactor
T_amb := 293.15;     K, temperature of ambient air
n := 6.67;           1/s revolutions of agitator
# temperature independent physical properties
# liquid in reactor (water),(VDI Wreheatlas, 6. Auflage, 1991, physical properties section)
M_r := 18.02;        kg/kmol, mole weight
```

```

R_r := 0.461522;    kJ/kg/K, gas constant
diffvol_r := 12.7;  diffusion volume, (VDI Wrmeatlas, 6. Auflage, 1991, Da33)
# ambient air (VDI Wrmeatlas, 6. Auflage, 1991, physical properties section)
M_a := 28.96;      kg/kmol mole weight
R_a := 0.28722;    kJ/kg/K gas constant
diffvol_a := 20.1; diffusion volume (VDI Wrmeatlas, 6. Auflage, 1991, Da33)
# borosilicate glass (reactor tanks)
cp_glass := 0.98;   kJ/kg/K, specific heat capacity
rho_glass := 2.23E3; kg/m^3, density
lambda_glass := 1.2E-3; kW/m/K, heat conductivity
# steel (steel cage of heat exchanger)
cp_st := 0.6;      kJ/kg/K, specific heat capacity
# coefficients for polynomials of temperature dependent physical
properties
# reactor liquid (water), (VDI Wrmeatlas, 6. Auflage, 1991, physical properties section)
order_r := 4;
rho_coeff_r(4) := 1.6045119E-5;
rho_coeff_r(3) := -1.9112884E-2;
rho_coeff_r(2) := 6.8714806;
rho_coeff_r(1) := 2.2203125E+2;
cp_coeff_r(4) := -3.4133333E-7;
cp_coeff_r(3) := 3.397056E-4;
cp_coeff_r(2) := -1.1226625E-1;
cp_coeff_r(1) := 1.6504143E+1;
lambda_coeff_r(4) := 0;
lambda_coeff_r(3) := -9.2E-9;
lambda_coeff_r(2) := 7.13116E-6;
lambda_coeff_r(1) := -7.0062587E-4;
eta_coeff_r(4) := -4.0981333E-9;
eta_coeff_r(3) := 4.1122154E-6;
eta_coeff_r(2) := -1.3815594E-3;
eta_coeff_r(1) := 1.5586862E-1;
pr_coeff_r(4) := -3.6213333E-5;
pr_coeff_r(3) := 3.6227016E-2;
pr_coeff_r(2) := -12.121255;
pr_coeff_r(1) := 1359.5265;
hv_coeff_r(4) := 0;
hv_coeff_r(3) := 0;
hv_coeff_r(2) := -2.430021;
hv_coeff_r(1) := 3.165845E+3;
pvap_coeff_r(4) := 1.597053E-6;
pvap_coeff_r(3) := -1.393776E-3;
pvap_coeff_r(2) := 4.0654822E-1;
pvap_coeff_r(1) := -3.9606168E+1;
rho_coeff_vap(4) := 8.2659163E-7;
rho_coeff_vap(3) := -7.1409841E-4;
rho_coeff_vap(2) := 2.0642705E-1;

```



```

rho_coeff_vap(1) := -1.9950098E+1;
# bath fluid (Baysilone M5)
order_b := 4;
rho_coeff_b(4) := 0;
rho_coeff_b(3) := 0;
rho_coeff_b(2) := -8.1250000E-01;
rho_coeff_b(1) := 1.1681844E+03;
cp_coeff_b(4) := 0;
cp_coeff_b(3) := 0;
cp_coeff_b(2) := 1.6000000E-03;
cp_coeff_b(1) := 1.0329600E+00;
lambda_coeff_b(4) := 0;
lambda_coeff_b(3) := 0;
lambda_coeff_b(2) := -2.2666667E-07;
lambda_coeff_b(1) := 1.8358067E-04;
eta_coeff_b(4) := 0;
eta_coeff_b(3) := 0;
eta_coeff_b(2) := -3.8106667E-05;
eta_coeff_b(1) := 1.5961503E-02;
pr_coeff_b(4) := 0;
pr_coeff_b(3) := 0;
pr_coeff_b(2) := -4.1640000E-01;
pr_coeff_b(1) := 1.8402966E+02;
# ambient air, see [4] for reference (physical properties section)
order_a := 4;
rho_coeff_a(4) := 0;
rho_coeff_a(3) := 1.205495E-5;
rho_coeff_a(2) := -1.121029E-2;
rho_coeff_a(1) := 3.439576;
lambda_coeff_a(4) := 0;
lambda_coeff_a(3) := 0;
lambda_coeff_a(2) := 7.3642857E-8;
lambda_coeff_a(1) := 4.0873107E-6;
nu_coeff_a(4) := 0;
nu_coeff_a(3) := 1.0353346E-10;
nu_coeff_a(2) := 3.3041402E-8;
nu_coeff_a(1) := -3.233218E-6;
pr_coeff_a(4) := 0;
pr_coeff_a(3) := 5.833333E-7;
pr_coeff_a(2) := -4.852464E-4;
pr_coeff_a(1) := 8.069223E-1;
# multiplication factor for external controller parameters
(estimated)
p.Kp := 0.06875;      multiplication factor for proportional constant
P.Ki := 1500;        multiplication factor for integral time
p.Kd := 1.2;         multiplication factor for differential time

```

distribution domains

```

yi := [CFDM, 4 ,50]; inner tank wall
yo := [CFDM, 4 ,50]; outer tank wall
zs := [CFDM, 4 ,50]; shell part of tempering jacket

```

Specified variables

```

r.P:= 0.002;          kW,          capacity of agitator

he.Vdot := 0.24E-3;   m3/s ,    volumetric flow rate through pump
chs.alpha := 0.0935839; kW/m2/K, heat transfer coefficient between bath fluid in heat
exchanger and steel cage of heat exchanger
chs.A_chs := 0.164;   m2,          area of heat exchange between bath fluid
in heat exchanger and steel cage of heat exchanger
st.m_st := 9.63804;   kg,          mass of steel cage around heat exchanger
csa.u := 1;           m/s,          velocity of air flow around heat exchanger in
thermostat
csa.l_csa := 0.165;   m ,          characteristic length for heat transfer between
steel cage of heat exchanger and forced air flow
around heat exchanger
csa.A_csa := 0.15;   m2,          area of heat exchange between steel cage of heat
exchanger and forced air flow around heat exchanger

ic.slope:=0.00909712; slope of the thermostat setpoint temperature
# Internal controller
ic.Tn := 80010;       s,          integral time of internal controller
ic.Tv := 7;          s,          differential time of internal controller
ic.xp := 3;          kJ,          range of proportional gain (kJ since energy is
controlled)

# External controller
p.Kc_exp :=1.31;     proportional constant
P.Ti_exp :=4;        integral time
P.Td_exp :=1;        differential time
# Adjusting factors
cra.est_cra := 0.00012; kW/K, estimation parameter for product of heat transfer
coefficient and area of heat exchange between reactor
liquid and ambient air
crc.est_g := 0.5;    factor for mass transfer coefficient at the surface
of reactor liquid
cis.est_alpha := 2;  factor for heat transfer coefficient between bath fluid
in the tempering jacket and surrounding tank walls
(identical with cib.est_alpha)
i.est_lambda := 0.7; factor for heat conductivity of inner and outer tank wall
i.est_cp := 0.8;     factor for heat capacity of inner tank wall
ob.est_cp := 1.6;    factor for heat capacity of bottom part of outer tank wall
os.est_lambda := 1.08864; factor for heat conductivity of shell part of outer tank
wall
os.est_cp := 1.3;    factor for heat capacity of shell part of outer tank wall

```

```

cich.cool_coeff_4 := -3.08959E-007; coefficients for polynomial for cooling duty of
                                thermostat
cich.cool_coeff_3 := 0.000572537;
cich.cool_coeff_2 := -0.288925;
cich.cool_coeff_1 := 41.8024;
cich.cool_min := 0.1;           minimum cooling coefficient

```

Initial conditions

```

r.T_r = 293.15;                K, temperature of reactor liquid
i.T_i(0:Si) = 293.15;         K, temperature of inner tank wall
b.T_b = 293.15;                K, temperature of bottom part of tempering jacket
s.T_s(0|+:Ls) = 293.15;       K, temperature of shell part of tempering jacket
ob.T_ob(0:So) = 293.15;       K, temperature of bottom part of outer tank wall
os.T_os(0:So) = 293.15;       K, temperature of shell part of outer tank wall
he.T_he = 293.15;             K, temperature of bath fluid in heat exchanger
st.T_st = 293.15;             K, temperature of steel cage of heat exchanger
ic.I_error = 0;                integral of error of internal controller
ic.PIDvalue = 0.2;            output of internal controller
ic.t=0;                         s, time
ic.delta_T_r = 0;              objective function for temperature trajectory
                                optimization
ic.T_set1 = 293.15;            K, pre specified thermostat setpoint temperature
ic.T_set = 293.15;            K, adjusted thermostat setpoint temperature
ic.TBuffer_given = 0;         K, reactor setpoint temperature
p.IError = 0;                  integral error of external controller

```

Optimize slope of thermostat setpoint temperature profile

```
# obtain by temperature trajectory optimization
```

```
# operation schedule
```

```
SCHEDULE
```

```
SEQUENCE
```

```
RESET com.ic.slope := 0;
```

```
END
```

```
CONTINUE FOR 1881.6
```

```
RESET com.ic.slope := -0.013066667;
```

```
END
```

```
CONTINUE FOR 5.4
```

```
RESET com.ic.slope := 0.0751;
```

```
END
```

```
CONTINUE FOR 322.8
```

```
RESET com.ic.slope := 0.020083333;
```

```
END
```

```
CONTINUE FOR 1651.8
```

```
RESET com.ic.slope := 0.022783333;
```

```
END
```

```

CONTINUE FOR 12
RESET com.ic.slope := 0.0044333333;
END
CONTINUE FOR 0.6
RESET com.ic.slope := -0.016267;
END
CONTINUE FOR 0.6
RESET com.ic.slope := -0.0499;
END
CONTINUE FOR 350.4
RESET com.ic.slope := 0;
END
CONTINUE FOR 1591.2
RESET com.ic.slope := -0.037583333;
END
CONTINUE FOR 484.8
RESET com.ic.slope := -0.014066667;
END
CONTINUE FOR 999.6
RESET com.ic.slope := -0.02925;
END
CONTINUE FOR 525
RESET com.ic.slope := -0.020066667;
END
CONTINUE FOR 1111.2
RESET com.ic.slope := 0.08725;
END
CONTINUE FOR 214.2
RESET com.ic.slope := 0.0;
END
CONTINUE FOR 849
END

```

A.2 Linear model

Specified parameters

```

V_he := 4.53E-3;    m3, volume of heat exchanger
# polynomial coefficient for bath fluid density
order_b := 4;
rho_coeff_b(4) := 0;
rho_coeff_b(3) := 0;
rho_coeff_b(2) := -8.1250000E-01;
rho_coeff_b(1) := 1.1681844E+03;
#polynomial coefficient for bath fluid heat capacity
cp_coeff_b(4) := 0;

```

```

cp_coeff_b(3) := 0;
cp_coeff_b(2) := 1.6000000E-03;
cp_coeff_b(1) := 1.0329600E+00;
#coefficient of linear model obtain by system identification
a = 0.5708;
b = 0.0005504;
c = 0.02294;
d = 0.0005481;
# multiplication factor for controller parameters (estimated)
kp = 0.1484;      multiplication factor for proportional constant
ki = 1500;        multiplication factor for integral time
kd = 1.2;         multiplication factor for differential time

```

Specified variables

```

# controller parameters
Kc_exp := 1.31;      proportional constant
Ti_exp := 4;         integral time
Td_exp := 1;         differential time
slope1 := 0.008      slope of thermostat setpoint temperature

```

Initial conditions

```

y = 293.15;          K, reactor temperature
x = 0;               reactor temperature slope
u = 293.15;          K, thermostat temperature
u1 = 293.15;         K, thermostat setpoint temperature
t = 0;               s, time
Tbuffer_given = 293.15; K, reactor setpoint temperature
IError = 0;          integral error
delta_y = 0;         objective function for trajectory optimization

```

Optimize slope of thermostat setpoint temperature profile

```

# obtain by temperature trajectory optimization
# operation schedule
SCHEDULE
SEQUENCE
RESET s.slope1 := 0;
END
CONTINUE FOR 1881.6
RESET s.slope1 := -0.013066667;
END
CONTINUE FOR 5.4
RESET s.slope1 := 0.0751;
END
CONTINUE FOR 322.8

```

```
RESET com.s.slope1 := 0.020083333;
END
CONTINUE FOR 1651.8
RESET s.slope1 := 0.022783333;
END
CONTINUE FOR 12
RESET s.slope1 := 0.004433333;
END
CONTINUE FOR 0.6
RESET s.slope1 := -0.016267;
END
CONTINUE FOR 0.6
RESET s.slope1 := -0.0499;
END
CONTINUE FOR 350.4
RESET s.slope1 := 0;
END
CONTINUE FOR 1591.2
RESET s.slope1 := -0.037583333;
END
CONTINUE FOR 484.8
RESET s.slope1 := -0.014066667;
END
CONTINUE FOR 999.6
RESET s.slope1 := -0.02925;
END
CONTINUE FOR 525
RESET s.slope1 := -0.020066667;
END
CONTINUE FOR 1111.2
RESET s.slope1 := 0.08725;
END
CONTINUE FOR 214.2
RESET s.slope1 := 0.0;
END
CONTINUE FOR 849
END
```

Appendix B

System identification

B.1 1 Liter reactor

estimation from experimental data set 1 (use for optimization in linear model)

#Discrete-time IDPOLY model:

$$A(q)y(t) = B(q)u(t) + e(t)$$

$$A(q) = 1 - 1.318 (+-0.00869) q^{-1} + 0.3193 (+-0.008674) q^{-2}$$

$$B(q) = 0.02812 (+-0.001083) q^{-30} - 0.02682 (+-0.00108) q^{-31}$$

Estimated using ARX from data set 1liter Loss function 4.20208e-005 and FPE 4.20489e-005 Sampling interval: 2

Continuous-time IDPOLY model:

$$A(s)y(t) = B(s)u(t) + C(s)e(t)$$

$$A(s) = s^2 + 0.5708 s + 0.0005504$$

$$B(s) = 0.02294 s + 0.0005481$$

$$C(s) = s^2 + 1.18 s + 0.4194$$

estimation from experimental data set 2 (just for comparison)

#Discrete-time IDPOLY model:

$$A(q)y(t) = B(q)u(t) + e(t)$$

$$A(q) = 1 - 1.004(+-0.01257) q^{-1} + 0.006654 (+-0.01254) q^{-2}$$

$$B(q) = 0.0523 (+-0.001709) q^{-30} - 0.05008 (+-0.001702) q^{-31}$$

Estimated using ARX from data set validation Loss function 8.29832e-005 and FPE 8.30855e-005 Sampling interval: 2

#Continuous-time IDPOLY model:

$$A(s)y(t) = B(s)u(t) + C(s)e(t)$$

$$A(s) = s^2 + 2.506 s + 0.002815$$

$$B(s) = 0.1276 s + 0.002804$$

$$C(s) = s^2 + 3.009 s + 1.262$$

B.2 6 Liter reactor

estimation from experiment 1

#ARX 2240

#Discrete-time IDPOLY model:

$$A(q)y(t) = B(q)u(t) + e(t)$$

$$A(q) = 1 - 0.7956(+0.01182) q^{-1} - 0.2036(+0.01181) q^{-2}$$

$$B(q) = 0.02671(+0.002499) q^{-40} - 0.02587(+0.0025) q^{-41}$$

#Continuous-time IDPOLY model:

$$A(s)y(t) = B(s)u(t) + C(s)e(t)$$

$$A(s) = s^2 + 0.7958 s + 0.0002798$$

$$B(s) = 0.01754 s + 0.0002778$$

$$C(s) = s^2 + 1.188 s + 0.3305$$

#ARMAX[22140]

#Discrete-time IDPOLY model:

$$A(q)y(t) = B(q)u(t) + C(q)e(t)$$

$$A(q) = 1 - 1.075(+0.04778) q^{-1} + 0.07591(+0.04775) q^{-2}$$

$$B(q) = 0.02603(+0.002258) q^{-40} - 0.0254(+0.002248) q^{-41}$$

$$C(q) = 1 - 0.3047(+0.04622) q^{-1}$$

#Continuous-time IDPOLY model:

$$A(s)y(t) = B(s)u(t) + C(s)e(t)$$

$$A(s) = s^2 + 1.289 s + 0.0004463$$

$$B(s) = 0.03571 s + 0.0004432$$

$$C(s) = s^2 + 1.691 s + 0.485$$

#OE [2218]

#Discrete-time IDPOLY model:

$$y(t) = [B(q)/F(q)]u(t) + e(t)$$

$$B(q) = 0.0007713 q^{-18} - 0.0007707 q^{-19}$$

$$F(q) = 1 - 1.998 q^{-1} + 0.9983 q^{-2}$$

#Continuous-time IDPOLY model:

$$y(t) = [B(s)/F(s)]u(t) + e(t)$$

$$B(s) = 0.0003858 s + 1.622e-007$$

$$F(s) = s^2 + 0.0008548 s + 1.629e-007$$

#BJ[222240]

#Discrete-time IDPOLY model:

$$y(t) = [B(q)/F(q)]u(t) + [C(q)/D(q)]e(t)$$

$$B(q) = 0.01445(+0.01195) q^{-40} - 0.0137(+0.01169) q^{-41}$$

$$C(q) = 1 + 0.1816(+0.6266) q^{-1} - 0.1948(+0.1909) q^{-2}$$

$$D(q) = 1 - 0.5135(+0.6318) q^{-1} - 0.4861(+0.6317) q^{-2}$$

$$F(q) = 1 - 0.9751(+0.7565) q^{-1} - 0.02411(+0.756) q^{-2}$$

#Continuous-time IDPOLY model:

$$y(t) = [B(s)/F(s)]u(t) + [C(s)/D(s)]e(t)$$

$$B(s) = 0.02532 s + 0.0006842$$

$$C(s) = s^2 + 0.7002 s + 0.1197$$

$$D(s) = s^2 + 0.3607 s + 5.053e-005$$

$$F(s) = s^2 + 1.863 s + 0.0006791$$


```

#P2DZ
#Process model with transfer function
      1+Tz*s
G(s) = K * ----- * exp(-Td*s)
      (1+Tp1*s)(1+Tp2*s)
with   K = 0.99145+-0.00012837
      Tp1 = 3532.2+-17.825
      Tp2 = 1070.2+-32.018
      Td = 60+-2.2908
      Tz = 1602+-44.499
#P3DZ Process model with transfer function
      1+Tz*s
G(s) = K * ----- * exp(-Td*s)
      (1+Tp1*s)(1+Tp2*s)(1+Tp3*s)
with   K = 0.99165+-0.00014949
      Tp1 = 3524.8+-17.123
      Tp2 = 954.3+-34.571
      Tp3 = 44.156+-4.4028
      Td = 57.763+-0.0058543
      Tz = 1522.7+-44.028
# estimation from experiment 2
#ARX[2240]
Discrete-time IDPOLY model:
A(q)y(t) = B(q)u(t) + e(t)
A(q) = 1-0.641 (+-0.011) q^-1 - 0.358 (+-0.01099) q^-2
B(q) = 0.000282 (+-0.0004077) q^-40 + 0.0007082 (+-0.0004081) q^-41
#Continuous-time IDPOLY model:
A(s)y(t) = B(s)u(t) + C(s)e(t)
A(s) = s^2 + 0.5136 s + 0.0001871
B(s) = 0.0001958 s + 0.0001871
C(s) = s^2 + 0.8458 s + 0.189
#ARMAX[22140]
#Discrete-time IDPOLY model:
A(q)y(t) = B(q)u(t) + C(q)e(t)
A(q) = 1 - 1.048 (+-0.02602) q^-1 + 0.04848 (+-0.026) q^-2
B(q) = 0.0004733 (+-0.0002066) q^-40 + 0.0002202 (+-0.0002086) q^-41
C(q) = 1 - 0.4875 (+-0.02258) q^-1
#Continuous-time IDPOLY model:
A(s)y(t) = B(s)u(t) + C(s)e(t)
A(s) = s^2 + 1.513 s + 0.0005516
B(s) = -4.205e-005 s + 0.0005516
C(s) = s^2 + 1.818 s + 0.4076
#OE[2215]
#Discrete-time IDPOLY model:
y(t) = [B(q)/F(q)]u(t) + e(t)
B(q) = 0.0002677 q^-15 - 0.0002495 q^-16
F(q) = 1 - 1.975 q^-1 + 0.9752 q^-2

```

#Continuous-time IDPOLY model:

$$y(t) = [B(s)/F(s)]u(t) + e(t)$$

$$B(s) = 0.0001309 s + 4.591e-006$$

$$F(s) = s^2 + 0.01257 s + 4.591e-006$$

#BJ[222 25]

#Discrete-time IDPOLY model:

$$y(t) = [B(q)/F(q)]u(t) + [C(q)/D(q)]e(t)$$

$$B(q) = -0.002304 (+-0.004876) q^{-25} + 0.002538(+0.005236) q^{-26}$$

$$C(q) = 1 + 0.3021 (+-0.5729) q^{-1} + 0.06766 (+-0.1951) q^{-2}$$

$$D(q) = 1 - 1.113 (+-0.6069) q^{-1} + 0.1133 (+-0.6069) q^{-2}$$

$$F(q) = 1 - 1.675 (+-0.5277) q^{-1} + 0.6756 (+-0.5274) q^{-2}$$

#Continuous-time IDPOLY model:

$$y(t) = [B(s)/F(s)]u(t) + [C(s)/D(s)]e(t)$$

$$B(s) = -0.001468 s + 7.083e-005$$

$$C(s) = s^2 + 1.702 s + 0.8411 \quad D(s) = s^2 + 1.089 s - 1.028e-005$$

$$F(s) = s^2 + 0.1961 s + 6.931e-005$$

#P2DZ

#Process model with transfer function

$$1+Tz*s$$

$$G(s) = K * \frac{1+Tz*s}{(1+Tp1*s)(1+Tp2*s)} * \exp(-Td*s)$$

with $K = 1.0001$

$$Tp1 = 2681.6$$

$$Tp2 = 0.001$$

$$Td = 60$$

$$Tz = -3.6273$$

#P2DZ

#Process model with transfer function

$$1+Tz*s$$

$$G(s) = K * \frac{1+Tz*s}{(1+Tp1*s)(1+Tp2*s)(1+Tp3*s)} * \exp(-Td*s)$$

with $K = 0.99985+-4.3777e-005$

$$Tp1 = 2593.8+-17.36$$

$$Tp2 = 646.01+-91.189$$

$$Tp3 = 11.127+-6.3474$$

$$Td = 56.591+-6.1338$$

$$Tz = 607.54+-84.359$$

Appendix C

PID controller

C.1 Internal controller

```
# Optional internal PID controller
error = T_set - T_he; #error is expressed directly in term of temperature instead of energy

$I_error = error;      #integral of error

PIvalue = 1/xp*(error +I_error/Tn);

Q_ic = (-Dvalue+PIvalue) # controller heat, calculated as provided by the the manufacture
Dvalue*xp*(1+Tv*D_error) =Tv*D_error;

D_error*V_he*(rho*cp+T_he*(rho*y_cp + cp*y_rho)) =slope*V_he*(rho*cp+T_he*(rho*y_cp + cp*y_rho))
-(E_in - E_out + Q_ic- Q_chs);

y_cp =3*cp_coeff_b(4)*(T_he)^2+2*cp_coeff_b(3)*(T_he)+cp_coeff_b(2);
y_rho = 3*rho_coeff_b(4) +2* rho_coeff_b(3) + rho_coeff_b(2);
```

C.2 External controller

```
# The differential error is related to the reactor temperature by
the following equation:
DError*mass_r*(Cp+(T_r-273.15)*(3*cp_coeff_r(4)*(T_r)^2+2*cp_coeff_r(3)*(T_r)+
cp_coeff_r(2)))=Constant*mass_r*(Cp+(T_r-273.15)*(3*cp_coeff_r(4)*(T_r)^2
+ 2*cp_coeff_r(3)*(T_r)^1 + cp_coeff_r(2)))-(-Q_cri -Q_crc+Q_cra+P);
```

Appendix D

Entities in gPROMS

Model section entities

PARAMETER

Parameter name as integer or real or logical (default value)

Parameter name as array (size) of integer

Parameter name as foreign object (foreign object class)

DISTRIBUTION DOMAIN

Domain name as (lower bound:upper bound)

Domain name as array (size) of (lower bound:upper bound)

UNIT

Unit name as unit model name

Unit name as array (size) of unit model name

VARIABLE

Variable name as variable type

Variable name as array (size) of variable type

Variable name as distribution (domain name) of variable type

STREAM

Stream name: Variable path (...) as stream type

Stream name: Variable path (...) as array of stream type

SET

Parameter path :=expression;

BOUNDARY

Boundary equations

EQUATION

Table D.1: *Optimization entities*

Specification	Comments
HORION	Time horizon specification
$\{IV\} : \{LB\} : \{UB\}$	Initial guess for t_f followed by t_f^{min} and t_f^{max}
INTERVALS	Intervals in control variable profiles
{number of intervals}	Specify number of intervals
$\{IV\} : \{LB\} : \{UB\}$	Initial guess, lower bound and upper bound for the length of each interval
PIECEWISE CONSTANT	Specification of a piecewise constant control variable
{variable name}	Its full gPROMS path name
{initial profile specification}	Optional
PIECEWISE LINEAR	Specification of a piecewise linear control variable
{variable name}	Its full gPROMS path name
{initial profile specification}	Optional
TIME INVARIANT	Specification of a time invariant parameter
{variable name}	Its full gPROMS path name
initial value specification	Optional
ENDPOINT EQUALITY	Specification of a variable on which an equality end point constraint is to be imposed
{variable name}	Its full gPROMS path name
{value}	Its value
ENDPOINT INEQUALITY	Specification of a variable on which an inequality end point constraint is to be imposed
{variable name}	Its full gPROMS path name
$\{LB : UB\}$	Lower bound and upper bound of constraint
INTERIOR POINT	Specification of a variable on which an interior point constraint is to be imposed
{variable name}	Its full gPROMS path name
$\{LB : UB\}$	Lower bound and upper bound of constraint
MAXIMISE	or MINIMISE
{variable name}	Full gPROMS path of objective function

Appendix E

Case study

Process section for crystallization of L-glutamic acid

Specified parameters

```
# in the gPROM model r is assume alpha form and s is assume beta
form
k_v := 0.5236;          volumetric shape factor
k_a := 3.1416;          area shape factor
k_gr := 0;              growth rate constant of alpha form
k_gs := 0.5E-07;        growth rate constant of beta form
k_dr := 1E-07;          dissolution rate constant of alpha form
k_ds := 0;              dissolution rate constant of beta form
k_nr := 0;              nucleation rate constant of alpha form
k_ns := 1E08;           nucleation rate constant of beta form
g := 1;                 growth rate order
n := -1;                nucleation rate order
L_nr := 1E-08;          size of seed of alpha form
L_ns := 1E-08; #0, for unseeded, size of seed of beta form
rho_s := 17000;         density of beta form
rho := 17000;           density of solution
rho_r := 17000;         density of alpha form
a_alpha := 0.44283;
a_beta := 0.35597;
b_alpha := 0.03656;
  b_beta := 0.03423;
```

Specified variables

```
V := 4.4E-04;
T_r := 390
```

Initial conditions

```
x = 0.12;
L_r = 9998.6752;
L_s = 9998.6752; # 0, for unseeded
M_r = 0.89;
M_s = 0.0089; # 0, for unseeded
A_r = 3.1412;
A_s = 0.31412; # 0, for unseeded
Nr = 99986752.48;
Ns = 999867524.8; # 0, for unseeded
m_f = 10;
```


References

- [API05] A. Arpornwichanop, P. Kittisupakorn, and I. M. Mujtaba. On-line dynamic optimization and control strategy for improving the performance of batch reactors. *Chemical Engineering and Processing*, 44, pp. 101–114, 2005.
- [GZ99] Gangadhar Gattu and Evangelos Zafiriou. A methodology for online setpoint modification for batch reactor in the presence of modeling error. *Chemical Engineering Journal*, 75, pp. 21–29, 1999.
- [hg] <http://www.julabo-gmbh.de/manual/us19532752.pdf>.
- [HJKA03] H. A. Mohameed, N. Abdel Jabbar, K. Takrouri, and A. Nasr. Model-based optimal cooling strategy for batch crystallization processes. *Trans IChemE*, 81, pp. 578–584, May 2003.
- [HJR00] H. J. M. Kramer, J. W. Dijkstra, and G. M. Van Rosmalen. Modeling of industrial crystallizers for control and design purposes. *Powder Technology*, 108, pp. 185–191, 2000.
- [hm] http://www.hws-mainz.de/sites/lieferkataloge/psp/psp06.html#psp06_01.
- [JN42] J. G. Ziegler and N. B. Nichols. Optimum settings for automatic controllers. *ASME Transaction*, pp. 759–768, November 1942.
- [Mer95] A. Mersmann, editor. *Crystallization Technology Handbook*. Marcel Dekker, Inc. New York, 1995.
- [NHI00] N. Aziz, M. A. Hussain, and I. M. Mujtaba. Performance of different types of controllers in tracking optimal temperature profiles in batch reactors. *Computer and Chemical Engineering*, 24, pp. 1069–1075, 2000.

- [OtHJ04] T. Ono, H. J. M. Kramer, J. H. ter Host, and P. J. Jansens. Process modeling of the polymorphic transformation of L-glutamic acid. *Crystal Growth and Design*, 4(6), pp. 1161–1167, July 2004.
- [PEBL04] P. Quintana, E. Bolanos, B. Miranda, and L. Salcedo. Mathematical modeling and kinetic parameter estimation in batch crystallization. *AIChE*, 50(7), pp. 1407–1417, July 2004.
- [PS88] P. L. Lee and G. R. Sullivan. Generic model control. *Computer and Chemical Engineering*, 12, pp. 573–580, 1988.
- [Ren] U. Renz. Heat and mass transfer, Lecture notes, Lehrstuhl für Prozesstechnik, Wärmeübertragung und Klimatechnik, RWTH Aachen.
- [RJT90] R. I. Risti, J. N. Sherwood, and T. Shripathi. Strain variation in the 100 growth sectors of potash alum single crystals and its relationship to growth rate dispersion. *Journal of Crystal Growth*, 102, pp. 245–248, 1990.
- [Sko04] Sigurd Skogestad. Simple analytical rules for model reduction and PID controller tuning. *Modeling, Identification and Control*, 25, pp. 84–120, 2004.
- [SN03] Joseph W. Schroer and Ka M. Ng. Process paths of kinetically controlled crystallization: Enantiomers and polymorphs. *Ind. Eng. Chem. Res.*, 42(10), pp. 2230–2244, 2003.
- [SPCC02] Vishak Sampath, Srinivas Palanki, J. C. Cockburn, and J. P. Corriou. Robust controller design for temperature tracking problems in jacketed batch reactors. *Journal of Process Control*, 12, pp. 27–38, 2002.
- [VW] 1991 VDI Wärmeatlas, 6. Auflage.